CYPRUS UNIVERSITY OF TECHNOLOGY

FACULTY OF ENGINEERING AND TECHNOLOGY

Doctor of Philosophy

Investigation of the Processing Parameters for Efficient Organic Solar Cells

Marios Neophytou

Limassol, 2012

CYPRUS UNIVERSITY OF TECHNOLOGY

Faculty of Engineering and Technology

Department of Mechanical Engineering and Materials Science and Engineering

Investigation of the Processing Parameters for Efficient Organic Solar Cells

By

Marios Neophytou

Limassol, 2012

Approved Thesis Committee
PhD Thesis

Investigation of the Processing Parameters for Efficient Organic Solar Cells

Presented by

Marios Neophytou

Academic Supervisor

_____

Stelios A. Choulis
Associate Professor

President of the Committee

_____

Costas N. Costa
Associate Professor

Member of the Committee

_____

Jenny Nelson
Professor

Member of the Committee

_____

Charalambos Doumanidis
Professor

Member of the Committee

_____

Polyvios Eleftheriou
Senior Lecturer

Cyprus University of Technology
November, 2012

Πνευματικά δικαιώματα

Η έγκριση της διδακτορικής διατριβής από Τμήμα Μηχανολόγων Μηχανικών και Επιστήμης και Μηχανικής Υλικών του Τεχνολογικού Πανεπιστημίου Κύπρου δεν υποδηλώνει απαραιτήτως και αποδοχή των απόψεων του συγγραφέα εκ μέρους του Τμήματος.

Acknowledgements

I would like to thank Associate Professor Stelios A. Choulis for introducing me to such an interesting and breathtaking topic and for his helpful advices, guidance and support.

Special thanks to Christoph Waldauf for knowledge transfusion, Roberto Pacios for his hospitality and funding, and the rest of the group for making my life exciting during my PhD internship at Ikerlan, Spain.

Also I would like to thank Achilleas Savva, Felix Hermerschmidt, Efthymios Georgiou, Dr Solon Economopoulos, Panayiotis Pouloupatis and Dr Myrsini Giannouli for fruitful discussions, crazy conversations and for all the fun we have in the lab. Dr Christos Chochos and Assoc. Professor Koutentis group at the Department of Chemistry (University of Cyprus) for synthesizing some of the conjugated polymers studied in this Thesis, as well as external collaborators at University of Erlangen, Imperial College London and Jaume University in Spain.

I would like to thank Assistant Professor Gregorios Itskos, Professsor Andreas Othonos, Dr Polyvios Eleftheriou and Dr Constantinos Christodoulou for their ideas, perspectives and experimental support.

I devote my heartiest appreciation to my parents for moral support, ethical guidance and boundless love.

Last but not least, a special thanks to Danae Constantinou for inspiring discussions and for making my life adorably difficult.

Dedicated to the Master of my Universe

Table of Contents

Table of Figures

Chapter 1 & 2:

Chapter 3:

Chapter 4:

Chapter 5:

Tables

Chapter 3

Chapter 4:

Chapter 5:

List of Abbreviations

AFM……...Atomic Force Microscopy

BHJ……..…….. ..BulkHeterojunction

CB……...……Chlovrobenzene

CF……. Chloroform

CTC……...… Charge Transfer Complex

CTS……. Charge Transfer States

EBL…… …Electron Blocking Layer

FF…….……Fill Factor

HOMO…… Hoghest Occupied Molecular Orbital

HTL……..Hole Transporting Layer

ITO……..Indium Tin Oxide

Jsc……..Short Circuit Current

LUMO……Lowest Unoccupied Molecular Orbital

oDCB…… ….ortho DiChlorobenzene

OPV……Organic Photovoltaic

P3HT…….Poly- 3 - hexylthiophene

PCBM…….…… Phenyl-C61-butyric acid methyl ester

PCE……...……Power Conversion Efficiency

PEDOT:PSS…… Poly(3,4-ethylenedioxythiophene):poly(styrenesulfonate)

SCLC……SpaceCharge Limited Current

Voc…….Open Circuit Voltage

Abstract

The field of organic photovoltaics (OPV) has been attracting great scientific attention over the last few years. New fields of applications are feasible as OPVs are lightweight, flexible and have the potential for truly low fabrication cost. At present, so-called bulk heterojunction structures based on blends of a conjugated polymer as electron donor and a soluble fullerene derivative as acceptor represent the OPV material system with the highest power conversion efficiency reported until now.

This thesis addresses several critical parameters in the processing issues of polymer:fullerene based organic solar cells. Primarily, a sedulous investigation concerning deposition parameters of an electron blocking-hole transporting interfacial layer (Poly(3,4-ethylenedioxythiophene):poly(styrenesulfonate) [PEDOT:PSS]) was performed. The conductivity and thickness effect of the layer on overall device performance was analyzed. Then the optically active layer consisting of the reference poly-3-hexylthiophene and phenyl-C61-butyric acid methyl ester (P3HT:PCBM) blend material system was investigated. Parameters such as composition ratio, layer thickness and annealing conditions were examined in order to achieve the reference organic solar cells for the newly founded Molecular Electronics and Photonics research unit with optimized and highly reproducible power conversion efficiency (PCE).

The processing steps described in this thesis yielded P3HT:PCBM devices with repeatable and consistent PCE performance higher than 3 % and now the process is used as a standard method to provide the reference solar cells in the Molecular Electronics and Photonics laboratory. During the processing steps of P3HT:PCBM, a

kink in the shape of the current density/voltage (J/V) characteristics was observed. Devices of different ratios of P3HT to PCBM were fabricated and sent for further studies at the Jaume University in Spain. The s-shaped characteristics were explained by capacitance measurements related to the presence of defect bands exhibiting Gaussian shape located at E approximate to 0.38 eV above the highest occupied molecular orbital level of the P3HT.

After establishing the reference process for P3HT:PCBM based solar cells new synthesized conjugated polymers donors were investigated in terms of their potential for organic solar cell applications. A perfluoro poly[(9,9-dioctylfluorenyl-2,7-diyl)-alt-5,5- (4',7'-di-2-thienyl-2',1',3'-benzothiadiazole)] (APFO-3) derivative and different fluorescent *boron-dipyrromethene* conjugated polymers (BODIPY) were characterized. Absorption and photo luminescent spectra as well as current density characteristics of the fabricated photovoltaic devices were compared to commercially available materials. Despite the exhibited low mobility and PCE values (in the range of 0.2-1.2 %), some of the newly synthesized polymers, like PBT and PBTT, are promising electron donors for further synthetic trials due to their high absorption coefficient and high photovoltage (over 1 V).

Furthermore a systematic study of inkjet printing processing parameters for organic solar cells applications was followed. Optimum parameters for inkjet printing active layer were firstly identified, proving that the viscosity of the inkjet formulation, substrate temperature, drop spacing and the height of the droplet in relation to the surface are critical factors to achieving high quality inkjet-printed polymer-fullerene

based active layers. The last part of the chapter focuses on replacing the expensive and brittle indium tin oxide (ITO) with an inkjet printed silver grid architecture. Investigation of an inkjet-printed silver nanoparticle grid combined with different conductivity PEDOT:PSS was performed. An ultimate control of the design requirements of current collecting grid based on the proposed inkjet-printed process to accurately control the uniformity and dimensions of the silver nanoparticle based grid was achieved. The performed measurements revealed higher transparency of the printed Ag grid when compared to different thicknesses of ITO. As a result a record power conversion efficiency of 1.96 % is achieved for ITO-free P3HT:PCBM based organic solar cells using the combination of PEDOT:PSS/inkjet printed nanoparticles based current collecting grids.

ΠΕΡΙΛΗΨΗ

Το πεδίο των οργανικών φωτοβολταϊκών (ΟΦ), έχει προσελκύσει μεγάλο επιστημονικό ενδιαφέρον τα τελευταία χρόνια. Νέα πεδία εφαρμογών είναι εφικτά με τα ΟΦ αφου αυτά είναι ελαφριά, εύκαμπτα και έχουν τη δυνατότητα για πραγματικά χαμηλό κόστος κατασκευής. Επί του παρόντος, τα λεγόμενα ΟΦ διεσπαρμένων ετεροεπαφών, τα οποία αποτελούνται από μίγμα ενός συζυγιακού πολυμερούς ως δότη ηλεκτρονίων και ενός διαλυτού παράγωγου του φουλλερενίων ως δέκτη, αντιπροσωπεύουν το σύστημα ΟΦ με την υψηλότερη απόδοση μετατροπής ισχύος που αναφέρθηκαν μέχρι τώρα στη βιβλιογραφία.

Η παρούσα εργασία ασχολείται με τη μελέτη διαφόρων κρίσιμων παραμέτρων επεξεργασίας του μίγματος πολυμερούς: φουλλερενίων για οργανικές ηλιακές κυψέλες. Διεξάγετε μια σε βάθος έρευνα σχετικά για τις παραμέτρους εναπόθεσης του υποστρώματος που διευκολύνει τη διέλευση και συλλογή των οπών, του Poly(3,4-ethylenedioxythiophene):poly(styrenesulfonate) PEDOT: PSS. Αναλύθηκε η επίδραση της αγωγιμότητας και του πάχους των υμενίων αυτών στη συνολική απόδοση της συσκευής. Κατόπιν, διερευνήθηκε το οπτικώς ενεργό υπόστρωμα που αποτελείται από μιγμα poly-3-hexylthiophene και phenyl-C61-butyric acid methyl ester (P3HT: PCBM). Παράμετροι όπως η σύσταση των δύο υλικών στο μίγμα, το πάχος των υποστρωμάτων και οι συνθήκες ανόπτησης εξετάστηκαν προκειμένου να επιτευχθούν ΟΦ συσκεύες αναφορας για την νεοϊδρυθείσα ερευνητική μονάδα των Μοριακών Ηλεκτρονικών και Φωτονικής. Τα βήματα βελτιστοποίησης επεξεργασίας που περιγράφονται στην παρούσα εργασία για συσκευές αποτελούμενες από P3HT:

PCBM απέδωσαν σταθερή και επαναλήψιμη ενεργειακή απόδοση υψηλότερη από 3%. Τώρα η διαδικασία χρησιμοποιείται ως πρότυπη μέθοδος για την δημιουργία ΟΦ αναφοράς στο εργαστήριο Μοριακής Ηλεκτρονικής και Φωτονικής. Κατά τη διάρκεια των σταδίων επεξεργασίας των συσκευών P3HT: PCBM, παρατηρήθηκε μια παράξενη συμπεριφορά στο σχήμα των γραφικών παραστάσεων πυκνότητας ρεύματος/τάσης (J / V). Συσκευές με διαφορετικές αναλογίες P3HT προς PCBM κατασκευάστηκαν και αποστάλησαν για περαιτέρω μελέτη στο Πανεπιστήμιο Jaume στην Ισπανία. Τα χαρακτηριστικά αυτά, εξηγήθηκαν με μετρήσεις χωρητικότητας, συνδέονται με την παρουσία ενεργειακών ζωνών που παρουσιάζουν ελάττωμα σχήματος Gaussian και βρίσκεται κατά προσέγγιση 0,38 eV πάνω από το υψηλότερο κατειλημμένο μοριακό τροχιακό (HOMO) του P3HT.

Μετά τη θέσπιση της διαδικασίας αναφοράς για ΟΦ με φωτοενεργό υπόστρωμα P3HT: PCBM, διερευνήθηκαν συσκευές με νέα συντεθειμένα συζυγιακά πολυμερή ως δωτές ηλεκτρονίων. Ένα παράγωγο του poly[(9,9-dioctylfluorenyl-2,7-diyl)-alt-5,5- (4’,7’-di-2-thienyl-2’,1’,3’-benzothiadiazole)] (APFO-3) και διαφορετικά πολυμερικά παράγωγα του boron dipyrromethene (BODIPY) χαρακτηρίστηκαν. Φάσματα απορρόφησης και φωτοφωταύγειας καθώς και J/V χαρακτηριστικά των κατασκευασμένων φωτοβολταϊκών διατάξεων συγκρίθηκαν με εμπορικά διαθέσιμα υλικά. Παρά τη χαμηλή κινητικότητα οπών που εμφάνισαν αλλά και τις χαμηλές τιμές ενεργειακής απόδοσης (στην περιοχή από 0,2 έως 1,2%), μερικά από τα νεοσυντιθέμενων πολυμερή, όπως PBT και PBTT, εμφανίζονται ως πολλά υποσχόμενοι δότες ηλεκτρονίων για περαιτέρω συνθετικές δοκιμές λόγω του υψηλού

συντελεστή απορρόφησης και της υψηλής τάσης ανοικτού κυκλώματος (Voc) που παρουσίασαν (πάνω 1 V).

Ακολούθως έλαβεν χώρα συστηματική μελέτη των παραμέτρων επεξεργασίας πιεζοηλεκτρικού εκτυπωτή για οργανικές ηλιακές κυψέλες. Σε πρώτο στάδιο αναγνωρίστηκαν οι παράμετροι που επηρεάζουν την ποιότητα των εναποτηθέμενων υμενίων και ακολούθως βελτιστοποιήθηκαν. Για την εκτύπωση του οπτικώς ενεργού υποστρώματος απεδείχθει ότι το ιξώδες του προς εκτύπωση διαλύματος, η θερμοκρασία υποστρώματος, η απόσταση μεταξύ των εκτυπωμένων σταγόνων καθώς και η απόσταση της εκτυπωτικής κεφαλής από το υπόστρωμα είναι κρίσιμοι παράγοντες για την επίτευξη υψηλής ποιότητας υμενίων για ΟΦ με μεγάλη ενεργειακή απόδοση βασιζόμενα σε μίγμα P3HT:PCBM. Το τελευταίο μέρος του κεφαλαίου επικεντρώνεται στην αντικατάσταση του ακριβού και εύθραυστου οξείδιου του κασσίτερου, ινδίου (ITO), με εκτυπωμένα πλέγματα από ασήμι. Πραγματοποιήθηκε διερεύνηση των συνθικών εκτυπωσης πλεγματων με νανοσωματίδια αργύρου σε συνδυασμό με PEDOT: PSS διαφορετικής αγωγιμότητας. Αποκτώντας απόλυτο έλεχο της διαδικασίας και κατανόντας πλήρως τις απαιτήσεις εκτύπωσης, επιτέυχθηκαν υψηλής ποίοτητας και ομοιομορφίας πλέγματα απο νανοσωματίδια αργύρου. Οι διεξαχθείσες μετρήσεις αποκάλυψαν μεγαλύτερη διαπερατότητα του εκτυπωμένου πλέγματος Ag σε σύγκριση με διαφορετικά πάχη ITO. Ως αποτέλεσμα επιτευχθηκε ρεκόρ απόδοσης ενεργειακής μετατροπής της τάξης του 1,96% για ΟΦ συσκευές χωρίς ITO με οπτικώς ενεργό υλικό μίγμα P3HT: PCBM και τον συνδυασμό του PEDOT: PSS / εκτυπωμένων νανοσωματίδιων αργύρου για συλλογή των φορτίων.

Chapter 1 - Introduction

In the last decade increasing concern about global warming led to an intense search for alternative, green and renewable energy resources such as water and wind power as well as solar radiation. When the latter reaches the surface of the earth, it can provide enough energy to supply the increasing global energy demand and it is considered as a viable candidate to replace the major energy resource at present: oil[1].

The discovery of the photovoltaic effect by Einstein in 1905 led to the performance development of photovoltaic devices based on inorganic materials. Despite the high efficiency of these devices today, the market growth is still far away from its expected maximum contribution. Some of the main reasons for that are the high environmental expense from toxic etching and high temperatures as well as vacuum operations needed during inorganic solar cell fabrication, resulting in non-commercially attractive production cost. In order to reduce this cost, thin film solar cells are preferred, mostly made by using gallium arsenide (GaAs), cadmium telluride (CdTe), and copper indium di-selinide ($CuInSe_2$). Although by using less material one would expect that cost is dramatically reduced in comparison with mono and poly-crystalline silicon cells, the need for high material purity keeps the cost at a similar level[2]. When efficient charge transfer processes between excited organic semiconductors and fullerene was discovered in the early 90's, photovoltaic devices applying this principle began to receive growing interest. Several device concepts have been developed, including dye-sensitized, small molecule and polymer-based solar cells.

Organic photovoltaics (OPVs) have great potential as clean energy resource due to the low cost of device fabrication using solution-based processing technology, low weight as the deposited material is on the nanometer scale, and their mechanical flexibility, which is compatible with foldable or rollable substrates[3, 4].

The decisive step towards more efficient OPVs was the realization of the heterojunction concept[5], where two different materials, an electron-donor and an electron-acceptor were stacked in a bi-layer structure, in order to dissociate the excitons[6]. On absorption of a photon, an electron in the highest occupied molecular orbital (HOMO) is excited to the lowest unoccupied molecular orbital (LUMO) in the donor phase. This bound photogenerated exciton migrates to an electron donor-acceptor interface where it dissociates into an electron-hole pair. At the interface weakly bound charge carriers can be separated because of the LUMO band offset of the two materials and transported to the respective contacts through percolating pathways in the different phases. In order for efficient dissociation to take place the exciton must be generated in close proximity to the donor-acceptor interface, since its diffusion length is typically around 10 nm[7, 8]. This need limits the part of the active layer that contributes to the photocurrent generation to a very thin region near the donor-acceptor interface. Excitons generated further than that distance are lost through recombination and thermalization processes.

The so-called bulk heterojunction (BHJ) concept assisted in overcoming this limitation[9]. These structures based on intimate mixtures of a conjugated polymer as electron-donor and the soluble fullerene derivative as electron-acceptor, represent the single cell device structure with the highest power conversion efficiency (PCE)

reported in the literature. This has been achieved by overcoming the exciton diffusion length bottleneck by creating interpenetrating networks of donor and acceptor materials.

In recent years, intense optimization of device structure, interfacial layer engineering, processing conditions and synthesis of new high performance polymer semiconductors led to certified PCE exceeding 9% for solar cells processed with conventional spin-coated or blading methods[10].

The technological attraction in organic solar cells is their compatibility with printing processes. However, up until today, limited work has been published on the processing conditions of printed organic solar cells since the major body of research is being done using spin coating or blading techniques. Among the various organic photovoltaic fabrication printing techniques, inkjet printing is emerging as a key process to generate patterned structures due to drop-on-demand (DoD) technology. Transferring the spin-coating or doctor blading process currently used for the fabrication of bulk heterojunction solar cells to an inkjet printing process holds dares which are challenging to overcome.

This thesis is primarily focused on establishing a reference cell using commonly used materials and lab deposition techniques leading to repeatable device performance. Secondly, newly synthesized electron donating conjugated polymers were investigated. A perfluoro derivative of APFO-3, which is the alternating polyfluorene copolymer poly[(9,9-dioctylfluorenyl-2,7-diyl)-alt-5,5-(4',7'-di-2-thienyl-2',1',3' benzothiadiazole)][11], was utilised to lower the polymer's optical band gap, thus increasing solar spectrum irradiance absorption. Different moieties were used to

increase push-pull mechanisms which alter the HOMO-LUMO levels. The same route was followed when synthesizing a family of *boron-dipyrromethene* (BODIPY) derivative polymers.

The knowledge gained was transferred to printing these materials using a piezoelectric printer. Commercially available regioregular P3HT and the soluble fullerene derivative $PC_{60}BM$ were used. In an effort to move towards a fully printed device, brittle ITO was replaced with printable current collecting Ag-grids covered with PEDOT:PSS. High transparency and conductivity were obtained while optimum overall device performance was reached. Results included in this thesis have been published in peer reviewed journals and presented at international conferences (please see Appendix for list of publications).

Chapter 2 - Materials, Working Principles and Deposition Techniques

2.1 Working principles of organic solar cells

All donor and acceptor materials have different absorption spectra. Photons from the sun are absorbed depending on the optical band gap of the respective material. Here we consider the conjugated polymer to be the photoactive part of the blend, even though absorption also takes place in the electron acceptor.[12, 13] When considering the bi-layer model of organic solar cells, incoming photons with energy equal to the band gap energy (Eg) are absorbed by the optically active layer. An electron is excited from the highest occupied molecular orbital (HOMO) to the lowest unoccupied molecular orbital (LUMO) of the conjugated polymer, creating a bound electron-hole pair called exciton. If an electron accepting material is within a distance smaller than the exciton diffusion length, the exciton diffuces to the interface where the electron moves from the donor's LUMO to the acceptor's LUMO. At this step, due to the low dielectric constants of the organic materials, no free carriers occur. Charged species are now loosely bound together forming a hybrid state called charge-transfer complex (CTC). This intermediate state complex will either recombine, resulting in loss of the provided energy and affecting both open circuit voltage and photocurrent generation, or dissociate fully to deliver free carriers. Charge transfer exciton dissociation only happens if a required driving force is present which is defined as the difference in ionization potential (I_p) of the excited donor and the electron affinity (χ) of the acceptor, minus the coulombic correlations. If the acceptor's electron affinity is large enough to overcome the exciton's binding energy, which is in the order of 200-

500 meV,[14, 15, 16] the exciton is dissociated into free carriers. The electrons move along the acceptor molecules towards the cathode and the positively charged carriers remain on the polymeric chains reaching the anode. In case the exciton does not manage to diffuse at the donor-acceptor interface during its short lifetime, it will undergo one of the competing mechanisms of recombination via photon emission or decaying via thermalization.

The diffusion length of the exciton is around 10 nm and low mobilities in the order of 2×10^{-4} $cm^2\ V^{-1}\ s^{-1}$ are generally present in organic materials.[17, 18] In combination with high exciton binding energy, excitons dissociate only at the donor-acceptor interface. The latter limits the amount of photogenerated charge carriers formed in a bi-layer structure as well as the effective thickness of the optically active layer. A way to tackle this limitation is by increasing the dissociation interface by blending the electron donor with the acceptor. Interpenetrating networks are then formed providing efficient pathways in pure phases for the split charge carriers to travel along the bulk and reach the respective electrodes. This notion is called bulk heterojunction (BHJ). With this structure more embedded photons are absorbed as thick layers may be formed with reduced recombination probability, providing significant increase in photogenerated charged species.

2.2 Operating modes

The Metal/Insulator/Metal (MIM) concept is usually used for the description of operating modes of organic diodes[19]. Despite the fact that this is a hasty approach; it can provide a first impression of the energetic levels within the solar cell. This concept only applies when the organic semiconductors are pure and when no notable space charges are built up during operation. Charge built up would result from unbalanced electron and hole transport.

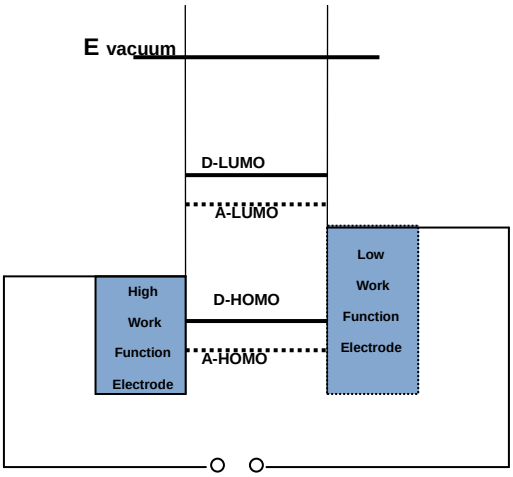

Figure 1: Flat band diagram in open circuit conditions

In Figure 1, the energetic diagram of a BHJ solar cell in open circuit condition is represented. The vacuum levels of the different materials are aligned and no electric field is flowing inside the device due to the absence of a driving force.

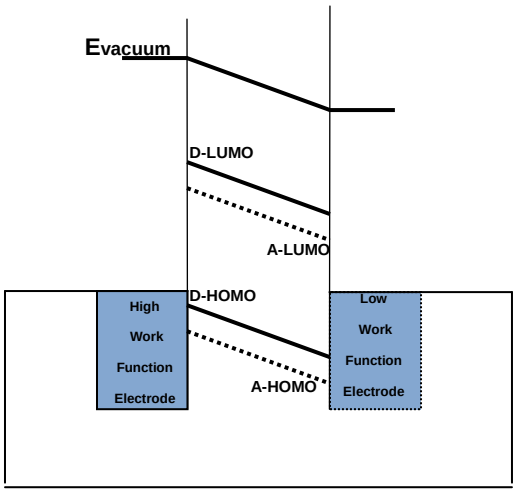

Figure 2: Flat band diagram in short circuit conditions

A Fermi level alignment (Figure 2) of the two electrodes occurs and the built-in field appears in the bulk, resulting in a constant slope for the HOMO and LUMO levels of the donor and acceptor as well as for the vacuum levels. When illuminated, photo generated charges can be drifted to the respective electrodes - holes to the High Work Function Electrode and electrons to the Low Work Function Electrode. Sample is under short circuit condition.

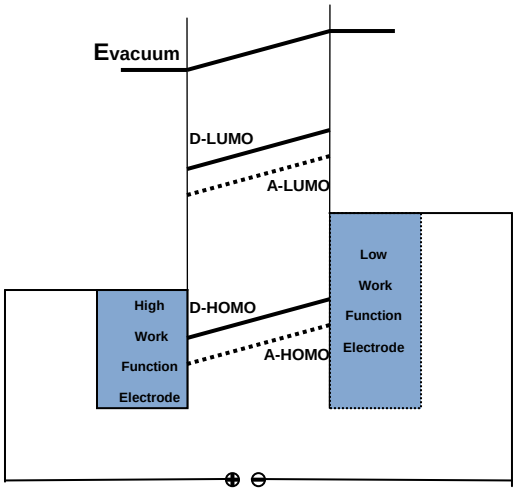

Figure 3: Flat band diagram in forward bias

When a diode is operated in the forward bias, as shown in Figure 3, electrons can be injected from the Low Work Function Electrode to the LUMO of the acceptor and holes from the High Work Function Electrode to the HOMO of the donor. The effective field created by the device will ensure the drift of electrons from Low to High Work Function Electrode and holes the other way around. If these charges are able to recombine and emit radiation, the device works as an Organic Light Emission Diode (OLED).

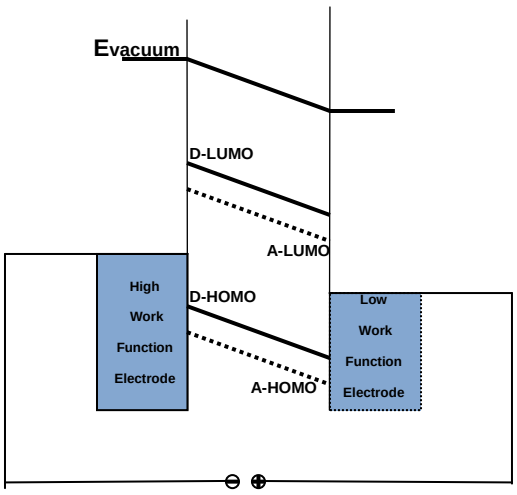

Figure 4: Flat band diagram in reverse bias

When a device is operated in reverse bias (Figure 4) charge injection is encumbered by the field present in the device. Under illumination, the generated charge carriers drift under a potentially strong electric field to the respective electrodes making the diode work as a photo detector.

2.3 Current Density Vs Voltage Characteristics (J/V)

The current-voltage characteristics of a solar cell with and without external illumination are shown on the graph below. In the dark, there is almost no current flowing. In the device in forward bias the contacts start to heavily inject for voltages higher than the open circuit voltage (Voc). Under illumination, current flows in the opposite direction to the injected currents. At Voc the maximum photogenerated current flows under short circuit conditions (Jsc). Jsc the generated photocurrent is balanced to zero (flat band condition). Between Voc and Jsc, in the fourth quadrant, the device generates power. At a precise point, the Maximum Power Point (Mpp), the product between current and voltage reaches its maximum value[20].

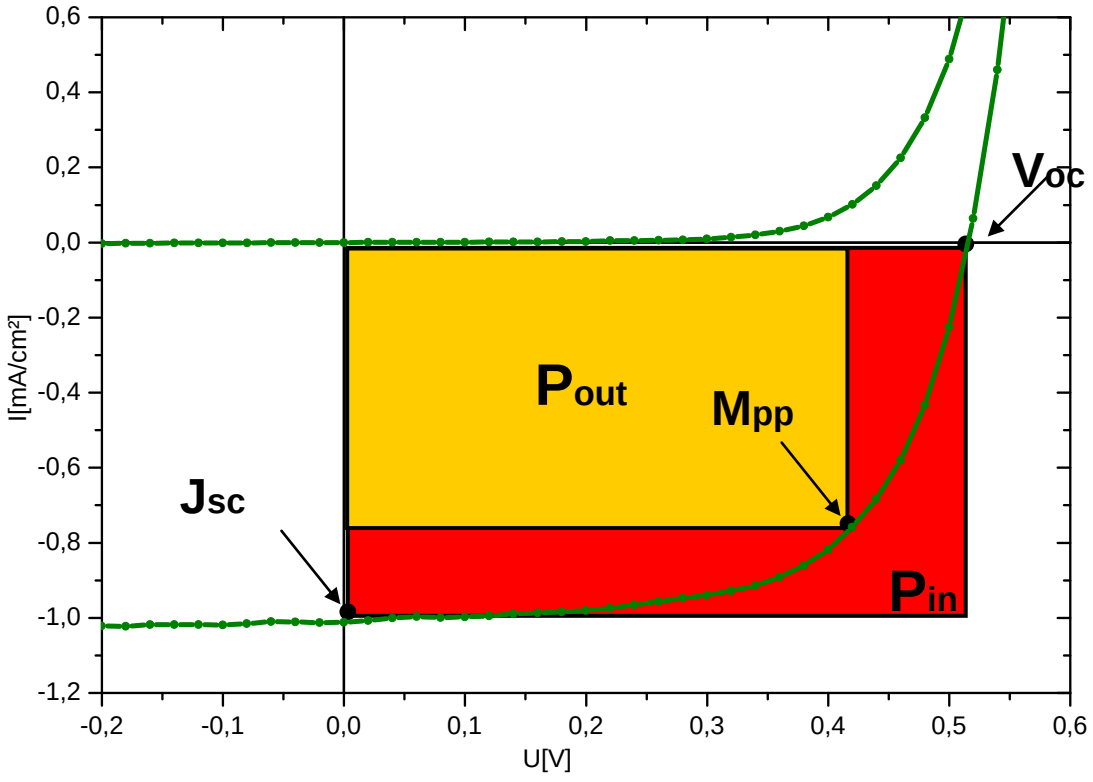

Figure 5: Typical dark and illuminated J/V characteristics of a solar cell

2.3.1 Open circuit Voltage (Voc)

The origin of Voc, which is the voltage of the solar cell when no current flows through the device, is a matter of controversial discussions. A model took into account the morphology of the bulk heteronjuction[21], but more recent studies have shown that the maximum value that Voc can theoretically reach is the energy difference between the HOMO of the donor and LUMO of the acceptor, and is defined as Built-in Voltage (Vbi)[22, 23] .

For BHJ device structure though limitations may arise and Voc may not exceed the work function difference between the anode and the metal cathode, as suggested by the Metal/Insulator/Metal (MIM) diode model[24, 25]. One concludes that Voc is always smaller than its theoretical value (Vbi), presumably due to losses at the photoactive layer-electrode interfaces[26]. It has already been demonstrated that Voc is strongly related to the BHJ material combination[27], light intensity, temperature[28] and electrode selection[24]. A format that relates Voc to externally measurable electro-optical spectra though was only recently suggested by Vandewal et al. With this theory the origin of the Voc of polymer:fullerene solar cells can be explained in terms of ground-state charge-transfer complex (CTC) formation between the polymer and the fullerene[29, 30]. The spectral position of the CT exciton correlates with the difference between the HOMO of the polymer and the LUMO of the fullerene, resulting into a strong tie between obtained Voc and this energetic difference[31, 32].

2.3.2 Short circuit Current (Jsc)

J_{SC} is the maximum current flowing in the device under illumination when no external voltage is applied[33]. The photocurrent is a result of (a) photoinduced exciton dissociation at the electron donor/acceptor interface, (b) free charge carrier transport in the active layer and (c) charge carrier collection by the respective electrodes. During transport, material defects or interface quality may cause these carriers to thermally recombine, reducing in this way the photogenerated current. A high internal electric field allows charges to flow towards the respective electrodes quickly minimizing recombination possibility. Assuming devices with the same cathode metal and active layer (system, thickness and solvent) the higher the work function difference between anode and cathode, the higher the internal electric field, thus photogenerated carriers extracted out of the device. A decrease in recombination benefits OPVs by increasing the photocurrent and fill factor. Two are the main routes for enhancing the internal electric field in organic solar cells. The first method is by tuning the optical band gap energy (Eg) of the electron donor photoactive material[34]. This simultaneously modifies the absorption spectrum and carrier transport in OPVs. The second method is by modifying the work function of the electrodes by choosing the appropriate metal[35, 36, 37]. A first estimation for the strength of the internal electric field depends on the surface potential difference, which represents the work function difference between anode and cathode metals, as well as the distance between these two electrodes[38]. At low photocurrent densities, due to low incident light intensity, the External Quantum Efficiency is not significantly influenced by the conductivity of the

anode, whereas for high light intensities a highly conducting electrode is needed to extract maximum power output from the device[39].

Charge transport in conjugated polymer films is mainly dominated by hopping of charge carriers between localized states as a consequence of the intrinsically amorphous nature of the polymers. Particularly, hopping transport of holes in pure polymeric films is field and temperature dependent owing to positional and energetic disorder limited charge carrier mobility[40].

2.3.3 Maximum power point (Mpp)

Between Voc and Jsc in the fourth J/V quadrant, a solar cell generates power and the power output is the product between Current and Voltage. At a specific V_{max} x J_{max} point, denoted as Maximum Power Point (Mpp), the power output reaches its maximum.

2.3.4 Fill Factor (FF)

Using the parameters mentioned above, Fill Factor may be calculated.

The Fill Factor of a solar cell is the measure of the power that can be extracted from the diode. FF is the ratio between Power output (Pout) and Power input (Pin), shown in the figure 1 with red and yellow color. The size of these two areas should ideally be similar; thus fill factor should be as close as possible to 1.

The higher the FF values obtained, the more the J/V characteristics resembles a constant current source with a maximum voltage and at the same time the higher the electric power that can be extracted from the device. Both serial (Rs) and parallel resistance (Rp) of a circuit equivalent can influence the FF. Under illumination high

Rs values lower the short circuit current, as charge carriers are recombined in the diode. In dark when Rp values are low, an extra Ohmic contribution is added on the diode curve which limits significantly the FF. Typical values for FF are 0.75 to 0.85 for inorganic solar cells and 0.55 to 0.7 for good organic solar cells.

Generally the fill factor can be calculated as:

$$FF = \frac{Vmpp * Jmpp}{Voc * Jsc} \qquad (1)$$

With this, the power conversion efficiency can be written as:

$$\eta = \frac{Pout}{Pin} \quad => \quad \eta = \frac{J_{mpp} * V_{mpp}}{Pin} \qquad (2)$$

Pin = (Light intensity) * (active area) (3)

$$(1),(2),(3) \Rightarrow \eta = \frac{J_{SC} \cdot V_{OC} \cdot FF}{LightIntensity * ActiveArea}$$

2.3.5 External Quantum Efficiency (EQE)

EQE represents the percentage of photoexcitons surviving both recombination via photon emission or decaying via thermalization, and those charge carriers finding the pathways through device morphology to reach the electrodes.

For bulk heterojunction structures the EQE has been increased from 29% [41] to 50% [42] and recently an EQE of 80% was reported[43]. Photons reach the photoactive layer of BHJ device with different energy, thus at different wavelengths. Despite the fact that at particular wavelengths high EQE values have been obtained, power conversion efficiencies are still low. One of the main reasons for that is the absorption spectral

mismatch of the organic absorbers to the solar spectrum. The enormous number of photons reaching the surface of the earth, peak at wavelengths around 700nm. Most studied organic absorbers absorb at lower wavelengths, P3HT and MDMO-PPV have their absorption maxima at around 520 and 440nm, losing that way a large amount of photons.

2.3.6 The Equivalent Circuit Diagram (ECD)

ECDs are frequently used to describe the electric behavior of more complex semiconductor devices with a network of ideal electrical components such as diodes, current or voltage sources and resistors[44]. Although some physical processes in organic semiconductors may be different, the same principal loss mechanisms apply for organic solar cells, and we may therefore apply the same circuit.

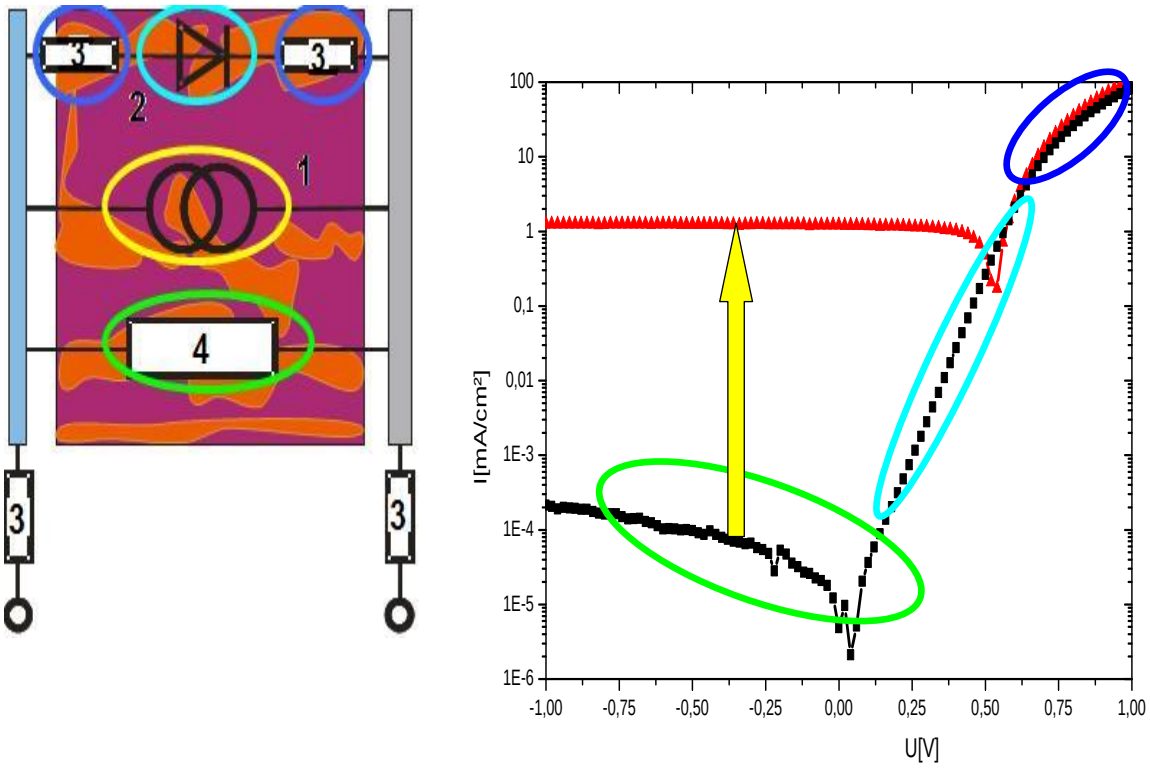

Figure 6 Simplified approach of the ECD of an OPV (left) and where its components are reflected on typical J/V characteristics in semi logarithmic form (right)

The ECD is consists of the following basic components:

1. A current source symbolizes the photogenerated current inside the illuminated cell. This current, flows in opposite direction in the diode and depends on the voltage across the device[45].

2. A diode responsible for the non linear shape of the J/V characteristics of a solar cell. (Not necessarily a Schottky type). The diode is dependent on the internal field of the solar cell resulting from the work function difference of the electrode materials. For similar systems variation in the angle of the slope suggests differences in internal morphology.

3. A series resistance that includes the Ohmic contributions of the electrodes, the contact between organic semiconductor and metal, and the resistivity of the optically active materials. This resistance typically decreases with decreasing thickness, increasing temperature and decreasing light intensity[46]. At high voltages all transport issues are collected in one serial resistance that reduces performance at high light intensities[47]. Minimizing series resistance mainly leads to FF and Jsc improvement thus, enhanced overall performaance.

4. A parallel or shunt resistance (Rp) illustrates the potential leakage current through the device. It increases with decreasing thickness and decreases considerably with increasing light intensity. At low voltages all shunting issues are collected in a total parallel resistance. The shunt may vary strongly

in orders of magnitude from device to device and it mostly represents process quality like impurities, active layer defects and selectivity of electrodes[48]. In order to achieve high efficiencies, Rp has to be maximized as it affects Voc and FF.

2.4 Materials

2.4.1 P3HT

Poly(3-hexylthiophene) (P3HT)[49], chemical structure is shown in Figure 7, is one of the most commonly studied electron donating material in organic solar cells. It has demonstrated promising physical properties such as environmental stability, reasonably high hole mobility and an improved absorption as compared with PPV and other commercially available polymers. It has been shown that an enhanced degree of crystallinity can be induced in P3HT films by thermal and vapor annealing by improving the hole mobility. High hole mobility is related mainly to side-chain induced self-organization. HOMO energy level lies at 4.9 eV and LUMO at 3.0 eV. The material was purchased from Rieke Metals,Inc (http://www.riekemetals.com/).

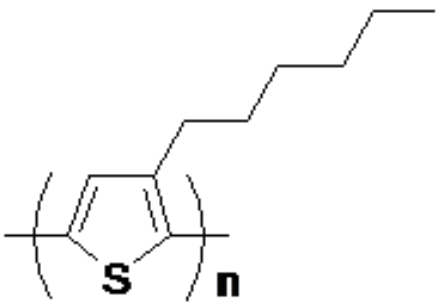

Figure 7 Chemical structure of P3HT

2.4.2 PCBM

C_{60} itself is not very soluble. Side groups were attached to increase its solubility for the use in solution-cast processes. The most widely used C60 derivative[9] in solar cell devices is 1-(3-methoxycarbonyl) propyl-1-phenyl-[6,6] methanofullerene (PCBM). It is highly soluble in common organic solvents and despite the fact that it has one double bond less than C_{60}, which means that electron acceptance is reduced, it still acts as an excellent electron acceptor. It has been stated that hole transport in a polymer is usually enhanced when the polymer is in a blend with PCBM (Figure 8)[50, 51, 52, 53, 54]. The reason for hole mobility enhancement in the blend phase is not really resolved yet, but based on transport studies in polymer/PCBM phase, authors have urged that PCBM actually participates in hole transportation. Ambipolar transport in PCBM films was demonstrated in field effect transistors measurements[55] and PCBM was found to transport holes and electrons with similar mobilities. Ambipolarity of PCBM in charge carrier transport terms was confirmed by Inganas et al.[56] while investigating electroluminescence in a ITO/PEDOT:PSS/PCBM/LiF/Al device configuration. The material was purchased from Nano-C and had a Homo energy level around 6.1eV and a LUMO around 4 eV.

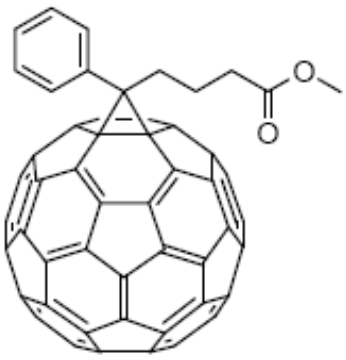

Figure 8 Chemical structure PCBM

2.4.3 ITO

Indium tin oxide (ITO) films have been widely employed in the organic electronics industry, as it is an important material for solar cells fabrication. ITO consists of a mixture of In_2O_3 (90%) and SnO_2 (10%) and has a bandgap of 3.7eV that allows no absorption of wavelengths longer than 350nm, and a Fermi level around 4.7eV. The strong excess of In atoms is n-doping the layer and thus increases the conductivity, leading to low sheet resistances. Films of ITO are sputtered on glass substrates and are commercially available. The transmission properties of ITO substrates do not change much for thicker films since the material does not absorb in the visible range. Increased surface roughness may cause shunts for very thick ITO layers in thin organic films.

2.4.4 PEDOT:PSS

PEDOT is an electrochemically stable conjugated polymer that provides electrical conductivity with optical transparency. Polystyrene sulfonic acid (PSS) works as a charge balancing dopant providing PEDOT water solubility and high electrical conductivity. In mixture, PSS-acid donates a proton from its HSO_3 group to a sulphur atom of PEDOT. This leads to a positive doping of PEDOT, while PSS guarantees charge neutrality. The role of PEDOT:PSS (Figure 9) on organic solar cells have been studied by UV photoemission spectroscopy. It has been demonstrated that PEDOT:PSS typically has a higher work function than ITO[57, 58, 59], matching more closely the HOMO level of the semiconducting polymers, hence reducing the barrier for hole transport. The hole injection barrier is mainly depended on work function of the PEDOT:PSS instead of that of ITO[60]. One additional benefit is the reduction of

the topological variation of sputtered ITO, as PEDOT:PSS is a film of optimized thickness that covers any possible pin holes generally present in ITO films and significantly smoothens its surface. Thick layers can cause large increase in series resistance, also influenced by the annealing treatment after deposition. Heat treatment after deposition increases the conductivity of the PEDOT:PSS layer up to two orders of magnitude by changing the film morphology. There are several different kinds of PEDOT:PSS commercially available and their conductivity, work function and chemical properties can be further modified to suit any particular application[61, 62, 63, 64, 65, 66].

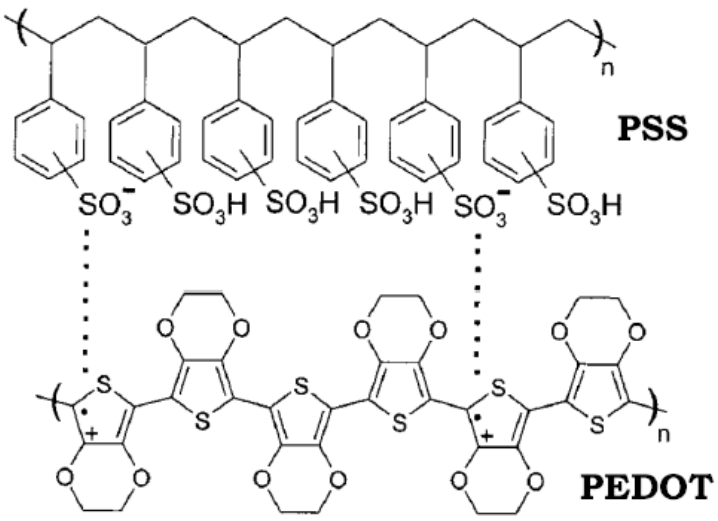

Figure 9 Chemical structure of the Hole transporting polymer PEDOT:PSS

2.4.5 Cathode

The cathode is typically realized by thermal evaporation of a low workfunction metal. The most common materials are Al and Ag. Differences in bond nature (stronger bonds in metal and weak van-der-Waals bonds in the organic semiconductor) and charge transport (mechanism dominated by thermally assisted hopping in organic semiconductor, band-like transport for metals) lead to direct transfer of charges between metallic and organic materials not possible. Many studies have been done to improve the carrier extraction efficiency and understand the physic of charge transfer. It has been shown that the efficiency of conjugated polymer/fullerene BHJ solar cells can be significantly enhanced when using thin interfacial layers like LiF and Ca between the optically active layer and Al, Ag top metal electrode respectively. According to Brabec et. al. a dipole moment is formed across the junction, due to either orientation of LiF or chemical reactions leading to charge transfer across the interface, is suggested as the reason for enhanced device performance [67].

2.5 Processing Technologies

The challenge we are facing today is up scaling from laboratory small area cells to large area, low cost high quality and efficient organic photovoltaics. The improvement of existing and new developing large area coating techniques for organic photovoltaics is essential for large-area Roll-to-Roll (R2R) processing. Efficient organic photovoltaics made by using Doctor Blading (DB) with similar device performance to the spin coating ones have been fabricated. The ability to use R2R technique to fabricate large area solar cells was then feasible[68]. Since then many printing techniques have been employed for the active layer deposition in polymer solar cells, such as screen printing, inkjet printing, gravure printing, offset, micro-contact and spray coating. Despite the fact that spin coating is the most commonly used deposition technique in laboratories globally, mainly due to the homogeneity of the film thickness, reduced particles, and reduced number of pinholes, it offers no control on the created pattern (0-dimensional) as the entire substrate is covered in the film forming process and no temperature control exists.

On the other hand, doctor blading is known to give sidelong resolution in the nanometer regime, offering 1-dimensinal control of the pattern and more freedom in depositing a semiconductor layer with an optimized film thickness. Screen printing, inkjet printing and gravure printing offer 2-dimentional pattering of the printed area. Pad printing also offers 2-dimensional control of the printed pattern and while the technique is not the best candidate for printing very large areas, it gives the ability to print well on curved, rough surfaces or surfaces with multiple curvatures (i.e. a golf ball). Screen printing, gravure printing and inkjet printing are especially suitable for

large area devices. One of the main reasons that the polymer solar cell technology is so attractive from a mass production point of view is that it provides the benefit to prepare devices using so many different printing methods[69].

2.5.1 Spin Coat

Spin Coating is a well understood and broadly used organic semiconductor deposition technique. Although it is not suitable for producing large scale OPVs, it is a quite common technique for small lab scale solar cells as it can provide high quality thin films with reduced dust particles and shunts.

Spin coating (Figure 10) is based on a centrifugal force developed by spinning which spreads the ink on the substrate surface. Most of the applied solution is ejected during spinning, making this deposition technique the most wasteful. Since a very small volume is required to complete the operation, waste is not critical. A range of layer thickness can be achieved by mainly adjusting the spinning speed. Lower speed yields thicker films. A limitation arises when aiming for extra thick layers as the centrifugal force for low speeds is significantly low and does not spread the ink homogeneously on the substrate. Other parameters that can be varied are the ink viscosity; spin time and substrate surface tension manipulation[70].

After the wet film is deposited it is subjected to several changes which include solvent evaporation, changes in viscosity, radial solution flow, molecular organization and orientation at the solid–liquid and air–liquid interfaces, phase separation of blends, diffusion of molecules in the films, etc. All these effects influence the overall behavior of organic solar cells. It is therefore logical that many scientific reports have dealt with various aspects of spin coating that are correlated with device operation [65].

Figure 10: Spin coater

2.5.2 Doctor Blading

Doctor Blading is a coating technique offering more deposition parametrers than Spin Coating as the final film thickness depends not only on the ink viscosity, solvent drying rate, solid concentration and surface tension but also on the controllable substrate temperature, blade height and blade speed. These important parameters can be varied providing a better control on the device fabrication and performance. The working principle behind this deposition technique is simple as it uses a coating knife to apply the diluted semiconductor evenly over the substrate[69]. A specific amount of solution is applied in the substrate-blade gap and the knife moves along the substrate with an adjustable velocity in the range of 2.5 to 70 mm/s. The deposited thin film, which due to blade height can be varied from a few nanometers to some micrometers, is then left to dry for some time. Drying time depends on the in use solvent evaporation rate and the substrate temperature that has been used during coating. The layer thickness can also be adjusted by changing the coating velocity. Higher blading speeds yield thicker films and vice versa, but may decrease film quality as the turbulent flow of the ink is critically affecting homogeneity of the obtained layer[63].

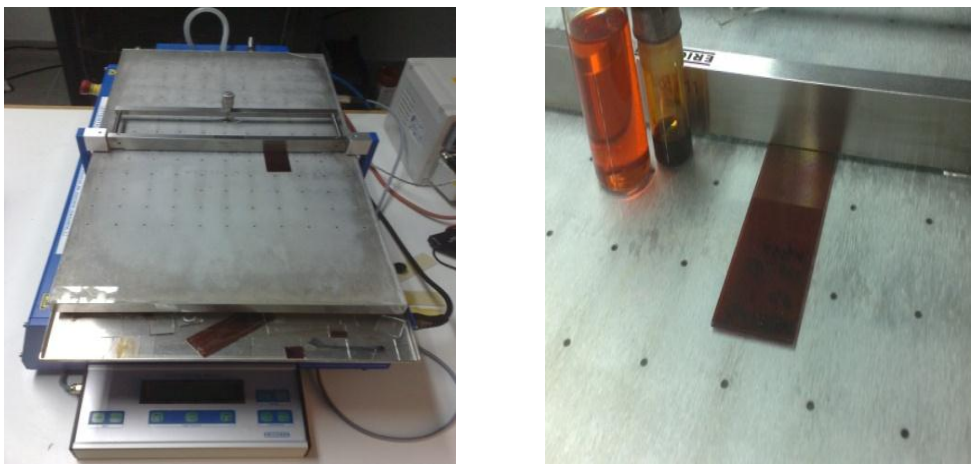

Figure 11: Doctor Blade, a suitable deposition methode for large areas Organic Solar Cells

2.5.3 Inkjet Print

Inkjet printing[71, 72] allows an accurate deposition of ink in defined spots on the substrate. An after-deposition patterning procedure of the printed films is eliminated due to the drop-on-demand (DOD) technology that inkjet printer incorporates. This technology allows the user to print high resolution films due to droplet generation in the nanoscale regime. The solution is kept inside a cartridge and it is printed without any contact between the printing head and the substrate allowing the usage of multiple types of substrates. Also, due to the fact that the printing head is resistant to organic solvents; it is possible to produce printable ink formulations based on almost all available solvents. As the ink is dropped from a distance of a few microns above the substrate, the solution spreading and wetting are crucial in order for the droplets to merge and form the desired pattern. The quality of droplet formation is dependent on both the rheology of the printed solution and the driving conditions of the printhead. The droplet may be formed by mechanical compression of the ink through the nozzles piezoelectrically and ink viscosities up to 10 mPa s^{-1} are suggested by the manufacturer that can be easily printed. Nevertheless more viscous solutions may be printed simply by varying the cartridge temperature from room temperature to 70°C and thus creating a pressure increase inside the cartridge. The temperature elevation keeps the solution viscosity at the lower end so that the droplet formation is feasible without any clogging at the nozzle-air interface. Nozzle clogging may also occur if the in use solvent has a high vapor pressure. Since the nozzles are open to atmospheric air, an easily evaporated solvent will locally increase the viscosity of the solution at a prohibitive printable value. It can even cause solid precipitation at the

nozzle orifice causing either clogging or even affecting the characteristics of the droplets in terms of velocity, volume and angularity (angle deviation). When having optimized waveform parameters the inkjet printhead droplets are coming out of the nozzle without any trace or tail which could affect the printed layer thickness and facture. With round, high quality and consistent drops the layer thickness can be controlled by simple parameter alternations. Some of these parameters are the selection between 1pL and 10pL per drop cartridge, the distance between the drops named Drop Spacing (DS), the firing voltage or even printing multiple drops per spot. The advantages offered by this technique and the good literature examples of its use make it the primer candidate for low-cost mass-production deposition technique for organic solar cells [69, 73].

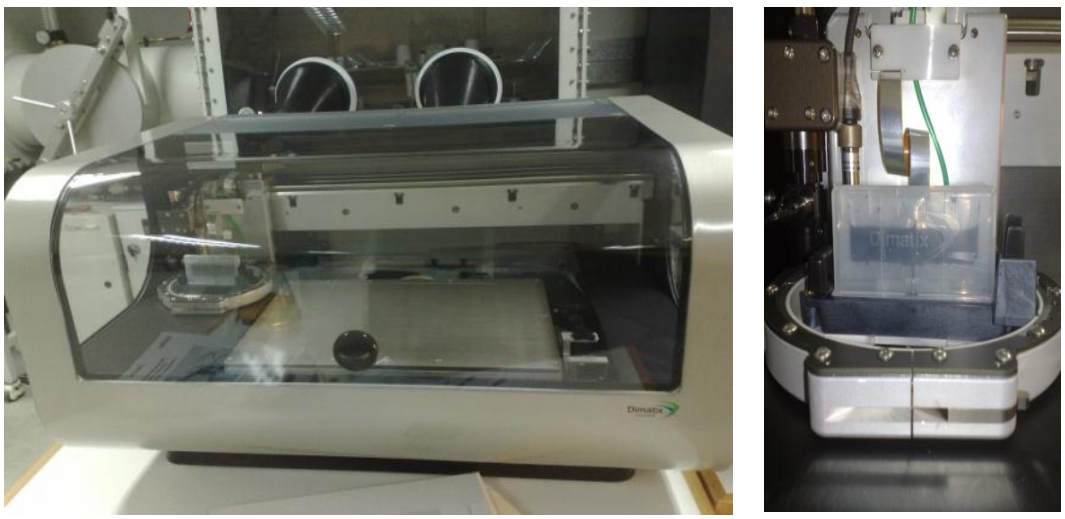

Figure 12: Drop-on-Demand technology of inkjet printer brings mass production R2R a step closer to implementation.

2.5.4 Measurements

In order to characterize the performance of the solar cell devices, current density Vs voltage (J/V) measurements were performed. The J/V curves allow the user to determine the maximum power output of a solar cell and thus the efficiency that the incoming photons transformed into electrons. During these measurements voltages usually from -1 to +1 Volts are applied to the cell under light illumination and in the dark. In both cases, the current output was measured using a Keithley 2420 power source in combination with computer software purchased from National Instruments. All the devices were produced in ambient conditions and thermal evaporation of the metal cathode was performed inside a N_2 atmosphere Glove-Box. Devices were encapsulated and measured in air, unless stated otherwise.

2.6 Bibliography

[1] http://www.nrel.gov/docs/fy10osti/48178.pdf (2010) U.S. Department of Energy

[2] (http://www.iea-pvps.org/) http://www.iea.org/papers/2010/pv_roadmap.pdf

[3] C.J. Brabec, V. Dyakonov, U. Scherf, Organic PhotoVoltaics: Materials, Device Physics, and Manufacturing Technologies; John Wiley & Sons: (2008)

[4] Deibel C, Dyakonov V. , Brabec C J, Organic bulk Heterojunction solar cells IEEE J. Sel. Top. Quantum Electron, 16 (6), 1517-1527, (2010)

[5] G. Yu, J. Gao, J. C. Hummelen, F. Wudl, A. J. Heeger, Polymer photovoltaic cells: enhanced efficiencies via a network of internal donor–acceptor heterojunctions, Science 270, 1789, (1995)

[6] C.W. Tang, Two-layer organic photovoltaic cell Appl. Phys. Lett. 48 183 (1986)

[7] O. V. Mikhnenko, H. Azimi, M. Scharber, M. Morana, P. W. M. Blom, M. A. Loi, Exciton diffusion length in narrow bandgap polymers, Energy Environ. Sci., 5, 6960, (2012)

[8] H. Wang, H.Y. Wang, B. R. Gao, L. Wang, Z. Y. Yang, X. B. Du, Q. D. Chen, J. F. Song, H. B. Sun, Exciton diffusion and charge transfer dynamics in nano phase-separated P3HT/PCBM blend films, Nanoscale, 3, 2280, (2011)

[9] G. Yu, J. Gao, J. C. Hummelen, F. Wudl, A. J. Heeger, Polymer photovoltaic cells: enhanced efficiencies via a network of internal donor–acceptor heterojunctions Science 270 1789, (1995)

[10]http://www.polyera.com/newsflash/polyera-achieves-world-record-organic-solar-cell-performance

[11] C. M. B. Svanstrom, J. Rysz, A. Bernasik, A. Budkowski, F. Zhang, O. Inganas, M. R. Andersson, K. O. Magnusson, J. J. B. Smith, J. Nelson, E. Moons, Device Performance of APFO-3/PCBM Solar Cells with Controlled Morphology, Adv. Mater., 21, 4398–4403, (2009)

[12] R. Koeppe , N. S. Sariciftci, Photoinduced charge and energy transfer involving fullerene derivatives Photochem. Photobiol. Sci., 5, 1122–1131, (2006)

[13] P. Schilinsky, Loss Analysis of the Power Conversion Efficiency of Organic Bulk Heterojunction Solar Cells, University of Oldenburg, (2005)

[14] A. Dkhissi, Excitons in organic semiconductors, Synthetic Metals 161, 1441– 1443, (2011)

[15] S. Gelinas, O. P. Labrosse, C. N. Brosseau, S. A. Seifried,C. R. McNeill, K. R. Kirov, I. A. Howard, R. Leonelli, R. H. Friend, C. Silva, The Binding Energy of Charge-Transfer Excitons Localized at Polymeric Semiconductor Heterojunctions, J. Phys. Chem. C, 115, 7114–7119, (2011)

[16] J. D. Servaites, M. A. Ratner, T. J. Marks, Organic solar cells: A new look at traditional models, Energy Environ. Sci.,, 4, 4410–4422, (2011)

[17] V. D. Mihailetchi, H. Xie, B. de Boer, L. J. A. Koster, P. W. M. Blom, Charge Transport and Photocurrent Generation in Poly(3-hexylthiophene): Methanofullerene Bulk-Heterojunction Solar Cells, Adv. Funct. Mater., 16, 699–708, (2006)

[18] E. von Hauff, V. Dyakonov, J. Parisi, Study of field effect mobility in PCBM films and P3HT:PCBM blends, Solar Energy Materials & Solar Cells 87, 149–156, (2005)

[19] C. J. Brabec, S. Gowrisanker, J. J. M. Halls, D. Laird, S. Jia, S. P. Williams, Polymer–Fullerene Bulk-Heterojunction Solar Cells, Adv. Mater., 22, 3839–3856, (2010)

[20] H. Hoppe, Nanomorphology – Efficiency Relationship in Organic Bulk Heterojunction Plastic Solar Cells, Linz University, (2004)

[21] L. He, S. Yijian, Y. Yang, Solvation-Induced Morphology Effects on the Performance of Polymer-Based Photovoltaic Devices , Adv. Funct. Mater., 11,420-424, (2001)

[22] L. J. A. Koster, V. D. Mihailetchi, P. W. M. Blom, Thickness dependence of the efficiency of polymer:fullerene bulk heterojunction solar cells Appl. Phys. Lett. 88, 243502 (2006)

[23] M. C. Scharber, D. Mühlbacher, M. Koppe, P. Denk, C. Waldauf, A. J. Heeger, C. J. Brabec, Design Rules for Donors in Bulk-Heterojunction Solar Cells—Towards 10% Energy-Conversion Efficiency Adv. Mater. 18, 789-794, (2006)

[24] V.D. Mihailetchi, P.W.M. Blom, J.C. Hummelen, M.T. Rispens, Cathode dependence of the open-circuit voltage of polymer:fullerene bulk heterojunction solar cells J. Appl. Phys., Vol. 94, No. 10, (2003)

[25] B.A. Gregg , M.C. Hanna. , Comparing organic to inorganic photovoltaic cells: theory, experiment, and simulation. J Appl Phys 93:3605, (2003)

[26] P.A.Troshin,R.N. Lyubovskaya, V.F.Razumov Organic Solar Cells: Structure, Materials, Critical Characteristics, and Outlook,Nanotechnologies in Russia Vol.3, (2008)

[27] A. Gadisa, M. Svensson, M. R. Andersson,, O. Inganas, Correlation between oxidation potential and open-circuit voltage of composite solar cells based on blends of polythiophenes: fullerene derivative Appl. Phys. Lett. 84, 1609, (2004)

[28] B. P. Rand, D. P. Burk, S. R. Forrest, Offset energies at organic semiconductor heterojunctions and their influence on the open-circuit voltage of thin-film solar cells Phys. Rev. B 75, 115327, (2007)

[29] K. Vandewal, K. Tvingstedt, A. Gadisa, O. Inganas, J. V. Manca, On the origin of the open-circuit voltage of polymer–fullerene solar cells , Nat. Mater. 8, 904 (2009)

[30] K. Vandewal, K. Tvingstedt, A. Gadisa, O. Inganäs, , J. V. Manca Relating the open-circuit voltage to interface molecular properties of donor:acceptor bulk heterojunction solar cells, Phys. Rev. B 81, 125204 (2010)

[31] B. C. Thompson and J. M. J. Fréchet, Polymer–Fullerene Composite Solar Cells , Angew. Chem., Int. Ed. 47, 58 (2008)

[32] G. Dennler, M. C. Scharber, C. J. Brabec, Polymer-Fullerene Bulk-Heterojunction Solar Cells Adv. Mater. 21,1323 (2009)

[33] C. J. Brabec, Organic photovoltaics:technology and market Sol. Energy Mater. Sol. Cells 83, 273-292, (2004)

[34] L.J. Koster, V.D. Mihailetchi, P.W.M. Blom, Ultimate efficiency of polymer fullerene bulk heterojunction solar cells, Appl. Phys. Lett., Vol. 78, No. 6, (2001)

[35] D.C. Olson, S.E. Shaheen, M.S.White, W.J.Mitchell, M.F.A.M. van Hest, R.T. Collins, D.S. Ginlley, Band-offset engineering for enhanced open-circuit voltage in polymer-oxide hybrid solar cells, Adv. Funct. Mater. 17, 264–269, (2007)

[36] C.J. Brabec, A. Cravino, D. Meissner, N.S. Sariciftci, M.T. Rispens, L. Sanchez, J.C. Hummelen, T. Fromherz, The influence of materials work function on the open circuit voltage of plastic solar cells, Thin Solid Films 430-404, 368–372, (2002)

[37] C.J. Brabec, A. Cravino, D. Meissner, N.S. Sariciftci, T. Fromherz, M.T. Rispens, L. Sanchez, J.C. Hummelen, Origin of the open circuit voltage of plastic solar cells, Adv. Funct. Mater. 11, 374–380, (2001)

[38] H. W. Tsai, Z. Pei, C. C. Chen, S. J. Cheng, W. S. Hsieh, P. W. Li, Y. J. Chan, Anode engineering for photocurrent enhancement in a polymer solar cell and applied on plastic substrate, Sol. Energy Materials and Solar Cells 95 (2), 611-617, (2011)

[39] S. Admassie, F. Zhang, A.G. Manoj, M. Svensson, M. R. Andersson, O. Inganäs, A polymer photodiode using vapor-phase polymerized PEDOT as an anode Solar Energy Materials & Solar Cells 90, 133–141, (2006)

[40] A. Gadisa, X. Wang, S. Admassie, E. Perzon, F. Oswald, F. Langa, M. R. Andersson, O. Inganäs, Stoichiometry dependence of charge transport in polymer/methanofullerene and polymer/C70 derivative based solar cells Organic Electronics 7, 195–204, (2006)

[41] G. Yu, J. Gao, J.C. Hummelen, F. Wudl, A.J. Heeger, Polymer Photovoltaic Cells: Enhanced Efficiencies via a Networko f Internal Donor-Acceptor Heterojunctions, Science 270, 1789, (1995)

[42] S. E. Shaheen, C. J. Brabec, N. S. Sariciftci, F. Padinger, T. Fromherz, J. C. Hummelen, 2.5% efficient organic plastic solar cells, Appl. Phys. Lett. 78, 841-843, (2001)

[43] P. Schilinsky, C. Waldauf, C.J. Brabec, Recombination and loss analysis in polythiophene based bulk heterojunction photodetectors Appl. Phys. Lett. 81, (2002)

[44] C. Deibel, V. Dyakonov, Polymer–fullerene bulk heterojunction solar cells, Rep. Prog. Phys. 73, 096401, 39, (2010)

[45] P. Schilinsky, C. Waldauf, J. Hauch, C. J. Brabec, Simulation of light intensity dependent current characteristics of polymer. J. Appl. Phys., Vol. 95, 2816, (2004)

[46] I. Riedel, J. Parisi,V. Dyakonov, L. Lutsen, D.Vanderzande, and J. C. Hummelen, Effect of temperature and illumination on the electrical characteristic of polymer-fullerene bulk-heterojunction solar cells. Adv. Funct. Mater., Vol. 14, 38, (2004)

[47] J. Xue, S. Uchida, B P. Rand, S.R.Forrest 4.2% efficient organic photovoltaic cells with low series resistances, Appl. Phys. Lett., Vol. 84, No. 16, (2004)

[48] C. Waldauf , "Simulation of Organic Solar Cells", European Spring School 2009 on Supramolecular Organized Nanostructured Materials for Optoelectronic Applications of the European Marie-Curie RTNs NANOMATCH & THREADMILL featuring: ICMol workshop on Molecular Materials Peníscola, Spain 19-24/04 (2009)

[49] Y. Kim, S. Cook, S. M. Tuladhar, S. A. Choulis, J. Nelson, J. R. Durrant, D. D. C. Bradley, M. Giles, I. McCulloch, C. S. Ha, M. Ree, A strong regioregularity effect in self-organizing conjugated polymer films and high-efficiency polythiophene:fullerene solar cells, Nature Materials 5, 197 - 203 (2006)

[50] K.G. Jespersen , F. Zhang , A. Gadisa , V.Sundstrom , A. Yartsev , O.Inganas, Charge formation and transport in bulk-heterojunction solar cells based on alternating polyfluorene copolymers blended with fullerenes, Organic Electronics 7 , 235–242, (2006)

[51] L. M. Andersson, F. Zhang,O. Inganäs, Bipolar transport observed through extraction currents on organic photovoltaic blend materials , Appl. Phys. Lett. 89, 142111, (2006)

[52] V. D. Michailetchi, L. J. Anton Koster, P. W.M. Blom, C. Melzer, Bert de Boer, J. K.J. van Duren, R. A. J. Janssen, Compositional Dependence of the Performance of poly(p-phenylene vinylene) Methanofullerene Bulk-Heterojunction Solar Cells., Adv. Funct. Mater.15 No5 , (2005)

[53] S. A. Choulis, J. Nelson, Y. Kim, D. Poplavskyy, T. Kreouzis, J. R. Durrant, D. D. C. Bradley , Investigation of transport properties in polymer:fullerene blends using time-of-flight photocurrent measurements , Appl. Phys. Lett., Vol. 83, No. 18, (2003)

[54] S. M. Tulathar, D. Poplavskyy, S. A. Choulis, J. R. Durrant, D. D.C. Bradley, J. Nelson, Ambipolar Charge Transport in Films of Methanofullerene and Poly(phenylenevinylene)/Methanofullerene Blends, Adv.Funct.Mater.,15, 1171-1182, (2005)

[55] T. D. Anthopoulos, C. Tanase, S. Setayesh, E. J. Meijer, J. C. Hummelen, P. W.M. Blonm,D. M. Deleew Ambipolar Organic Field Effect Transistors Based on a Solution-Processed Methanofullerene. Adv. Matter.,16, 23-24, (2004)

[56] A. Gadisa, F. Zhang, D. Sharma, M. Svensson, M. R. Andersson, O. Inganäs, Improvements of fill factor in solar cells based on blends of polyfluorene copolymers as electron donors, Thin Solid Films 515, 3126–3131, (2007)

[57] N. Koch, A. Kahn, J. Ghijsen, J.J. Pireaux, J. Schwartz, R.L. Johnson, A. Elschner, Conjugated organic molecules on metal versus polymer electrodes: Demonstration of a key energy level alignment mechanism Appl. Phys. Lett. 82 ,70, (2003)

[58] J. Huang, P.F. Miller, J.S. Wilson, A.J. de Mello, J.C. de Mello, D.D.C. Bradley, Investigation of the effects of doping and post-deposition treatments on the conductivity, morphology, and work function of poly(3,4- ethylenedioxythiophene) /poly(styrene sulfonate) films Adv. Funct. Mater. 15 , 290, (2005)

[59] N. Koch, A. Vollmer, A. Elschner, Influence of water on the work function of conducting poly(3,4-ethylenedioxythiophene)/poly(styrenesulfonate) Appl. Phys. Lett. 90 , (2007)

[60] Th. Kugler, W. R. Salaneck, H. Rost, and A. B. Holmes, Polymer band alignment at the interface with indium tin oxide: consequences for light emitting devices, Chem. Phys. Lett., 310, 391 – 396, (1999)

[61] M. G. Helander, Z. B. Wang, M. T. Greiner, Z. W. Liu, K. Lian, Z. H. Lu, The effect of UV ozone treatment on poly(3,4-ethylenedioxythiophene): poly(styrenesulfonate) Appl. Phys. Lett. 95, 173302 (2009)

[62] C. Tengstedt, A. Kanciurzewska, M. P. de Jong, S. Braun, W. R. Salaneck, M. Fahlman, Ultraviolet light-ozone treatment of poly(3,4-ethylenedioxy-thiophene)-based materials resulting in increased work functions, Thin Solid Films 515, 2085 (2006)

[63] Y.J. Lin, F.M. Yang, C.Y. Huang, W.Y. Chou, J. Chang, Y.C. Lien, Increasing the work function of poly(3,4-ethylenedioxythiophene) doped with poly(4-styrenesulfonate) by ultraviolet irradiation Appl. Phys. Lett. 91, 092127 (2007)

[64] T. W. Lee, O. Kwon, M. G. Kim, S. H. Park, J. Chung, S. Y. Kim, Y. Chung, J. Y. Park, E. Han, D. H. Huh, J. J. Park, L. Pu, Hole-injecting conducting-polymer compositions for highly efficient and stable organic light-emitting diodes, Appl. Phys. Lett. 87, 231106 (2005)

[65] D. J. D. Moet, P. de Bruyn, and P. W. M. Blom, High work function transparent middle electrode for organic tandem solar cells , Appl. Phys. Lett. 96, 153504 (2010)

[66] T. Nagata, Seungjun Oh, T. Chikyow, Y. Wakayama Effect of UV–ozone treatment on electrical properties of PEDOT:PSS film, Organic Electronics 12, 279–284, (2011)

[67] C. J. Brabec, S. E. Shaheen, C. Winder, N. S. Sariciftci, P. Denk, Effect of LiF/metal electrodes on the performance of plastic solar cells, Appl. Phys. Lett., Vol. 80, No. 7, (2002)

[68] P. Schilinsky, C. Waldauf, C. J. Brabec, Performance Analysis of Printed Bulk Heterojunction Solar Cells, Adv. Funct. Mater., 16, 1669–1672, (2006)

[69] F.C. Krebs, Fabrication and processing of polymer solar cells: A review of printing and coating techniques, Solar Energy Materials & Solar Cells 93, 394–412, (2009)

[70] K. Norrman, A. Ghanbari-Siahkali, N.B. Larsen, Studies of spin-coated polymer films, Annu. Rep. Prog. Chem. Sect. C 101, 174–201, (2005)

[71] C. N. Hoth, P. Schilinsky, S. A. Choulis, C. J. Brabec Printing Highly Efficient Organic Solar Cells Nano Letters 8 , 2806-2813, (2008)

[72] C. N. Hoth, S.A.Choulis, P. Schilinsky, C.J.Brabec, High Photovoltaic Performance of Inkjet Printed Polymer:Fullerene Blends, Adv. Mater. 19,22, 3973-3978 (2007)

[73] C. N. Hoth, Ph.D. Thesis, University of Oldenburg, Germany, (2009)

Chapter 3 - Establishing a reference Device System

The importance of establishing a reproducible reference process with commercially available materials is always a high priority, especially when a laboratory has only recently been established. In this chapter, fabrication and optimization processes of the well known polymer:fullerene system P3HT:PCBM for efficient organic solar cells are described. A normal device architecture, where electrons are collected at the metal electrode and holes at the ITO/PEDOT:PSS side, was chosen as the reference cell in our group. The solar cells studied in this chapter were fabricated by doctor blade technique which, as previously stated, has fewer limitations in comparison to spin coating, due to the ability to control substrate temperature, blade height and deposition speed. A mixture of solvents was also used in order to further manipulate morphology and enhance overall performance. During the optimization process s-shaped curves were witnessed and as revealed by capacitance measurements are attributed to gap defects of the polymer.

3.1 Establishing the Reference

3.1.1 Theoretical Model

A theoretical model was recruited to provide important parameters for device optimization, since the laboratory was not yet equipped with basic optical and morphological characterization instruments. A Visual Basic based curve-fitting software was chosen. Both dark and illuminated current density vs. voltage characteristics are depicted in a semi-logarithmic form. By overlapping measured with respective simulated curves, equalized device parameters are ensured. As shown in Figure 1, parameters such as parallel resistance R_p, series resistance R_s, refractive index n, saturation current J_0, $\mu \times \tau$ product (the area covered during the lifetime of an exciton) and contact probability can be acquired from the model. Information and conclusions about blend systems may be extracted when the obtained data are combined with ones from the literature. These data can then be used to enhance overall device performance.

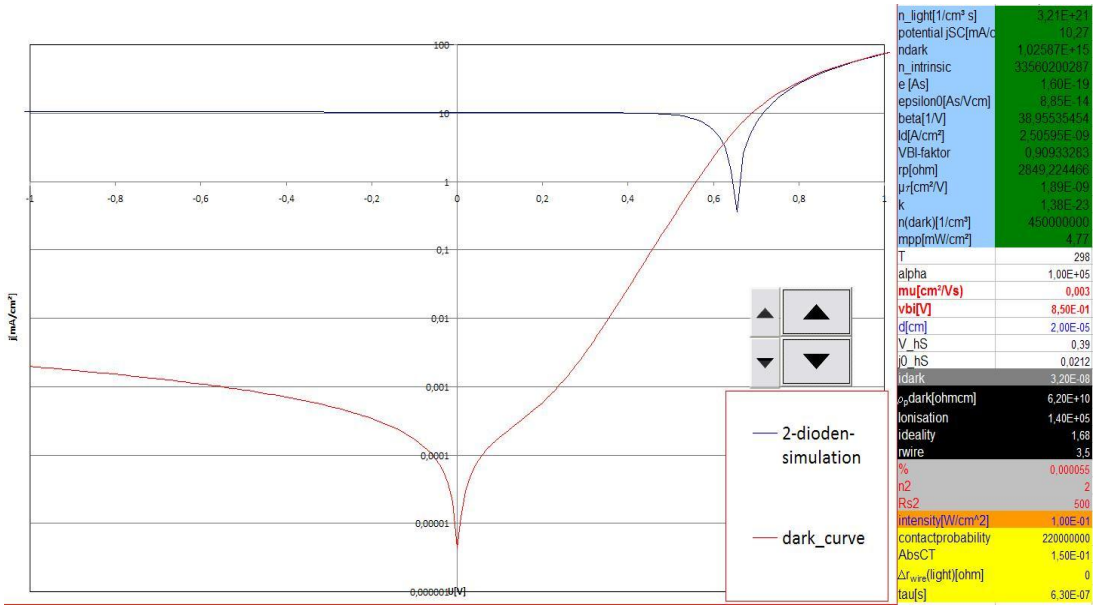

Figure 1: A fitting simulation aimed to cover for the lack of basic characterization equipment. Several parameters can be obtained critical for device optimization.

3.1.2 Experimental

Pre-patterned 4 Ω/square indium tin oxide (ITO) substrates protected with a photoresist layer were purchased from MicroLIQUID (http://www.microliquid.com/). Substrates were cleaned with acetone for 10 minutes in an ultrasonic bath in order to remove the protective layer and were then sonicated in an isopropanol solution for a total of 20 minutes. The substrates were then dried with an air-gun and on a hotplate at around 70 °C to ensure residual solvent removal. During the latter step samples were covered with a Petri dish. Figure 2a shows the sputtered ITO pattern. Then, as shown in Figure 2b, a thin PEDOT:PSS hole transporting layer (HTL), purchased from Heraeus Clevios™ (www.clevios.com) was doctor bladed on top of the substrate followed by a thicker optically active film of P3HT:PCBM blend (Figure 2c), both at conditions that will be further discussed later. PEDOT:PSS solutions used in this thesis were further diluted with isopropanol

(IPA) in a 1:3.2 ratio so that the contact angle of the ink formulation was reduced, resulting in better wettability on the ITO substrates. Then the formed layers were dried on a hot-plate at 140 °C for 20 minutes so that remaining water inside the layer was removed. Substrate edges were cleaned with a Q-tip first using the blend solvent and then using water (Figure 2d). In this way leakage current and series resistance were minimized after metal deposition which followed. After that, a droplet of UV-activated epoxy resin glue was placed between the 4 contacts and an encapsulation glass to seal the device and ensure longer lifetime (Figure 2f).

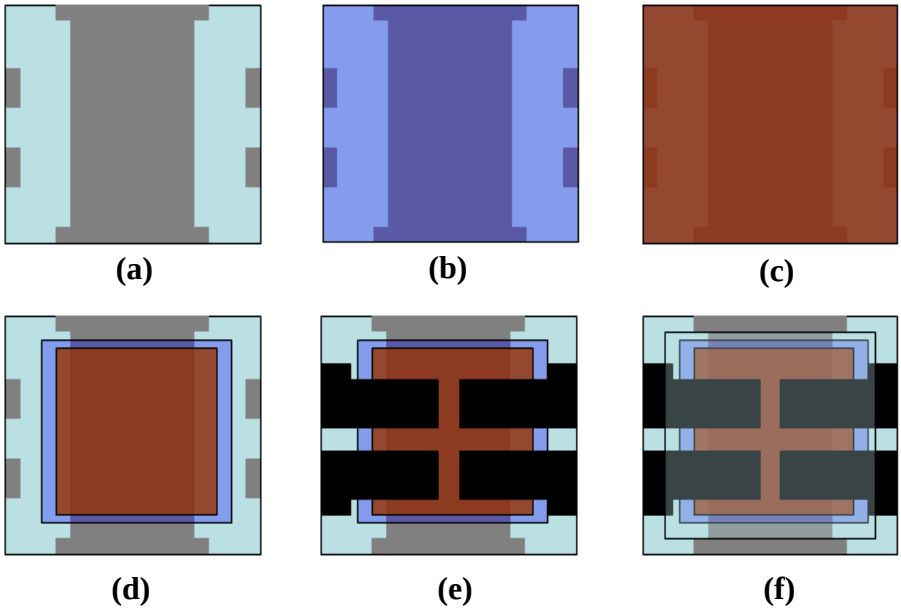

Figure 2: Schematically depicted device structure (a) as purchased. PEDOT:PSS is doctor bladed on top of ITO (b), followed by active layer deposition (c). To eliminate loss mechanisms the edges are cleaned (d) and the metal cathode is thermally evaporated on top (e). To ensure long lifetime of the photovoltaic cells, an encapsulation glass substrate seals the device (f).

3.2 Results and Discussion

3.2.1 PEDOT:PSS

3.2.1.1 Comparing Hole Transporting Layers (HTLs)

While investigating PEDOT:PSS optimum deposition conditions, various products were tested. Photovoltaic devices with Clevios P VP AL 4083 and Clevios PH were fabricated and obtained current density vs voltage (J/V) characteristics are shown in Figure 3.

Despite their small variations concerning product characteristics, the main difference between these two types of PEDOT:PSS lies in the PSS content of the dispersion which is closely related to the conductivity of the deposited layers, as discussed below. Layers fabricated with Clevios PH exhibited higher conductivity. Though devices were identical, their parameters exhibited differences concerning overall performance. The main values for both PEDOT:PSS layers are summarized in Table 1.

Table 1: Summary of device performance for different PEDOT:PSS products. Exhibited differences are mainly attributed to PEDOT:PSS resistivity values.

PEDOT:PSS	V_{oc} (V)	J_{sc} (mA/cm^2)	FF (%)	PCE (%)
Clevios P VP AL 4083	0.54	8.9	42	2.0
Clevios PH	0.56	9.4	47	2.4

When the HTL is deposited, a grain-like structure of the PEDOT:PSS, where a non-homogeneous distribution of the PEDOT and the PSS parts within the grains, has

been proposed[1, 2]. A conductive PEDOT-rich core surrounded by insulating PSS-rich shell areas is the prevailing view on PEDOT:PSS morphology[3]. Larger PSS domains result in higher resistivity layers, which is reflected in J/V characteristics as series resistance (R_s). Lower conductivity layers as a result of higher PSS content, lead to unbalanced hole and electron mobility. High PSS content limits charge carrier transportation (reduced FF), as holes struggle to pass through the PEDOT:PSS interfacial layer. At the same time slightly lower J_{sc} is a result of either small thickness variations of the active layer or higher series resistance. J_{sc} reduction has been associated with R_s by others[4]. The above-mentioned device losses are explained by the lower conductivity of Clevios P VP AL 4083.

Organic photovoltaic solar cells were also fabricated with higher conductivity PEDOT:PSS (Clevios PH 500) but devices exhibited a high shunt ratio, suggesting that further optimization is needed for that particular product type.

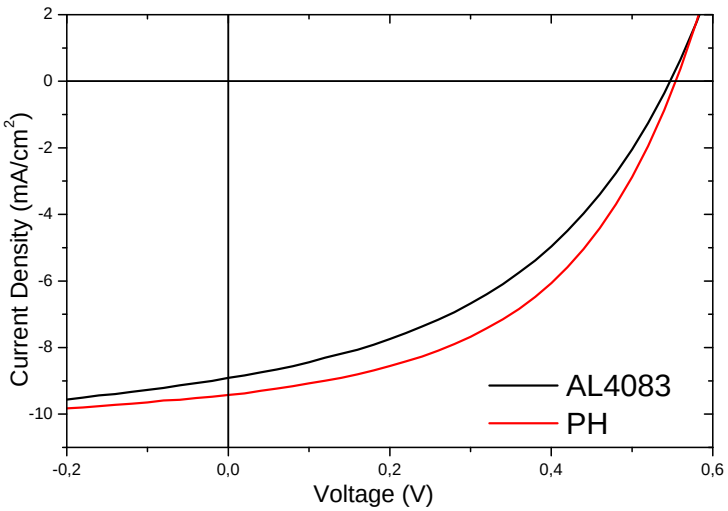

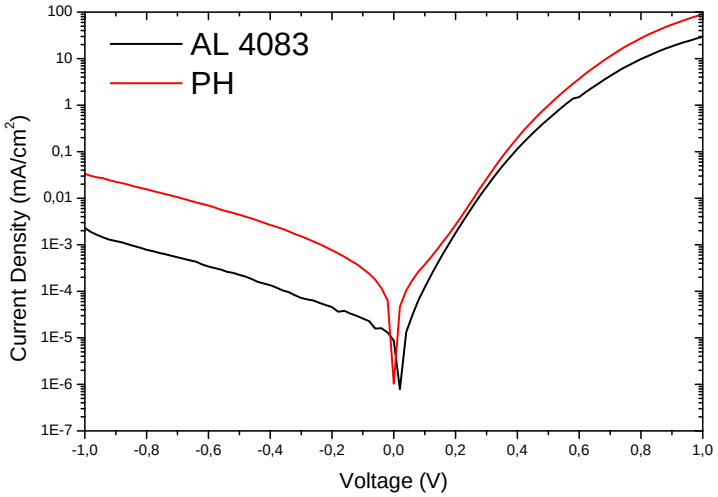

Figure 3: Devices fabricated with Clevios PH and AL 4083 PEDOT:PSS were analyzed. Current density vs. voltage characteristics under 1 sun illumination (top) and in semi logarithmic form (bottom).

3.2.1.2 Thickness

Another important aspect that was investigated in this chapter is the PEDOT:PSS layer thickness. The two main phenomena affecting device performance in relation to layer thickness are light interference and layer morphology. Depending on the thickness of PEDOT:PSS, constructive or destructive interference of light at certain wavelengths may occur, which will be demonstrated experimentally later. At higher thicknesses larger PEDOT-rich grains are formed and distance between the grains is reduced. This decreases the PSS edges that isolate conductive PEDOT areas, allowing better connectivity between grains and thereby better conductivity. An improved connecting network throughout the bulk also reduces sheet resistance resulting in fill factor improvement[5]. However, this happens to the detriment of transparency and thus negatively affects solar light harvesting.

Figure 4 summarizes the J/V characteristics of devices fabricated with different PEDOT:PSS layer thickness.

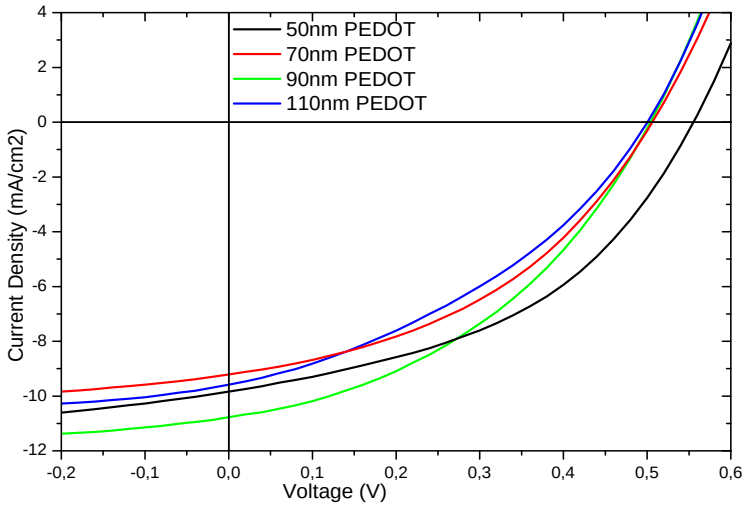

Figure 4: Current density vs Voltage (J/V) characteristics with respect to PEDOT layer thickness. Hole transporting layer thickness plays an important role in overall device performance. A work function reduction is suggested for layers thicker than 50 nm.

The data in Table 2 shows that devices with a 50 nm HTL layer exhibited improved device performance, while obtained J_{sc} and FF for the rest of the devices linearly decrease with increasing PEDOT:PSS thickness. A surprisingly high J_{sc} was observed for the device with a 90 nm PEDOT:PSS layer, but this is due to an underestimation of the evaporated metal area resulting in a larger than calculated device area. Current density reduction is a result of a reduced number of embedded photons in the optically active layer due to limited transmittance (Figure 4) of the thicker PEDOT:PSS layers. Despite losses in transmittance, an expected decrease in sheet resistance would allow higher FF values. Nevertheless, higher layer roughness resulted in unfavorable morphology of the active layer deposited on top of PEDOT:PSS. Deposited layers of 110 nm thickness exhibited root mean square (rms) roughness of 10.4 nm.

Table 2: Summary of obtained photovoltaic parameters when devices with different PEDOT:PSS layer thicknesses were measured under 100mW/cm^2 illumination. Optimum layer thickness was found to be 50 nm as other layers exhibited hindered internal driving force.

Thickness (nm)	V_{oc} (V)	J_{sc} (mA/cm^2)	FF (%)	PCE (%)	Roughness (nm)
50	0.550	9.8	44.3	2.40	1.8
70	0.506	9.2	42.0	1.96	2.1
90	0.504	10.7	40.8	2.21	7.0
110	0.508	8.8	39.1	1.76	10.4

Another current density limiting factor is the wavelength peak that transmits through each layer. In Figure 5, transmittance measurements were performed on each PEDOT:PSS layer and a trend was revealed. The 50 nm layer exhibited 3 main peaks at 420 nm, 526 nm and 670 nm. For the thicker layers the transmittance values were significantly blue shifted. Because the absorption maxima for P3HT:PCBM lie between 490 and 540 nm this blue shift only causes a reduction in absorption. This inverse proportionality of layer thickness to peak wavelength distance, is shown through the following mathematical expression (1)[6].

$$\chi = \frac{\lambda_1 \lambda_2}{\lambda_2 - \lambda_1} \frac{1}{n} \quad (1)$$

Where x = layer thickness

λ_1, λ_2 = peak wavelengths

n = refractive index

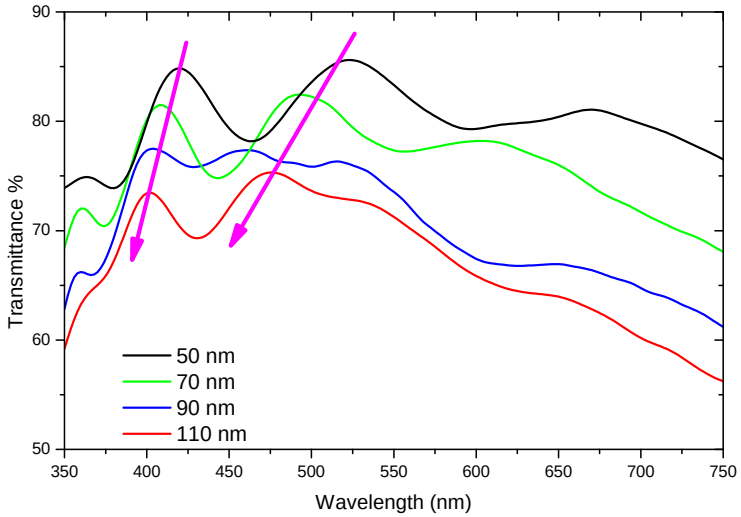

Figure 5: Various PEDOT:PSS layers were deposited on top of ITO. Transmittance measurements were performed. Spectra showed a blue shifted transmittance resulting in photocurrent density reduction.

Though optimum devices presented a V_{oc} of 0.55 V, reduced values were obtained for the 70, 90 and 110 nm devices. It is assumed that higher PEDOT:PSS layer roughness can result in an unfavorable morphology for exciton dissociation in the active layer but the consistency of the V_{oc} values for the 3 devices suggests otherwise (Table 2). Regardless of their thickness, all layers were annealed under the same conditions with residual water affecting device performance. A work function (WF) reduction[7, 8] seems to be the case, with hindered internal driving force proven to play a major role in overall device performance. The work function difference of the two electrodes creates an internal electric field that assists in exciton dissociation efficiency and drives the carriers towards the respective electrodes. When the WF difference is reduced, so is the exciton dissociation ability and in turn the V_{oc}.

3.2.1.3 UV-Ozone Treatment

It has been suggested that PEDOT:PSS conductivity and work function are increased when treated with UV-ozone (UV-O_3)[9]. This could lead to series resistance reduction and thus improvement in FF values. Although others have stated that improved charge carrier collection is also observed and revealed in the J/V graphs as increased shunt resistance (R_{shunt}), this did not apply in our case. Devices with Clevios PH were UV-O_3 treated for 10 minutes and the resulting device performance is summarized in Figure 6 and Table 3.

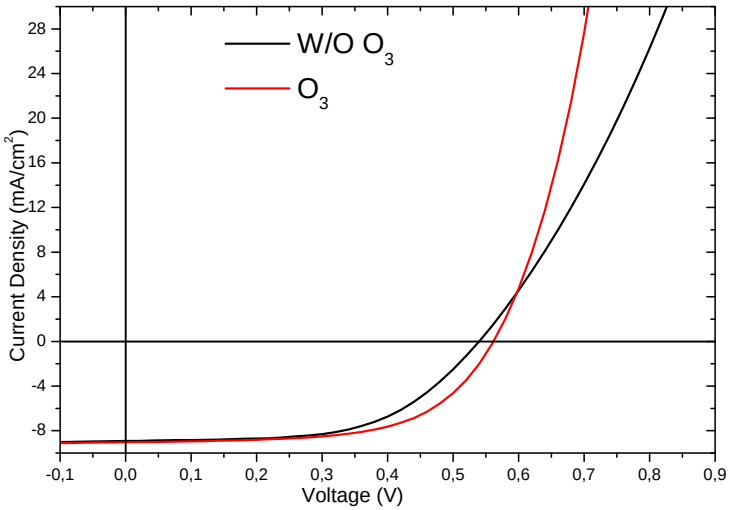

Figure 6: Current density vs Voltage for UV-ozone treated PEDOT:PSS layers compared to untreated films. A series resistance reduction resulted in improved FF and V_{oc}.

UV-ozone treatment decomposes the conjugated chemical bonds of the PSS aromatic ring reducing the insulating excess of PSS-rich domains surrounding PEDOT-rich grains, as discussed above. In this way, charges are easily transported towards the respective electrode – a fact that is mirrored on FF improvement for treated samples. Regardless of the slight differences in J_{sc} due to experimental thickness errors, V_{oc} increase is recognized as work function increase of treated

PEDOT:PSS. Atomic oxygen oxidizes the layer surface and is absorbed to form molecular oxygen. Due to its higher electron affinity O_2 withdraws electrons from PEDOT:PSS resulting in negatively charged surfaces with a positively charged layer underneath. This resulting dipole formation increases the work function[10,11].

Table 3: Device parameters comparison of as-cast and plasma-ozone treated PEDOT:PSS layers.

Clevios PH	Voc (V)	Jsc (mA/cm^2)	FF (%)	PCE (%)
Plasma - O_3	0.56	9.1	60	2.65
As cast	0.53	8.9	55	2.4

3.2.2 Active Layer Optimization

3.2.2.1 Various Solvents

The past few years has seen a wide range of different solvents reported in the literature utilized for depositing the active layer[12, 13, 14]. Most frequently used is the chlorinated solvent family such as chlorobenzene (CB), ortho-dichlorobenzene (o-DCB) and chloroform (CF)[15]. In each case the solvent choice depends on deposition technique limitations, the absence of a clean room and on local "ambient" conditions. In an effort to determine the most suitable pristine or solvent mixture for our laboratory needs, various devices were fabricated. Though a more environmental approach by employing non-halogenated solvents was also made, low device performance did not allow further studies at that point. From collected data (Figure 7) we focused on CB because of higher yielded FF values and on CF due to the higher photocurrent potential it exhibited. Discussion on how we attempted to benefit from these two solvents will follow later on. Primarily the goal was to optimize the optically active layer with widely used pristine CB.

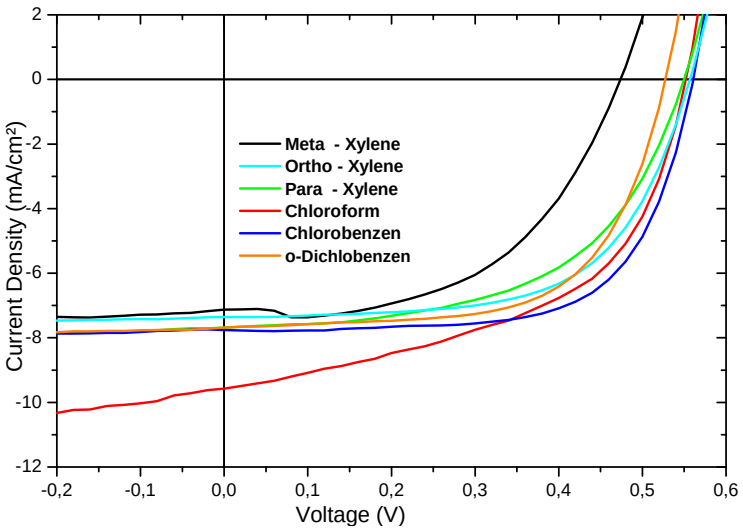

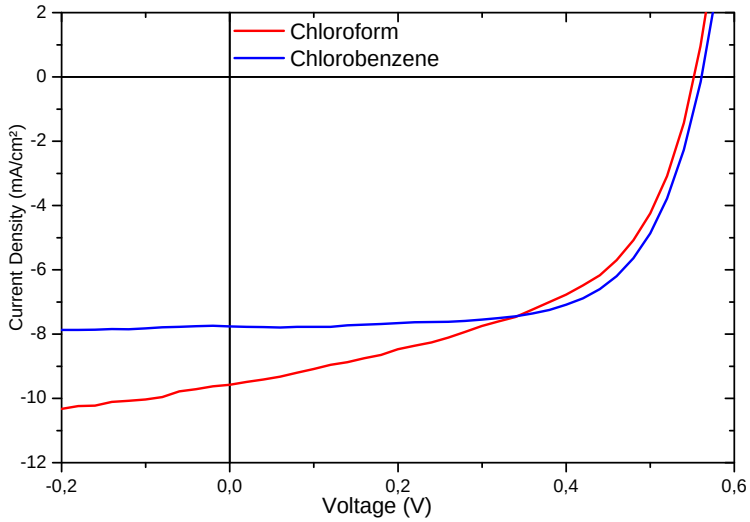

Figure 7: J/V characteristics of organic photovoltaic cells cast from various solvents (top). Judging from obtained data, chlorobenzene (CB) and chloroform (CF) were the most promising (bottom).

3.2.2.2 Blend Composition

As a first step, since both concentrations are extensively reported in the literature[16, 17], devices with ratios of 1:0.8 and 1:1 of P3HT:PCBM were fabricated[18]. Graphs with J/V characteristics of these devices in the dark and under illumination (Figure 8) are shown.

Device behavior under dark conditions in negative and medium positive bias, around 0.4 V, is almost identical. Only small differentiation between the two active layer compositions occurs at the higher positive voltage region, representing R_s. The devices fabricated with 1:1 ratio demonstrate improved R_s value than the 1:0.8 ones. Although the 1:1 cells could suggest improved FF, only the 1:0.8 cells, when illuminated, showed higher photocurrent density and enhanced FF. This paradox is attributed to the 10 % increase of PCBM concentration in the 1:1 film. It is assumed that electron and hole mobilities are not balanced in this composition, resulting in

bimolecular charge recombination. At the same time, lowering the overall percentage of the polymer in the mixture from 60 % (1:0.8) to 50 % (1:1) resulted in weaker photon absorbance and thus lower J_{sc} values.

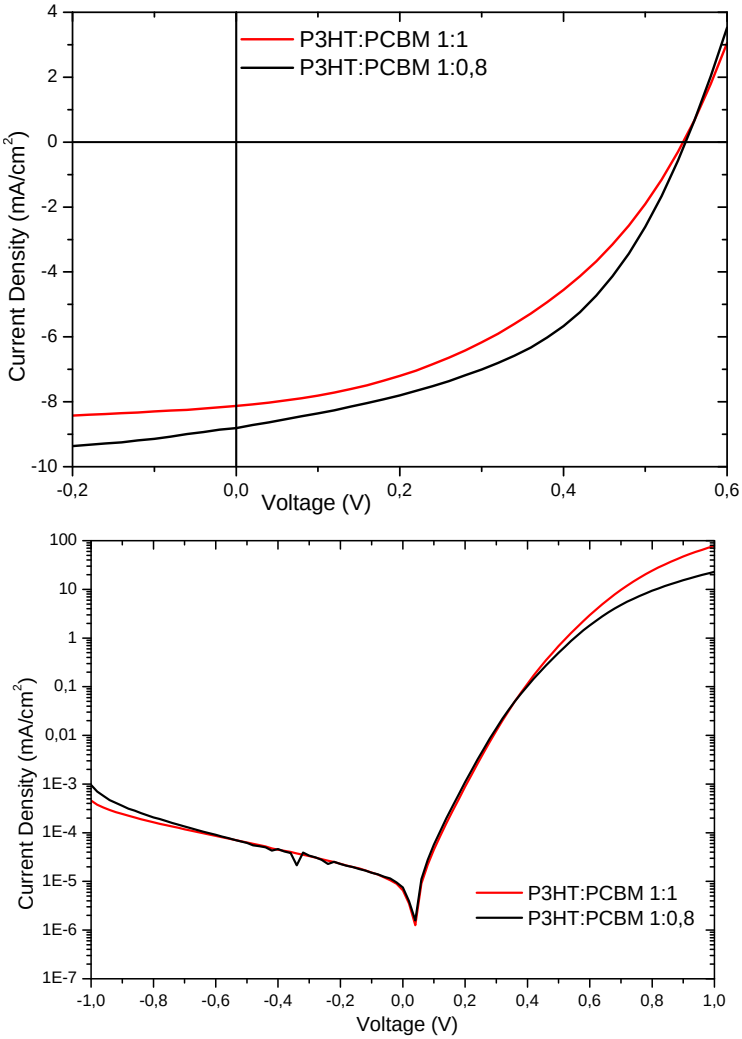

Figure 8: An increase in PCBM composition ratio, in the order of 10 %, reduces incident photon absorption. This is shown on the light (upper plot) and dark (bottom plot) J/V characteristics of 1:1 and 1:0.8 P3HT:PCBM ratio,

3.2.2.3 Thermal Annealing Effect

The morphology of the cast organic semiconductor plays a crucial role in device performance. In BHJ solar cells the optimization of internal continuous percolated pathways for the charge carriers in order to reach the appropriate electrodes limits

geminate and bimolecular charge recombination and thus enhances device performance. Local nanoscale morphology is improved by thermal annealing as the latter increases the degree of crystallinity of ideally both electron donor and acceptor[19, 20]. Figure 9 shows the J/V characteristics of a device, measured pre and post thermal annealing (top). From the dark curve one can conclude that the rectification ratio is improved for annealed cell and shows reduced leakage current (higher R_p) as well as R_s. This was accompanied by an increase in FF and J_{sc}, as depicted in the illuminated characteristics. Prior to annealing, small polymer:fullerene domains were formed in an "over mixed" morphology with increased exciton dissociation area, explaining higher V_{oc}, but with inefficient pathways for the charge carriers to travel towards the electrodes. After annealing the domains became larger, mainly due to vertical segregation of the system, with internal continuous pathways formed but with a decreased exciton splitting interface.

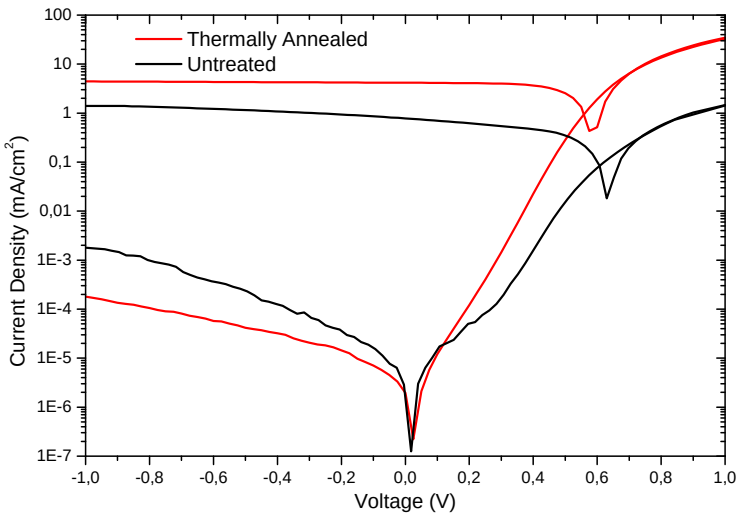

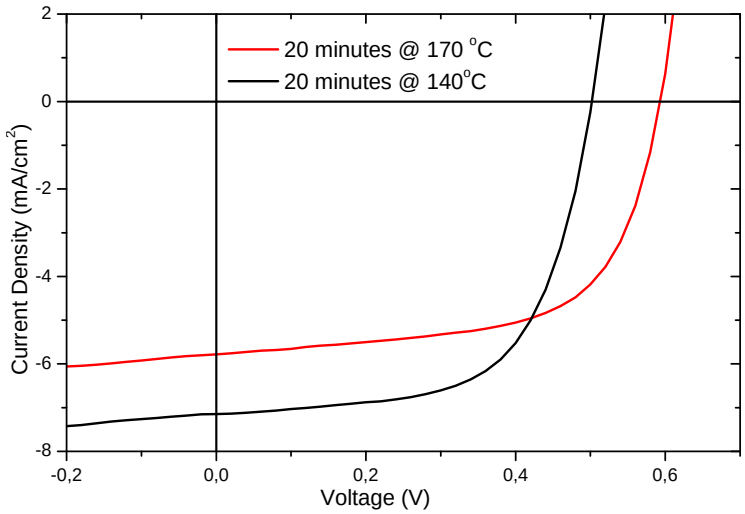

Figure 9: Thermally annealed and untreated device J/V characteristics (top) and different temperature annealing (bottom). At 170 °C J_{sc} reduction was demonstrated while at 140 °C it was V_{oc}.

In order to further improve device performance, the annealing temperature itself was investigated. Similar devices were fabricated and post evaporation thermally treated on a hot plate inside inert atmosphere at 140 °C and 170 °C for 20 minutes[21]. Solar cells annealed at 170 °C showed higher V_{oc} values. On the other hand those at 140 °C show enhanced J_{sc}. It is known that the minimum annealing temperature that leads to improved device performance lies above the glass transition temperature (T_g) of the blend – in this case around 120 °C [22] . Firstly, residual solvent is evaporated and then the morphology is defined by the degree of phase separation and crystallinity of P3HT and PCBM. At higher temperatures or longer than optimum annealing time, each component tends to self-organize, form domains and thus reduce charge transportation ability. Though carrier mobility is reduced due to morphological changes taking place at higher temperatures, increased dissociation interfaces occur resulting in higher V_{oc} for cells annealed at 170 °C. Absorption measurements were performed for the above-mentioned devices. As shown in Figure 10, devices

thermally annealed at 170 °C exhibited not only a blue shifted absorption peak (~15 nm) but also a narrower spectrum than that of 140 °C. This is assigned to a large disorder in the blend and agrees well with experimental data reported by others[23]. Due to the above-mentioned reasons one can easily explain the J_{sc} reduction of devices annealed at 170 °C.

When the delocalization length of the conjugation throughout the polymeric chain is disrupted, absorption maxima exhibit a blue shift. Also reduced interchain interactions may result in the same effect.

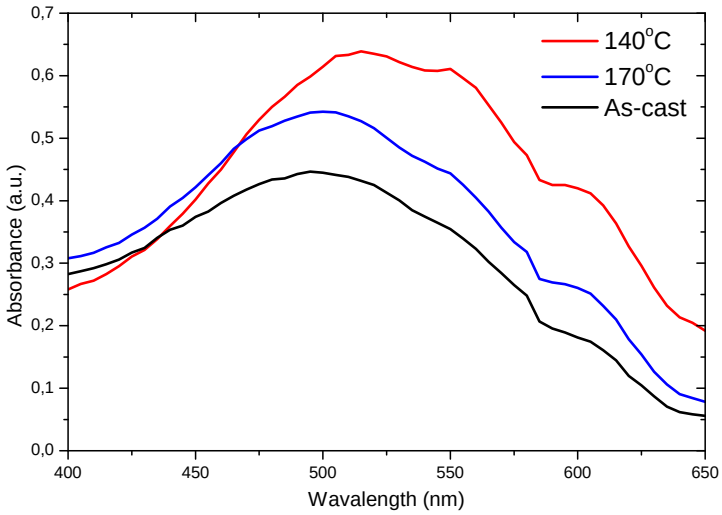

Figure 10: Absorption maxima of as-cast blends, and ones thermally annealed at 140 °C and 170 °C.

When devices are annealed at 170 °C for longer periods of time, a completely different morphology of the active layer is observed. PCBM is segregated from the blend and forms large needle-like aggregations underneath both the metal cathode and in between contacts area (Photo 1). It is possible that when extensively annealing at temperatures higher than T_g, PCBM undergoes a phase transition because of extensive demixing and excessive particle diffusion. Halos surrounding the aggregations are deficient of PCBM caused by molecule migration out of the

polymeric matrix. Also, by the size of aggregations, it seems that they are restricted beneath the metal cathode[17, 24].

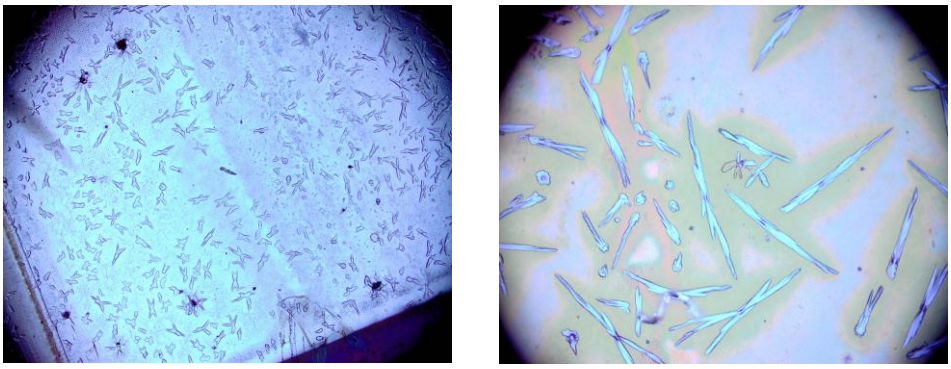

Photo 1: PCBM crystals underneath metal electrode (left) and in between cathodes area (right), revealed after thermal annealing at 170 °C. P3HT and PCBM have a tendency to self organize in the blend, in a destructive way in this case.

3.2.2.4 Solvent Annealing Effect

Depending on the boiling point of the solvent used the evaporation rate changes while fabricating organic photovoltaic devices. This can lead to nanoscale morphological differentiation of the active layer and thus improved overall device performance. A slow evaporation rate facilitates the growth of highly crystalline P3HT domains. The electron accepting molecules are steadily ejected from those domains resulting in vertical or lateral segregation of the blend composites. On the other hand, rapid solvent removal results in a more uniform distribution of P3HT and PCBM inside the blend[25, 26]. This limits charge carrier mobility and photon absorption. P3HT regains crystallinity if thermal treatment follows and in our experience lower temperatures and time are needed. Rapid solvent evaporation leads to thicker layers being formed, under the same conditions, with polymer chain density reduced. When solvent is evaporated and thermal annealing follows, PCBM

requires less energy to be expelled from crystalline P3HT as more unoccupied space is available. In order to control the evaporation rate we have performed experiments using different approaches. Blends of P3HT:PCBM in CB were doctor bladed on top of optimized PEDOT:PSS. Immediately after layer deposition, some substrates were covered with Petri dish while others were left in ambient conditions. Inside Petri dish the surrounding environment was saturated with solvent vapors prohibiting the layer from drying rapidly. Different volume size Petri dishes were also used but for the sake of simplicity data are not included. The improvement in FF and J_{sc} values for the slow drying device is due to percolating paths forming across the width of the layer thereby allowing the photogenerated species to travel towards the relative electrodes and be collected. This assumption is also supported by absorption measurements shown in Figure 14. From dark J/V characteristics of Figure 11, a reduction in leakage current is observed together with improved series resistance and consequently improved rectification ratio. As described above, P3HT and PCBM domains are formed, with the latter moving towards the metal electrode facilitating better ohmic contact at the organic:metal interface.

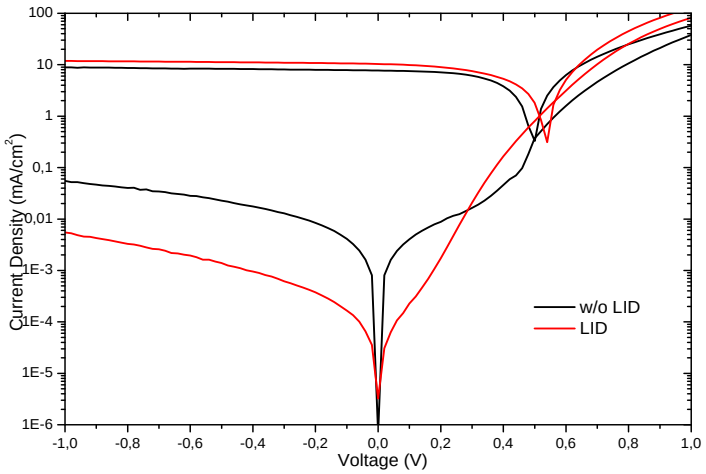

Figure 11: J/V characteristics of devices with and without lid. Slow evaporation rate of cast solvent results in improved morphology. P3HT and PCBM domains are formed increasing percolated networks for most favorable charge carrier transportation and collection.

3.2.2.5 Annealing Time

Despite the fact that vapor annealing influenced and improved morphology, further optimization in order to achieve higher PCE with commercially available P3HT:PCBM blend was needed. A combination of conclusions that had been reached up to now concerning annealing temperature and evaporation rate were employed. After deposition of the metal cathode, layers were exposed to 140 °C for different times[27, 28, 29]. For clarity only 20, 22 and 24 minutes data are shown below (Figure 12). Previous devices made yielded mainly low current density, so higher active layer thicknesses were aimed. As one would expect, thicker films (~270 nm) provided lower FF due to transport and recombination issues but at the same time increased photocurrent as more photons were absorbed (Table 4). Regardless of thickness, devices annealed for 24 minutes showed limited performance. This is because carriers could not migrate towards electrodes as the morphology suffered large scale phase demixing. Loss mechanisms, with geminate and bimolecular recombination being the most probable, dominated device operation and influenced

V_{oc} as well. Optimum annealing time was set to 22 minutes at 140 °C as both cells at different blade speeds, provided similar overall device performance.

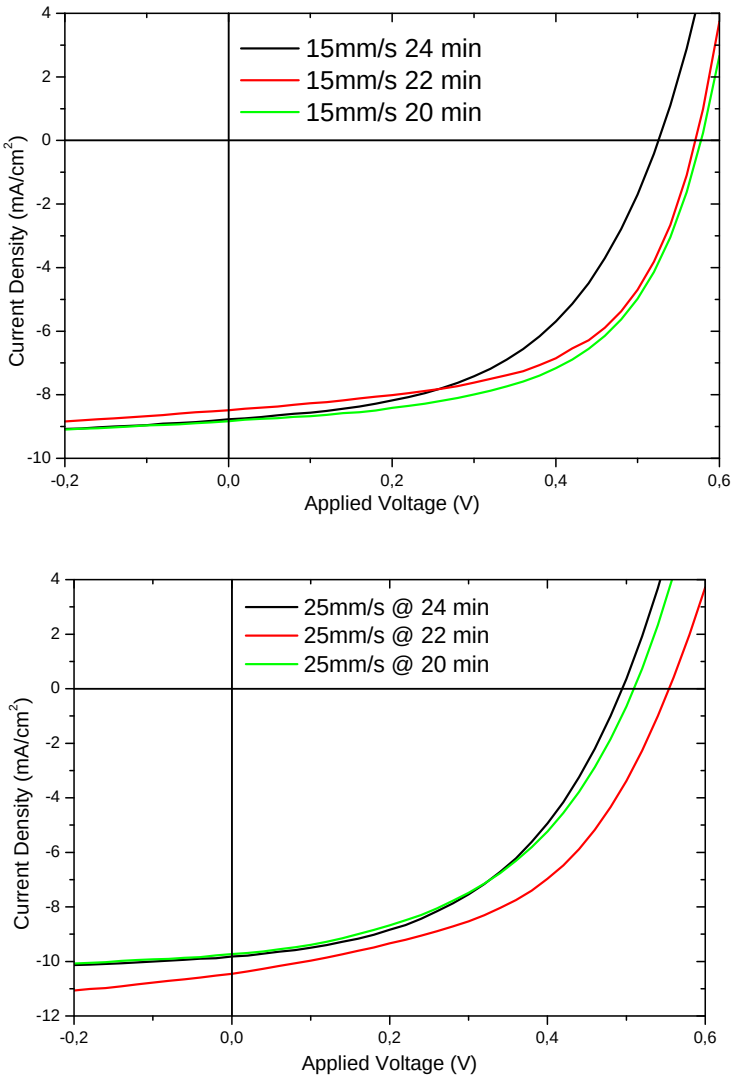

Figure 12: Photocurrent density vs. voltage characteristics for devices annealed at 140 °C for different lengths of time. Thicknesses of 180 nm by doctor blading at 15 mm/s (top) and 270 nm at 25 mm/s (bottom) were chosen.

Table 4: Active layer thickness dependence on thermal annealing time in relation to photovoltaic device parameters.

Annealing Time	V_{oc} (V)	J_{sc} (mA/cm2)	FF (%)	PCE (%)	Thickness (nm)
20	0,51	9,7	46.3	2.2	270
22	0,55	10,4	48.5	2.7	270
24	0,49	9,8	47.1	2.2	270
20	0,58	8,8	56.7	2.8	180
22	0,57	8,5	56.3	2.7	180
24	0,52	8,8	51.2	2.3	180

Further thickness optimization to 230 ± 5 nm and by employing all above mentioned conclusions, resulted in a photon to electron power conversion efficiency higher than 3 %. V_{oc} of 0.57 V and FF of 45.1 % were accompanied by 11.55 mA/cm^2 J_{sc}. The latter, according to Brabec *et al.*, corresponds to an internal quantum efficiency (IQE) of 90 % [30].

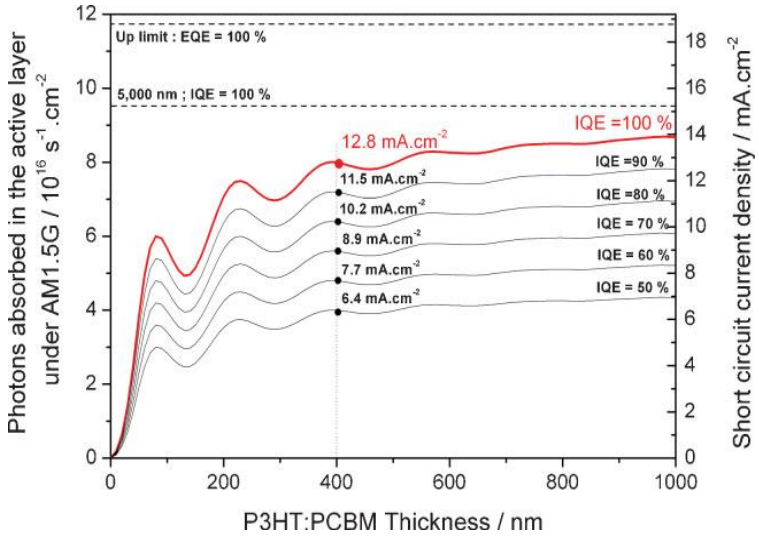

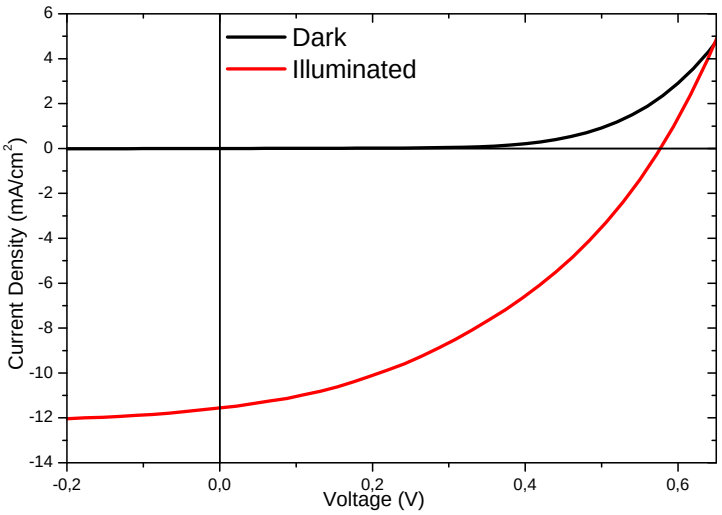

Figure 13: J/V characteristics of the reference device under illumination and in dark conditions. A PCE of 3% was achieved (bottom).

Absorption measurements show an absorption increase for annealed devices suggesting induced ordering of the polymeric chains. In all annealing conditions two peaks and a shoulder were observed at ~520, ~550 and ~600 nm, respectively. The lowest energy peak is attributed to an interchain electronic transition where the exciton is intermolecular and is delocalized over neighboring chains [31]. An increase in absorbance, when comparing thermal, solvent vapor and combination of both annealing treatments, is observed for the solvent annealing method (Figure 14). Combined treatment enhanced photon collection as the polymer's crystallinity and conjugation length were increased.

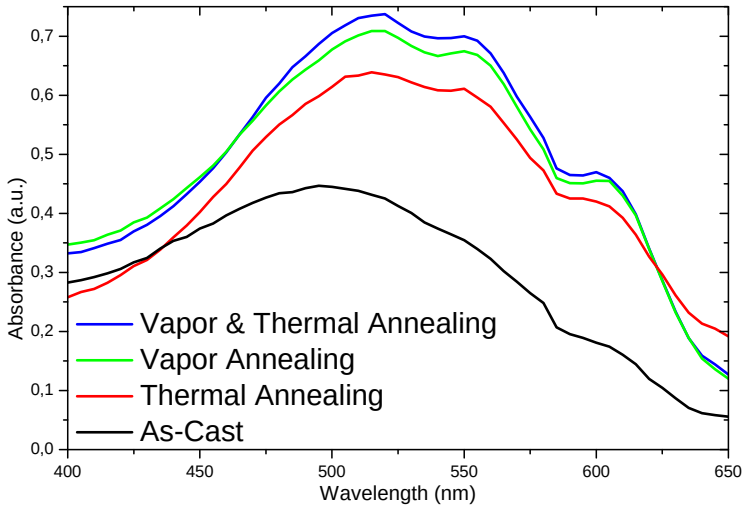

Figure 14: UV-Vis absorption of different post treatment types of P3HT:PCBM layers.

3.2.2.6 Solvent Mixture

For P3HT:PCBM blends use of certain solvents results in higher photosensitivity due to improved photon to electron conversion ability while others favor charge transportation that consequently leads to larger FF. In order to further manipulate morphology, high (131 °C) and low (61 °C) boiling point solvents CB and CF were mixed. In an effort to benefit from solvent blending[32,33], resulting in both high J_{sc} and good transport properties, devices with different concentrations of CF in CB were made. As also discussed for Figure 7, CF cells presented the highest photocurrent potential while those fabricated with CB showed enhanced FF. The low evaporation rate for pristine CB resulted in larger phases of the composite materials inside the film and formed percolated pathways facilitating charge carrier transportation. Geminate recombination however, was increased as exciton dissociation area was limited. On the other hand, CF's rapid evaporation rate provided smaller and uniformly mixed crystalline P3HT-rich and PCBM-rich clusters. This morphology, despite an increased exciton splitting interface, favored

bimolecular recombination as it could not offer continuous pathways for charge transportation towards the electrodes. The suggested morphology for both pristine solvents is schematically depicted below[34] (Figure 15).

Figure 15: Suggested morphology for slow (left) and fast (right) solvent evaporation.

External quantum efficiency (EQE) for pristine and solvent mixture devices (data not shown) exhibited only small variations suggesting that efficiency peaking should be looked into on the nanoscale morphology of the active layer.

Table 5: Optimum PCE of pristine solvents and solvent mixture

Solvent	PCE (%)
Chloroform	2.75
Chlorobenzene	2.85
Mixture	3.20

From the curve fitting software that was employed to compensate the lack of morphology characterization instruments, mobility lifetime (μ x τ) product values for the different ratios of CF into CB were exported. In Figure 16 (μ x τ) product was plotted in relation to the ideality factor of the cells. The latter takes values from $1 \leq n \leq 2$ and affects the power output of the device (4^{th} quadrant). Ideality factor is

extracted from dark J/V characteristics at medium positive voltages and with saturation current (J_o) as the main diode parameter.

The ideality factor linearly increases when using a solvent mixture ratio closer to pure CB, while the ($\mu \times \tau$) product saturates at a maximum of 60 % for CB. Phases seem to grow with the addition of CB due to the delayed drying process and this improves the transport properties towards the properties of the pure material (Figure 15). It is assumed that solvent evaporation took place in two phases because of boiling point difference. First, chloroform was evaporated forming small domains with high dissociation area. It was then followed by the chlorobenzene evaporation that led to clusters growing in such way that obtained morphology was improved.

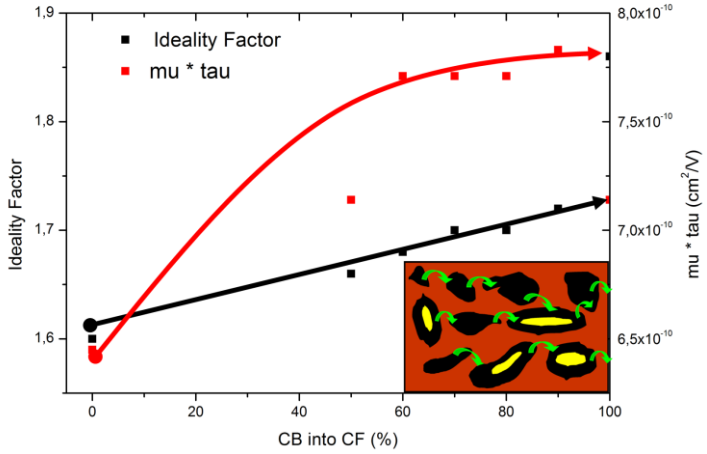

Figure 16: Ideality factor values and mu tau product were plotted against CF content into CB. At a mixing ratio of 40:60 CF:CB, optimum morphology was achieved, as schematically depicted (inset)

It is clear that internal morphology alters from pristine CB towards CF through different solvent ratio mixtures. These changes are also reflected in ideality factor alteration, thus the latter could provide a small indication of any morphological changes.

As illustrated below (Figure 17), the ratio of 40 % CF in CB showed enhanced device performance in comparison to pristine solvents. Solvent mixture composition ratio provides a nanoscale morphological control over the electron donor and acceptor interpenetrating networks, resulting in improved charge carrier transportation. The obtained morphology resulted in a photon to electron power conversion efficiency in the range of 3.2 % (Table 5).

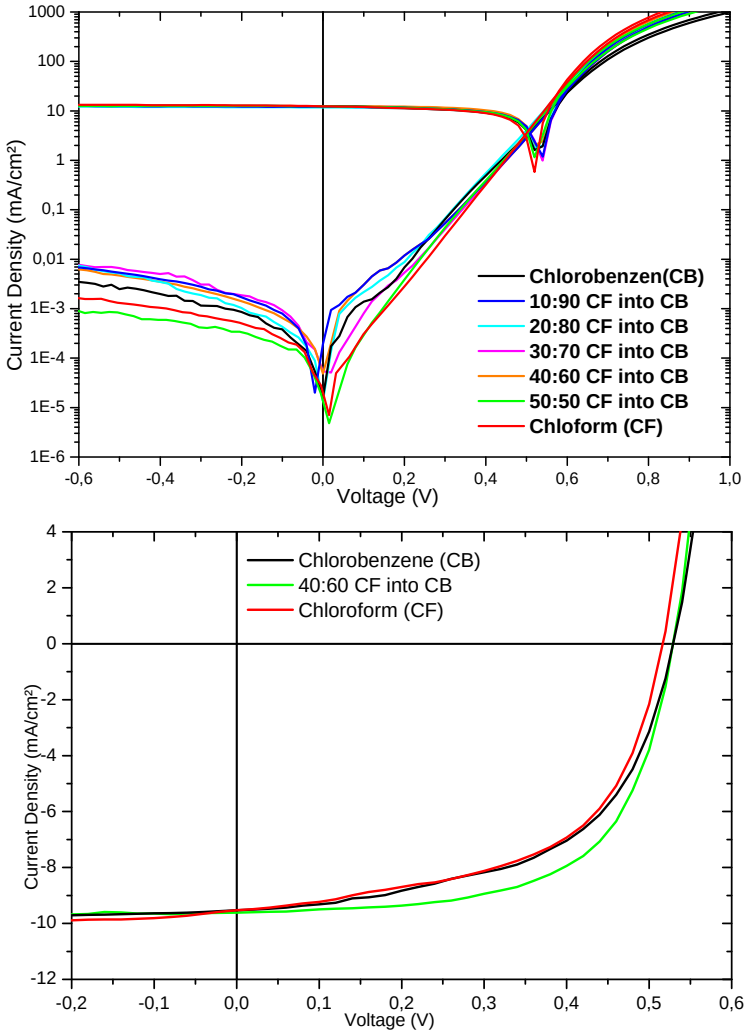

Figure 17: J/V characteristics of devices fabricated with mixed solvent in semi logarithmic scale (top) and optimum mixing ratio with pristine solvents (bottom)

3.2.2.7 Gap Defects[1]

During P3HT:PCBM optimization, s-shaped curves were witnessed when measuring J/V characteristics. These kinks (Figure 18) only appeared in the illuminated J/Vs, and were also reported in the literature for normal[35] and inverted[36] architecture solar cells. As schematically shown below, device characteristics appeared as if a second diode existed. Usually the kink was observed in the fourth quadrant and around maximum power point of the device. Gap defects were implied, with FF and J_{sc} mainly affected. For inorganic semiconductors, impurities in high concentrations lie behind similar device degradation. The density and energy levels of defect states within the gap of P3HT were studied in relation to PCBM ratio. Capacitance measurements were performed for both bias voltage (C_v) and frequency (C_f). The origin of the defects was found to belong to the polymer and they were identified as immobilized free radicals, vacancies and ends of polymeric chains. These resulted in two sets of states close or far away of P3HT's HOMO that corresponds to neutral and acceptor-like bands. Acceptor-like bands formed a second diode within the bulk that acted competitively to the neutral bands and generated extensive loss mechanisms[37].

[1] This work has been published as P. P. Boix, G. G. Belmonte, U. Muñecas, M. Neophytou, C. Waldauf, R. Pacios, Determination of gap defect states in organic bulk heterojunction solar cells from capacitance measurements at Applied Physics Letters, 95 (23), art. no. 233302, (2009).

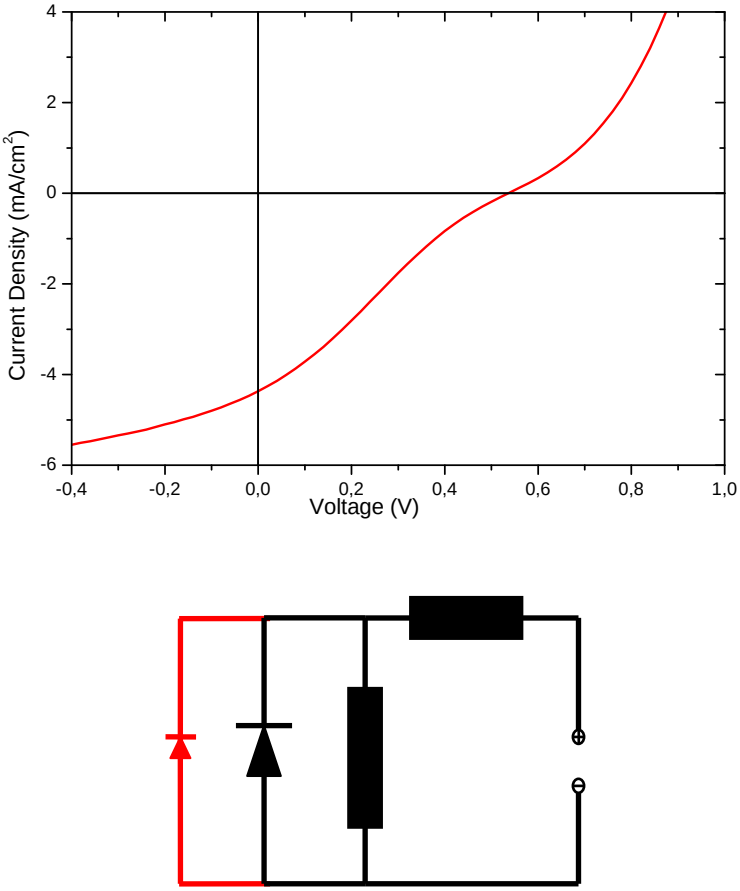

Figure 18: S-shaped kink illuminated J/V characteristics (upper plot) and the suggested macroscopic device model in order to explain this phenomenon (bottom plot).

3.3. Conclusions

The need of a reference system with reproducible results is imperative, especially in a new laboratory. In this chapter the route for achieving such a reference solar cell was described. Selecting PEDOT:PSS out of a range of different products, optimizing layer thickness and the effect of plasma-ozone treatment on device performance was described.

Concerning the optically active layer, various casting solvents were analyzed. Thermal and vapor annealing were discussed with respect to overall device performance. Exposure time of 22 minutes at 140 $^{\circ}$C in combination with slow solvent evaporation rate resulted in a PCE above 3 %. Similar results were obtained with a mixture of chlorobenzene and chloroform. The origin of s-shaped illuminated curves that were witnessed was identified to be P3HT gap defects originating from free radicals, vacancies and ends of polymeric chains.

3.4 Bibliography

[1] U. Lang, E. Muller, N. Naujoks, J. Dual, Microscopical Investigations of PEDOT:PSS Thin Films, Adv. Funct. Mater. 19, 1215–1220, (2009)

[2] M. M. de Kok, M. Buechel, S. I. E. Vulto, P. van de Weijer, E. A. Meulenkamp, S. H. P. M. de Winter, A. J. G. Mank, H. J. M. Vorstenbosch, C. H. L. Weijtens, V. van Elsbergen, Modification of PEDOT:PSS as hole injection layer in polymer LEDs, phys. stat. sol. (a) 201, No. 6 (2004)

[3] X. Crispin, S. Marciniak, W. Osikowicz, G. Zotti, A. W. Denier Van Der Gon, F. Louwet, M. Fahlman, L. Groenendaal, F. De Schryver, W. R. Salaneck, Conductivity, Morphology, Interfacial Chemistry, and Stability of Poly(3,4-ethylene dioxythiophene)–Poly(styrene sulfonate): A Photoelectron Spectroscopy Study, J. Polym. Sci. B 41, 2561-2583, (2003)

[4] R.A. Street, K.W. Song, S. Cowan, Influence of series resistance on the photocurrent analysis of organic solar cells, Organic Electronics 12, 244–248, (2011)

[5] Y. Galagan, E. W. C. Coenen, S. Sabik, H. H. Gorter, M. Barink, S. C.Veenstra, J. M. Kroon, R. Andriessen, P. W. M. Blom, Evaluation of ink-jet printed current collecting grids and busbars for ITO-free organic solar cells, SOL. ENERG. MAT. SOL. C. 104, 32–38, (2012)

[6] N. M. Ahmed, Z. Sauli, U. Hashim, Y. A. Douri, Investigation of the absorption coefficient, refractive index, energy band gap, and film thickness for Al0.11Ga0.89N, Al0.03Ga0.97N, and GaN by optical transmission method, Int. J. Nanoelectronics and Materials **2,** 189-195, (2009)

[7] N. Koch, Organic Electronic Devices and Their Functional Interfaces, ChemPhysChem 8, 1438 – 1455, (2007)

[8] N. Koch, A. Vollmer, A. Elschner, Influence of water on the work function of conducting poly(3,4-ethylenedioxythiophene)/poly(styrenesulfonate), Appl.Phys. Lett. 90, 043512, (2007)

[9] T. Nagata, S. Oh, T. Chikyow, Y. Wakayama, Effect of UV–ozone treatment on electrical properties of PEDOT:PSS film, Org. Electron. 12,279-284, (2011)

[10] C. Tengstedt, A. Kanciurzewska, M. P. de Jong, S. Braun, W. R. Salaneck, M. Fahlman, Ultraviolet light–ozone treatment of poly (3,4-ethylenedioxy-thiophene)-based materials resulting in increased work functions, Thin Solid Films 515, 2085–2090, (2006)

[11] M. G. Helander, Z. B. Wang, M. T. Greiner, Z. W. Liu, K. Lian, Z. H. Lu, The effect of UV ozone treatment on poly (3,4-ethylenedioxythiophene) : poly(styrenesulfonate), Appl. Phys. Lett. 95, 173302 (2009)

[12] M. Trung Dang, G. Wantz, H. Bejbouji, M. Urien, O. J. Dautel, L. Vignau, L. Hirsch, Polymeric solar cells based on P3HT:PCBM: Role of the casting solvent, Solar Energy Materials & Solar Cells 95, 3408–3418, (2011)

[13] J.F. Chang, B. Sun, D.W. Breiby, M.M. Nielsen, T.I. Solling, M. Giles, I. McCulloch, H. Sirringhaus, Enhanced mobility of poly(3-hexylthiophene) transistors by spin-coating from high-boiling-point solvents, Chem. Mater. 16, 4772–4776, (2004)

[14] H. Yu, Different solvents effect on the performance of the solar cells based on poly(3-hexylthiophene):methanofullerenes, Synthetic Metals 160, 2505–2509, (2010)

[15] M. T. Dang, L. Hirsch, G. Wantz, P3HT:PCBM, Best Seller in Polymer Photovoltaic Research, Adv. Mater., 23, 3597–3602, (2011)

[16] M. Sanyal, B. S. Hansberg, M. F. G. Klein, C. Munuera, A. Vorobiev, A. Colsmann, P. Scharfer, U. Lemmer, W. Schabel, H. Dosch, E. Barrena, Effect of Photovoltaic Polymer/Fullerene Blend Composition Ratio on Microstructure Evolution during Film Solidification Investigated in Real Time by X-ray Diffraction, Macromolecules, 44, 3795–3800, (2011)

[17] D. Chirvase, J. Parisi, J. C. Hummelen, V. Dyakonov, Influence of nanomorphology on the photovoltaic action of polymer–fullerene composites, Nanotechnology 15, 1317–1323, (2004)

[18] S. S. van Bavel, M. Barenklau, G. de With, H. Hoppe, J. Loos, P3HT/PCBM Bulk Heterojunction Solar Cells: Impact of Blend Composition and 3D Morphology on Device Performance, Adv. Funct. Mater., 20, 1458–1463, (2010)

[19] I. A. Howard, R. Mauer, M. Meister, F. Laqua, Effect of Morphology on Ultrafast Free Carrier Generation in Polythiophene:Fullerene Organic Solar Cells, J. AM. CHEM. SOC., *132*, 14866–14876, (2010)

[20] B. Ray, P. Nair, M. A. Alam, Annealing dependent performance of organic bulkheterojunction solar cells: A theoretical perspective, Solar Energy Materials & Solar Cells 95, 3287–3294, (2011)

[21] H. Kim, W. W. So, S. J. Moon, The importance of post-annealing process in the device performance of poly(3-hexylthiophene): Methanofullerene polymer solar cell, Solar Energy Materials & Solar Cells 91, 581–587, (2007)

[22] H. Kim, W. W. So, S. J. Moon, Effect of Thermal Annealing on the Performance of P3HT/PCBM Polymer Photovoltaic Cells, J KOREAN PHYS SOC, 48, 3, (2006)

[23] D. Chirvase, Z. Chiguvare, M. Knipper, J. Parisi, V. Dyakonov, J. C. Hummelen, Temperature dependent characteristics of poly(3-hexylthiophene)-fullerene based heterojunction organic solar cells, J. Appl. Phys., Vol. 93, 6, 15, (2003)

[24] A. J. Pearson, T. Wang, R. A. L. Jones, D. G. Lidzey, Rationalizing Phase Transitions with Thermal Annealing Temperatures for P3HT:PCBM Organic Photovoltaic Devices, Macromolecules, 45, 1499−1508, (2012)

[25] G. Li, Y. Yao, H. Yang, V. Shrotriya, G. Yang, Y. Yang, "Solvent Annealing" Effect in Polymer Solar Cells Based on Poly(3-hexylthiophene) and Methanofullerenes, Adv. Funct. Mater., 17, 1636–1644, (2007)

[26] S. Miller, G. Fanchini, Y.Y. Lin, C. Li, C.W. Chen, W. F. Su, M. Chhowalla, Investigation of nanoscale morphological changes in organic photovoltaics during solvent vapor annealing, J. Mater. Chem., 18, 306–312, (2008)

[27] M. Campoy-Quiles, T. Ferenczi, T. Agostinelli, P.G. Etchegoin, Y. Kim, T.D. Anthopoulos, et al., Morphology evolution via self-organization and lateral and vertical diffusion in polymer: fullerene solar cell blends, Nature Materials 7, 158–164, (2008)

[28] L. Zeng, C.W. Tang, S.H. Chen, Effects of active layer thickness and thermal annealing on polythiophene: fullerene bulk heterojunction photovoltaic devices, Applied Physics Letters 97, 053303–053305, (2010)

[29] H. Kim, M. Shin, J. Park, Y. Kim, Effect of long time annealing and incident light intensity on the performance of polymer: fullerene solar cells, IEEE Transactions on Nanotechnology 9, 400–406, (2010)

[30] G. Dennler, M. C. Scharber, C. J. Brabec, Polymer-Fullerene Bulk-Heterojunction Solar Cells, Adv. Mater., 21, 1323–1338, (2009)

[31] S. T. Turner, P. Pingel, R. Steyrleuthner, E. J. W. Crossland, S. Ludwigs, D. Neher, Quantitative Analysis of Bulk Heterojunction Films Using Linear Absorption Spectroscopy and Solar Cell Performance, Adv. Funct. Mater, 21, 4640, (2011)

[32] Y.S. Kim, Y. Lee, J. K. Kim, E.O. Seo, E. W. Lee, W. Lee, S. H. Han, S. H. Lee, Effect of solvents on the performance and morphology of polymer photovoltaic devices, Current Applied Physics 10, 985–989, (2010)

[33] F. Reisdorffer, O. Haas, P. Le Rendu, T.P. Nguyen, Co-solvent effects on the morphology of P3HT:PCBM thin films, Synthetic Metals 161, 2544– 2548, (2012)

[34] J. H. Huang, F. C. Chien, P. Chen, K. C. Ho, C. W. Chu, Monitoring the 3D Nanostructures of Bulk Heterojunction Polymer Solar Cells Using Confocal Lifetime Imaging, *Anal. Chem.*, *82*, 1669–1673, (2010)

[35] Y. Hirose , A. Kahn, V. Aristov, P. Soukiassian, V. Bulovic, S.R. Forrest, Chemistry and electronic properties of metal-organic semiconductor interfaces: Al, Ti, In, Sn, Ag, and Au on PTCDA. Physical Review B, 54: 13748–13758, (1996)

[36] D. Gupta, M. Bag, and K. S. Narayan, Correlating reduced fill factor in polymer solar cells to contact effects, Appl. Phys. Lett., vol. 92, 093301, 1-3, (2008)

[37] P. P. Boix, G. G. Belmonte, U. Muñecas, M. Neophytou, C. Waldauf, R. Pacios, Determination of gap defect states in organic bulk heterojunction solar cells from capacitance measurements, Appl. Phys. Lett. 95, 233302, (2009)

Chapter 4 - Processing and Device Analysis studies for newly synthesized polymers

In order to further improve PCE and overall device performance, the optical band gap of the electron donating polymer can be altered. In this chapter, by applying the knowledge and similar fabrication parameters gained in Chapter 3 for our reference device, newly synthesized polymers are investigated. Initially, a perfluorinated derivative of APFO-3 polymer is studied. The introduction of fluorine (the most electronegative element) is expected to lower the end-polymer's energy levels and result in improved photovoltage values. Moreover, a family of conjugated polymers based on the BODIPY moiety was optically and electrically characterized.

4.1 Pentafluoro Derivative[1]

4.1.1 Introduction

The rapid increase in PCE observed the last few years for organic solar cells is mainly attributed to better understanding of the physics governing charge generation, transportation and collection. As mentioned in Chapter 2 overall photovoltaic device performance depends on obtained Voc, Jsc and FF values. The challenges in designing a new p-type conjugated polymer lie in fulfilling a number of diverse and sometimes overlapping properties such as increased light harvesting from smaller optical band gap, optimal charged species transportation and lowered HOMO level for Voc enhancement. To this end, various moieties and organic groups have been utilized. Fluorinated organic molecules have received great attention in chemistry due to interesting and unique properties such as oxidation stability[1], low degradation[2] and high hydrophobicity[3]. These features are assigned to the high electronegativity of fluorine, which has the smallest electron withdrawing atoms of the periodic table (van der Waals radius 0.25 Å larger than hydrogen). Upon incorporation in conjugated polymers, fluorine is expected to stabilize the lowest unoccupied and the highest occupied molecular orbitals, LUMO and HOMO, respectively[4]. Moreover, concerning conjugated polymers, there is an established notion that a weak donor-strong acceptor copolymerization approach can yield desirable optoelectronic characteristics in the

[1] This work has been published as M. Neophytou, H. A. Ioannidou, T. A. Ioannou, C. L. Chochos, S. P. Economopoulos, P. A. Koutentis, G. Itskos, S. A. Choulis, 2-(2,3,4,5,6-Pentafluorophenyl)-1H-benzo[d]imidazole, A Fluorine-Rich Building Block for the Preparation of Conjugated Polymer Donors for Organic Solar Cells Applications in Polymer Chemistry.

end-material[5, 6]. As fluorine can enhance the electronegativity of a given moiety, the use of fluorinated analogues in organic solar cells has led to enhanced power conversion efficiencies[7, 8, 9].

Based on the considerations mentioned above, we opted to include the perfluorophenyl moiety into a polymeric structure aiming at increasing the acceptor character of the well studied benzo[*d*]imidazole functional unit, before polymerizing with an electron donor co-monomer. Optical and current density characteristics of these materials were investigated and compared with those of benzo[1,2,5]thiadiazole, the donor-acceptor-donor (D-A-D) thiophene-benzo[1,2,5]thiadiazole-thiophene (TBZT) segment and the well-studied donor-acceptor (D-A) polyfluorene copolymer APFO-3[10, 11].

4.1.2 Experimental

Film absorption was carried out using a Lambda 1050 UV/Vis/NIR spectrophotometer (Perkin Elmer). Polymers were diluted in chlorobenzene and were homogeneously deposited on 3 × 7 cm microscopic glasses with doctor blading. Blade speed was set at 30 mm/sec while the substrate temperature was at 60 °C.

For device preparation, pre-patterned ITO substrates were cleaned primarily with acetone and then with isopropanol in an ultra sonic bath for 10 min. Afterwards, a thin layer of PEDOT/PSS (Clevios^{TM} PH) was doctor bladed on top with a measured thickness of 50 nm. Thermal annealing of the deposited layer was performed to ensure the removal of any residual solvent from the deposited film. On top of that, the optically active layer consisting of APFO-3 and PFTPFBZT (Figure 1) blended with

PCBM at different ratios in each case, was deposited[12]. Polymers and fullerene derivative were separately diluted overnight in chlorobenzene[13] at 70 °C and were mixed 1 h prior deposition. Various parameters were used to achieve an average thickness of 70 nm for both layers. Thickness measurements, performed with a Veeco profilometer, were followed by thermal deposition of the bi-metal cathode consisting of 1 nm of LiF and 80 nm of Al. The effective photovoltaic area was defined by the geometrical overlapping between anode and cathode and was measured to be 9 mm^2. A Keithley 2420 source meter recorded the current density vs voltage (J/V) characteristics under 100 mW/cm^2 irradiance and at 1.5 A.M. conditions with a Newport solar simulator.

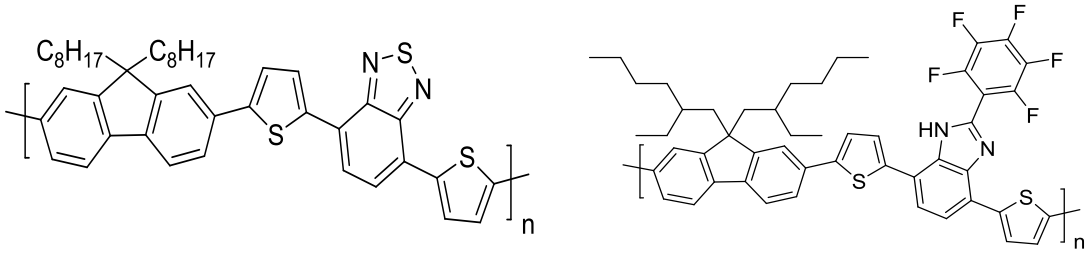

Figure 1: Chemical structures of the APFO-3 and PFTPFBZT

4.1.3 Results and Discussion

The characterization of the synthesized materials took place both in solution and in the solid state. Since the synthesized polymer shares structural similarities to the APFO-3 copolymer, the building blocks and the polymers were examined side-by-side to help elucidate the role of the fluorinated benzimidazole *versus* the

benzothiadiazole units when forming donor-acceptor-donor (D-A-D) triads with thiophene.

The polymer PFTPFBZT in thin films exhibits single absorption peaks at 451 nm. In contrast, the APFO-3 spectrum shows two well-resolved peaks at 383 and 530 nm. The two-peak absorption is typically considered as an optical signature of a successful push-pull molecule interaction[14] exhibiting intramolecular charge transfer. The single-peaked spectrum and the relatively large optical bandgap of 2.25 eV of PFTPFBZT indicate a rather unsuccessful attempt at the donor-acceptor approach. Furthermore, when compared to established light harvesting polymers such as regioregular RR-P3HT and APFO-3, the newly synthesized PFTPFBZT shows a lower absorption coefficient by a factor of ~2 (Figure 2).

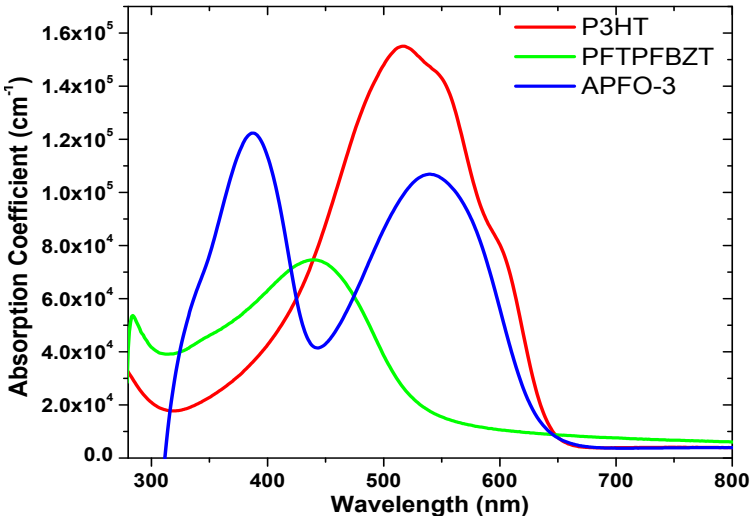

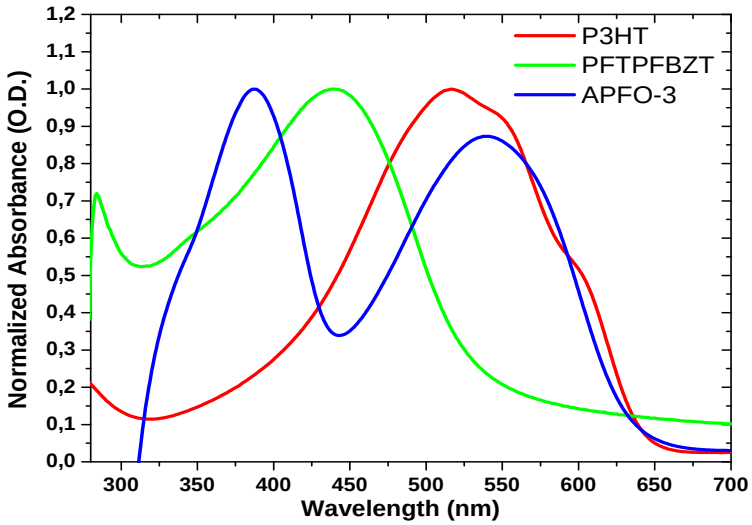

Figure 2: Absorption coefficient (upper) and normalized absorption (bottom) spectra of PFTPFBZT (green line) compared to regioregular P3HT (red line) and APFO-3 (blue line).

The PFTPFBZT polymer was evaluated on its power conversion efficiency in polymer-fullerene solar cells. Figure 3 summarizes J/V device performance for both APFO-3/PCBM and PFTPFBZT/PCBM systems.

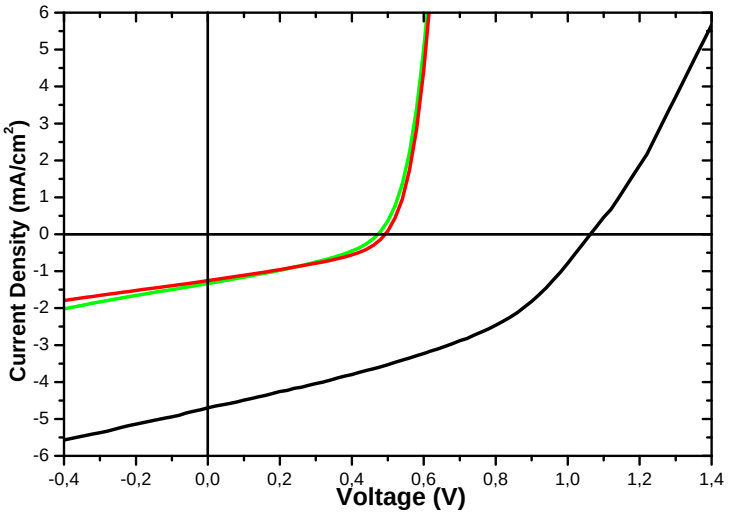

Figure 3: J/V characteristics of photovoltaic devices based on PFTPFBZT/PCBM at 1:3 (green line) and 1:4 (red line) ratio compositions and compared with APFO-3/PCBM (black line) that was used as reference device.

The obtained photovoltaic parameters such as open circuit voltage (Voc), short circuit current density (Jsc), fill factor (FF) and power conversion efficiency (PCE) of the 3 blends are summarised in Table 1.

Table 1: Summarizes photovoltaic parameters acquired from illuminated J/V device characteristics.

Active Layer	Voc (V)	Jsc (mA/cm^2)	FF (%)	PCE (%)
APFO-3/PCBM (1:4)	0.96	4.49	40.5	1.75
PFPFBZT/PCBM (1:3)	0.47	1.33	36	0.22
PFPFBZT/PCBM (1:4)	0.49	1.25	38.8	0.24

When PFTPFBZT/PCBM was used as the optically active layer, lower Voc values were obtained in comparison with devices with APFO-3/PCBM. This could be partially explained by the difference in HOMO of the two fluorene-based copolymers, as the difference between electron donor's HOMO and electron acceptor's LUMO mainly defines photovoltage. The obtained Voc values are significantly lower than the theoretical maximum potential and in combination with FF values; this suggests possible recombination losses and morphological limitations obtained for both PFPFBZT/PCBM concentrations. A small Voc and FF enhancement in the case of the 1:4 blend is mainly attributed to the slight (5 %) increase of PCBM into the blend, possibly resulting in minor morphological improvement. In general, only incoming photons with energy larger than the optical band gap (E_g) of the polymer are absorbed by the active layer. Low Jsc values for PFPFBZT are due to the moderate E_g of 2.25 eV, which was calculated from the UV-Vis spectrum. Concerning the 1:4 ratio

devices, despite the fact that more PCBM results in higher Voc values, this reduces the effective photon absorber (polymer) proportion in the blend and the consequence is reflected as lower Jsc value when comparing it to the 1:3 blend.

4.1.4 Conclusions

A novel polymer bearing the pentafluorophenyl moiety as a side chain has been studied. The aim was to investigate the effect of a strong electron withdrawing monomer unit, when copolymerized with the well studied electron donating moiety of fluorine. Upon copolymerization with fluorene, a copolymer with a relatively high bandgap of 2.25 eV was obtained. Optical and electrochemical characterization strengthened the notion that, most likely, intramolecular interactions did not take place, resulting in a minimal lowering of the energy bandgap. Efficient emission quenching of the polymer emission within a blend with PCBM, however, indicates the presence of a fast exciton dissociation at the polymer:fullerene interface. Photovoltaic efficiency measurements were carried out using PCBM and showed a maximum power conversion efficiency of 0.24 %.

4.2 The BODIPY family[2]

4.2.1 Introduction

As stated previously in paragraph 2.3.2, conjugated low band gab (Eg < 2eV) polymers that absorb broader sun spectrum and have better transport properties than existing ones, are needed in order to achieve higher PCE. These should possess a functional LUMO alignment with the electron acceptor's energy levels, with lowered donor's LUMO and a deep HOMO level in respect to vacuum level. The former will reduce the interfacial exciton dissociation ability of the system and the latter will increase polymer oxidation and degradation stability and at the same time will increase the open circuit voltage of the device (Voc). In this chapter a class of fluorescent 4,4′-difluoro-4-bora-3a,4a-diaza-s-indacenes conjugated polymers (BODIPY) is described, that are considered novel electron donor candidates for organic photovoltaics by achieving high photovoltage values. BODIPY dyes have recently attracted considerable attention owed mainly to their interesting optical properties[15,16]. Despite being introduced a few years ago, a large number of donor-acceptor hybrids have already been prepared, either with fullerenes or with other molecular electron acceptors, which is a testament to their potential. Polymers incorporating the BODIPY moiety, however, are still scarce and solar cells with BODIPY-based polymers as the electron donor yield relatively low efficiencies[17, 18], attributed mainly to low charge carrier mobilities[19].

---

[2] This work is in preparation as M.Neophytou D. Baran, C. J. Brabec and S. A. Choulis, *Photovoltaic loss analysis of BODIPY:PCBM based organic solar cells*, Organic Electronics, (2012).

In light of the above, several new BODIPY-based polymers synthesized within the MEP research unit were selected and studied with the homopolymerized BODIPY poly(*4,4-difluoro-4-bora-3a,4a-diaza-s-indacene*) (PB) set as reference. Different moieties were introduced to the polymeric backbone creating 4 new polymers using: ethelene (PBE), thiophene (PBT), dithiophene (PBTT) and thiophene-benzothiadozole-thiophene (PBTBT) as comonomers (Figure 4). The effect of each additional structural unit on matching the sunlight spectrum or improving charge carrier mobility and photovoltaic device performance were investigated. The chemical structures of these polymers are schematically depicted in Figure 4.

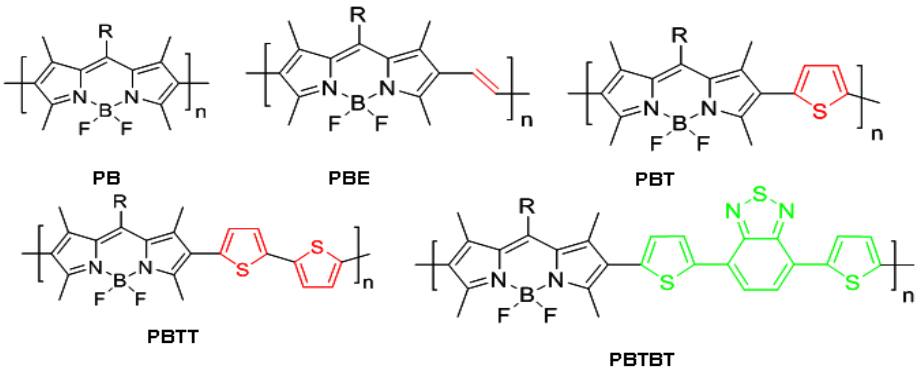

Figure 4: Chemical structure of newly synthesized BODIPY polymers.

4.2.2 Experimental

Absorption measurements were carried out with a Perkin Elmer Lambda 1050 UV/Vis/NIR spectrophotometer. Thin films of each polymer were doctor bladed on glass substrates in ambient conditions. In order to measure hole mobility space charge limited current (SCLC) devices were fabricated for only polymer and polymer:fullerene derivative blends. Charge carriers were selectively suppressed by the addition of an extra PEDOT:PSS layer on top of the optically active film. Pre

patterned ITO glass substrates were cleaned in an ultrasonic bath with acetone and isopropanol. The deposited optically active layer was sandwiched between the two electrodes, consisting of an ITO/PEDOT:PSS anode and a thermally evaporated metal bi-layer Ca/Ag cathode. Devices were fabricated in ambient conditions. A standard silicon diode calibrated Newport Corporation (http://www.newport.com/) solar simulator with an input power of 100 mW/cm^2 white light illumination was employed for the current density versus voltage (J/V) characteristics of the fabricated devices. Data obtained in dark and under illumination were analyzed. Atomic force microscopy (AFM) images for morphological analysis of the active layers were acquired with a Veeco Model D3100 in tapping mode. Height images are shown with 5 × 5 μm image size.

4.2.3 Results and Discussion

As light harvesting is mainly attributed to the polymer and is an important component for photovoltaic materials, optical absorbance was the first property to be investigated. Pristine BODIPY-polymers were diluted in chlorobenzene (CB) and were doctor bladed on glass substrates at 70 °C. The samples were probed at two different spots and similar spectra concerning line shape and strength, were obtained, suggesting layer homogeneity. All polymers showed dominant absorption coefficient peaks in the region of 565-600 nm (Figure 5) attributed to the BODIPY moiety and a higher energy absorption band in the 300-450 nm region, with PBE exhibiting the broader absorbance in the UV-Visible. Polymer PB shows weak absorption strength

and a long wavelength tail probably attributed to enhanced light scattering. PBTT and PBE polymers display significantly higher absorption coefficient in comparison to other BODIPY polymers and to the well studied P3HT, which was used for comparison.

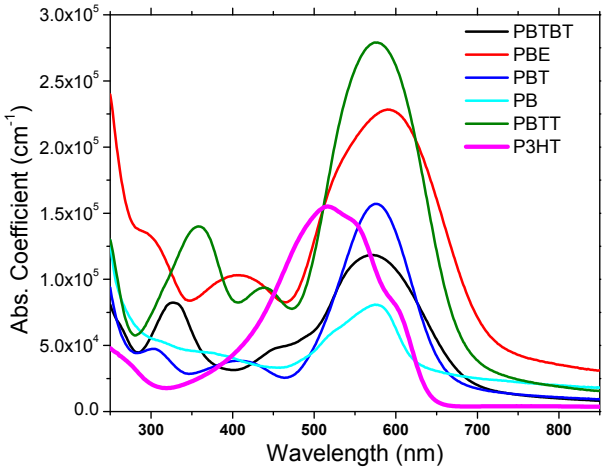

Figure 5: Optical absorption coefficient and normalized absorption spectra in the UV-Vis region of pristine BODIPY polymers in comparison with P3HT

Redox properties of BODIPY-based polymers were evaluated using cyclic voltammetry. Electrochemical band gap and HOMO-LUMO energy levels are summarized in Table 2.

Table 2: Summary of absorption, emission and energy levels of the BODIPY polymers

Compounds	λ_{max}^{sol} (nm)	λ_{max}^{film} (nm)	E_g^{opt} (eV)	Pl_{max}^{sol} (nm)	Pl_{max}^{film} (nm)	E_{LUMO} (eV)
PB	580	577	1.97	603	690, 740	3.47
PBT	568	577	1.87	659	696	3.56
PBTT	560	576	1.81	679	716	3.60
PBE	604	592	1.73	688	735	3.55
PBTBT	552	573	1.79	674	720	3.59

To assess the photophysical properties (Figure 6) of the above mentioned polymers the photoluminescence (PL) response was measured. Solid state layers were deposited from chlorobenzene solution and were measured under a photo-excitation wavelength of 575-580 nm, which corresponds to the respective absorption peak maxima of each polymer.

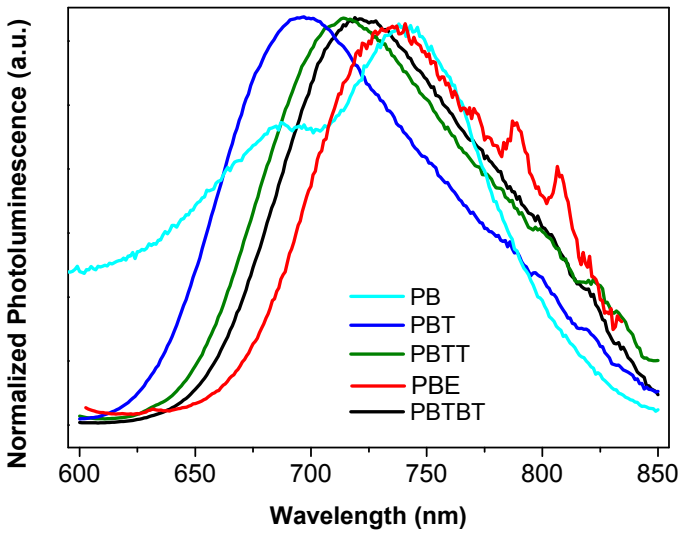

Figure 6: Normalized photoluminescence (PL) for newly synthesized polymers containing the BODIPY moiety

Interesting points are the large apparent Stokes shifts in solutions in all materials except in the case of PB. The large Stokes shift indicates a high energetic relaxation of excitations after absorption as a result of diffusion and/or energy transfer to local parts of the molecules (Table 2). Slightly larger Stokes shifts are seen in the films, as expected[20].

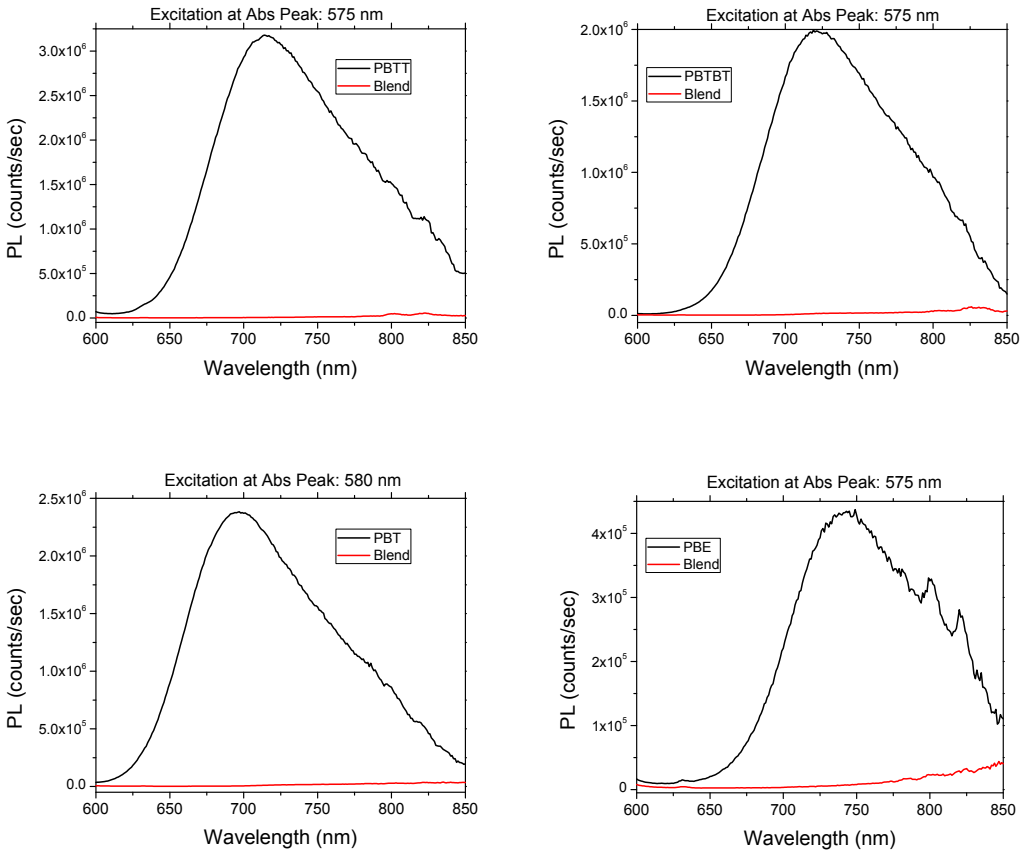

Figure 7: Emission spectra of pristine BODIPY polymers (black line) and polymer:PCBM blends (red line) depicting efficient phtoluminescence quenching.

As shown in Figure 7, highly efficient emission quenching is observed for the high intensity peak at 720 mn of PBTBT upon addition of PCBM. For polymer PBE, a weak emission centered around 740 nm is seen. The peaks observed in the near-IR region most probably come from the substrate. Highly efficient quenching of blend emission is observed at PBT with a longer wavelength emission appearing at $\lambda s>700$ nm that could possibly be due to charge transfer (CT) exciton radiative recombination. The highly photoluminescent PBTT with peak at ~715 nm is also efficiently quenched when blended with PCBM. The emission spectra for PBTT:

PCBM blends provide no indication of CT exciton radiative recombination nor remnant emission from the polymer (close to unity polymer exciton dissociation). Any differences in PL quenching can be understood in terms of the strength of electron donor:acceptor interaction, which clearly affects the excited states.

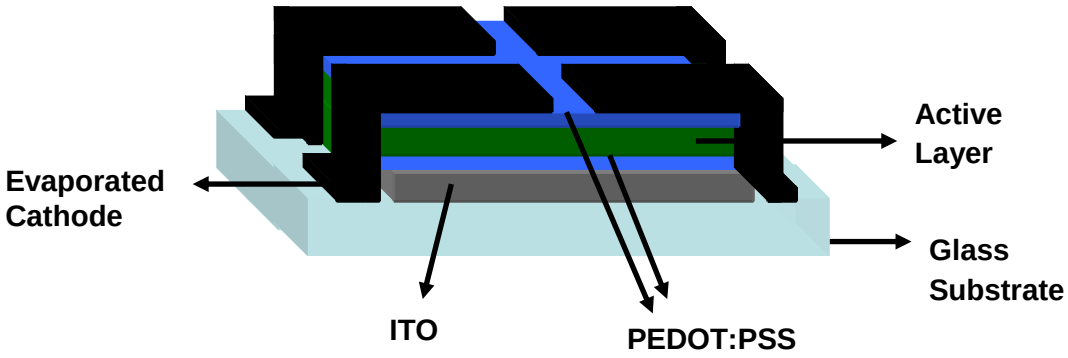

Figure 8: Device architecture for the SCLC measurements. Negatively charged carriers are suppressed by the insertion of an extra PEDOT:PSS layer below the evaporated metal cathode.

Various types of charge transport mechanisms have been deployed for organic semiconductors, but for this chapter SCLC measurements were chosen as they are closer to device operational conditions[21]. It has been reported that charge carrier's mobility can be determined from dark current density Vs voltage (J/V) characteristics by utilizing the appropriate electrodes which suppress one of the two species[22, 23, 24]. In theory, as charged species have to travel within the bulk a relatively long way until they reach respective electrodes, hopping between the polymeric chains takes place. In this way SCLC may also provide an indication about interpolymer interactions. Herein, hole-only devices consisting of ITO/PEDOT/polymer or polymer:fullerene derivative/PEDOT/Ag were fabricated and characterized. The SCLC device structure

is schematically depicted in Figure 8. Mobility data are shown in Table 2 and SCLC measurements were approximated by the following equation:

$$J_{SCLC} = \frac{9}{8} \varepsilon_0 \varepsilon \mu \frac{V^2}{L^3} e^{\frac{0,89\beta}{\sqrt{L}}\sqrt{V}} \quad (1)$$

Where β is the field activation factor, L is the thickness of the specimen, V the applied voltage, $\varepsilon_o\varepsilon$ are defined as electrical permittivity and μ is the hole zero field mobility.

Table 3: Space charge limited current measurements for pristine polymers and polymer:fullerene blends.

Sample	B	Mobility (μ) [cm²/V.s]
PBTBT	0	1.43×10^{-5}
PBTBT:$PC_{70}BM$	1.38×10^{-4}	6.60×10^{-6}
PBE	0	4.01×10^{-5}
PBE:$PC_{70}BM$	1.84×10^{-4}	1.60×10^{-5}
PBT	0	6.12×10^{-6}
PBT:$PC_{60}BM$	2.3×10^{-4}	4.41×10^{-6}
PB	0	2.60×10^{-5}
PB:$PC_{60}BM$	1.78×10^{-4}	3.60×10^{-5}
PBTT	0	4.2×10^{-5}
PBTT:$PC_{60}BM$	8.81×10^{-5}	6.9×10^{-5}

Hole mobility of almost two orders of magnitude higher than previously reported in the literature[25] were obtained with PBTT presenting the higher values in the order of 4.2×10^{-5} cm^2/Vs, which was increased to nearly 7×10^{-5} cm^2/Vs when $PC_{60}BM$ was added, in a final ratio of 1:4. Fullerene addition on the other hand, diminished hole

mobility for other polymers, with PBTBT exhibiting lower values by nearly one order of magnitude. These mobility values can be explained as reduced polymer-polymer interactions due to the fact that polymers had low molecular weight. As will be discussed below, this could also contribute to increased nanoscale phase separation morphology for the polymer:fullerene blends.

To get a better insight into the morphology of the polymer:fullerene blends, tapping mode AFM height and phase images were taken. Figure 9 shows the topography of each polymer when blended with electron acceptor. PBTBT and PBT films provide smoother surface characteristics with root mean squared (rms) (height differences) of 18 nm and 30 nm respectively. PB, PBE and PBT exhibit higher rms values in the order of 200 nm suggesting unfavorable morphology and the formation of large domains. The higher phase segregation for PBE:$PC_{70}BM$ films correlates well with the photovoltaic performance data (Figure 10) and weak PL intensity reported. Smoother layers would result in a better contact of the active layer with the evaporated metal cathode but, as discussed below for J/V characteristics, this is not the case. Both PBTBT and PBT polymers exhibit high Rs values and vertical segregation is the most likely explanation for this phenomenon.

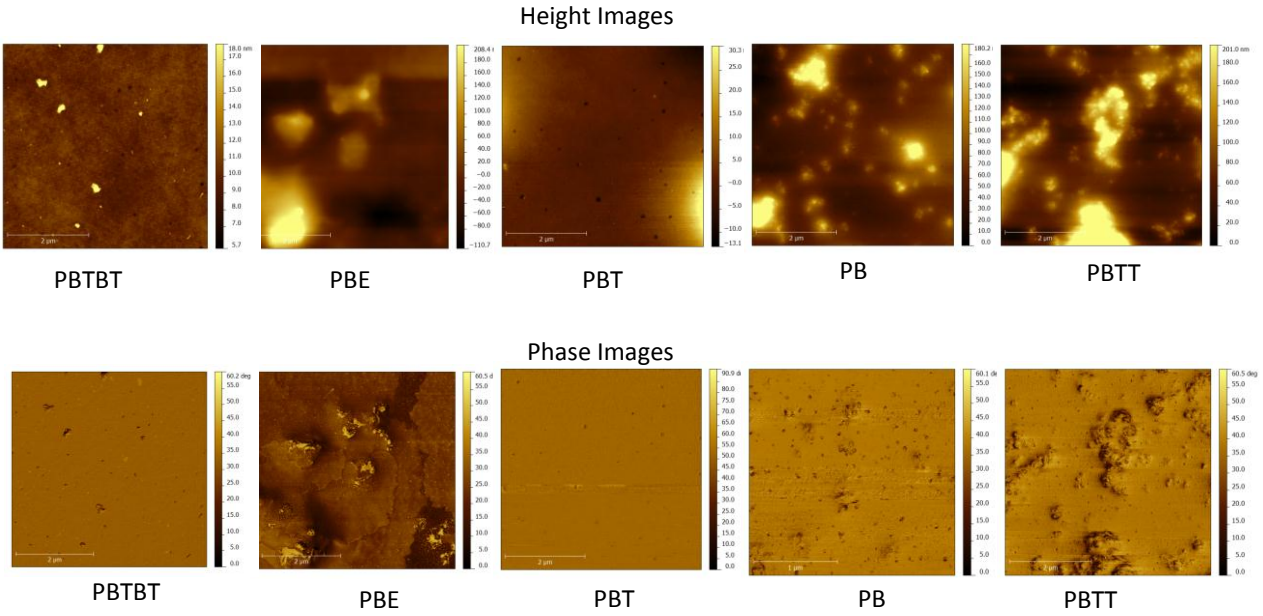

Figure 9: Tapping mode AFM (a) height and (b) phase images of the optically active layer

The thienyl thiophene derivative (PBTT) exhibited the best device performance. This could be attributed to enhanced internal light scattering and thus improved light absorption, which comes in compliance with higher absorption coefficient data. At the same time, large domains formed for PE photovoltaic devices, which lead to interconnected anode and cathode resulting in shunts for the fabricated solar cell devices. In all cases donor:acceptor domains exceed the exciton's dissociation length (~10nm)[26,27] explaining low hole mobility from SCLC and limited FF from J/V data. A solar cell device structure of ITO/PEDOT:PSS/active layer/Ca/Ag was used and the optimum electron donor:acceptor ratio was found to be 1:4. After thermal evaporation of the cathode, devices were measured under 1 sun 1.5 A.M. conditions and the resulting parameters are summarized in Figure 11. From illuminated J/V characteristics (Figure 10), PBTT exhibits the highest photocurrent value, as expected

from the absorption spectra of Figure 5, while PBE which also showed a high absorption coefficient, demonstrated significantly lower values. In combination with low V_{oc} in the case of PBE, unfavourable morphology and hindered exciton dissociation ability is suggested.

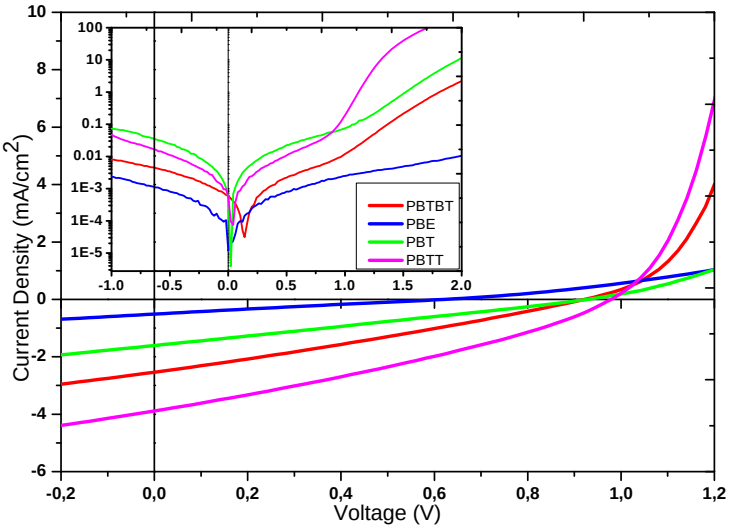

Figure 10: Current density vs. voltage representative characteristics of BODIPY:fullerene derivatives under 100 mW/cm^2 illumination and in dark conditions (inset)

This is in accordance with AFM data where inefficient phase morphology was observed, resulting in extensive exciton recombination. High photovoltage values are observed for the other polymers in compliance with the cyclic voltammetry values and HOMO-LUMO energy difference. For the polymers PBTBT and PBT, ohmic contributions between metal contact and the active layer is the drawback as seen in high serial resistance (Rs) which limits fill factor values and is also suggested by the SCLC measurements. In general, fill factor depends on the charge carrier mobility of

the polymer and available pathways so that carriers reach respective electrodes and the internal driving force.

Ultimately, PBTT exhibits the best solar cell device performance between all BODIPY derivatives being reported in this chapter with a short circuit current (J_{sc}) of 4 mA/cm^2, V_{oc} of around 1 V, fill factor of 34 % and photon to electron conversion efficiency of 1.2 %. Thermal annealing had no noticeable effect on the device performance as it does on the P3HT:PCBM system.

It was not possible to obtain assessable signals from devices using PB polymer. This was mainly due to solubility problems but also because of the presence of internally deficient interpenetrating networks.

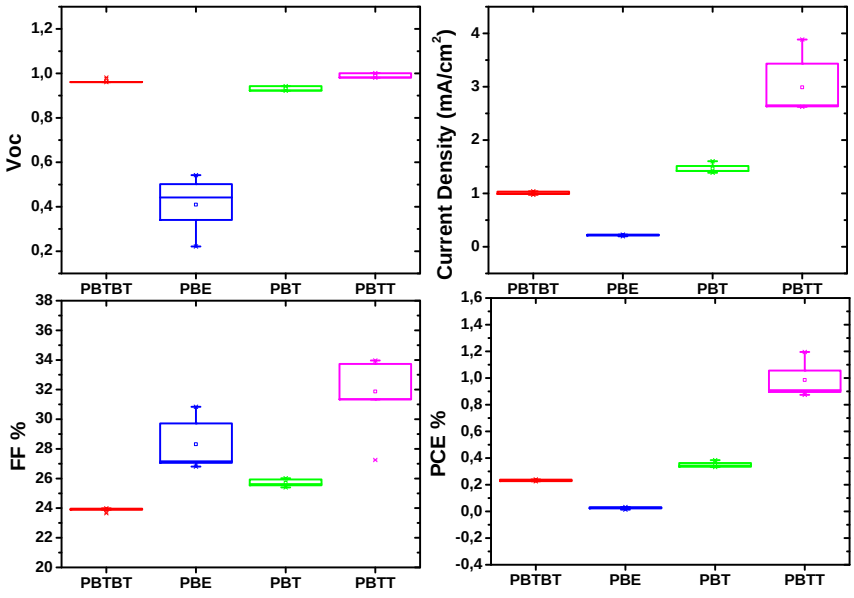

Figure 11: Summary of the device performance for polymer :fullerene blends

4.2.4 Conclusion

In summary, low charge carrier mobility, light harvesting ability and morphology are the main bottlenecks for enhanced PCE. However, despite the exhibited low mobility values, the newly synthesized BODIPY-based polymers are attractive candidates as electron donors due to their high absorption coefficient and high photovoltage values, exceeding 1 V. Mobility of charge species could be improved using higher molecular weight polymers. If higher carrier mobility can be achieved, the amount of electron donating polymer in the blend can be increased, and thicker films can be fabricated resulting in better photon absorption.

4.3 Bibliography

[1] M.P.C. Conrad, M. S. Shoichet, Synthesis and thermal stability of hybrid fluorosilicone polymers, Polymer 48, 5233-5240, (2007).

[2] K. Reichenbächer ,H.I. Süss, J. Hulliger, Fluorine in crystal engineering-"the little atom that could", Chem. Soc. Rev.,34, 22-30, (2005).

[3] M.G. Dhara, S. Banerjee, Fluorinated high-performance polymers: Poly(arylene ether)s and aromatic polyimides containing trifluoromethyl groups, Prog. Polym. Sci. 35, 1022–1077, 1023, (2010).

[4] B. C. Schroeder, Z. Huang, R. S. Ashraf, J. Smith,P. D'Angelo, S. E. Watkins, T. D. Anthopoulos, J. R. Durrant, I. McCulloch, Silaindacenodithiophene-Based Low Band Gap Polymers – The Effect of Fluorine Substitution on Device Performances and Film Morphologies, Adv. Funct. Mater., 22, 1663–1670, (2012).

[5] J. D. Yuen, J. Fan, J. Seifter, B. Lim, R. Hufschmid, A. J. Heeger, F. Wudl, High Performance Weak Donor_Acceptor Polymers in Thin Film Transistors: Effect of the Acceptor on Electronic Properties, Ambipolar Conductivity, Mobility, and Thermal Stability, J. Am. Chem. Soc., 133, 20799–20807, (2011).

[6] H. Zhou, L. Yang, S. Stoneking, W. You, A Weak Donor−Strong Acceptor Strategy to Design Ideal Polymers for Organic Solar Cells, ACS Appl. Mater. Interfaces, 2 (5), pp 1377–1383, (2010).

[7] S.C. Price, A. C. Stuart, L. Yang, H. Zhou, W. You, Fluorine Substituted Conjugated Polymer of Medium Band Gap Yields 7% Efficiency in Polymer-Fullerene Solar Cells, J. Am. Chem. Soc., 133, 4625–4631, (2011).

[8] H. Zhou, L. Yang, A. C. Stuart, S. C. Price, S. Liu, W. You, Development of Fluorinated Benzothiadiazole as a Structural Unit for a Polymer Solar Cell of 7% Efficiency, Angew. Chem. Int. Ed., 50, 2995 –2998, (2011).

[9] Y. Liang, Z. Xu, J. Xia, S. T. Tsai, Y. Wu, G. Li, C. Ray, L. Yu, For the Bright Future—Bulk Heterojunction Polymer Solar Cells with Power Conversion Efficiency of 7.4%, Adv. Mater., 22, E135–E138, (2010).

[10] C. M. B. Svanstrom, J. Rysz, A. Bernasik, A. Budkowski, F. Zhang, O. Inganas, M. R. Andersson, K. O. Magnusson, J. J. B. Smith, J. Nelson, E. Moons, Device Performance of APFO-3/PCBM Solar Cells with Controlled Morphology, Adv. Mater., 21, 4398–4403, (2009).

[11] C. M. Bjorstrom, S. Nilsson, A. Bernasik, A. Budkowski, M. Andersson, K. O. Magnusson, E. Moons, Vertical phase separation in spin-coated films of a low bandgap polyfluorene/PCBM blend—Effects of specific substrate interaction, Applied Surface Science 253, 3906–3912, (2007).

[12] L. M. Andersson, F. Zhang, O. Inganäs, Stoichiometry, mobility, and performance in bulk hetetrojunction solar cells, Applied Physics Letters, vol. 91, p. 071108, (2007).

[13] S. Nilsson, A. Bernasik, A. Budkowski, E. Moons, Morphology and phase segregation of spin-casted films of polyuorene/pcbm blends, Macromolecules, vol. 40, pp. 8291-8301, (2007).

[14] M. H. Chen, J. Hou, Z. Hong, G. Yang, S. Sista, L. M. Chen, Y. Yang, Efficient Polymer Solar Cells with Thin Active Layers Based on Alternating Polyfluorene Copolymer/Fullerene Bulk Heterojunctions, Adv. Mater., 21, 4238–4242, (2009).

[15] F. Li, S. I. Yang, Y. Ciringh, J. Seth, C. H. Martin, D. L. Singh, D. Kim, R. R. Birge, D. F. Bocian, D. Holten, J. S. Lindsey, Design, Synthesis, and Photodynamics of Light-Harvesting Arrays Comprised of a Porphyrin and One, Two, or Eight Boron-Dipyrrin Accessory Pigments, J. Am. Chem. Soc., 120, 10001-10017, (1998).

[16] M. D. Yilmaz, O. A. Bozdemir, E. U. Akkaya, Light Harvesting and Efficient Energy Transfer in a Boron-dipyrrin (BODIPY) Functionalized Perylenediimide Derivative, Org. Lett., Vol. 8, No. 13, (2006).

[17] T. Rousseau , A. Cravino , T. Bura , G. Ulrich , R. Ziessel, J. Roncali, Multi-donor molecular bulk heterojunction solar cells: improving conversion efficiency by synergistic dye combinations, J. Mater. Chem.,19, 2298-2300, (2009).

[18] T. Rousseau, A. Cravino, T. Bura, G. Ulrich, R. Ziessel, J. Roncali, BODIPY derivatives as donor materials for bulk heterojunction solar cells, Chem. Commun., 1673-1675, (2009).

[19] B. S. Kim, B. Ma, V. R. Donuru, H. Liu, J. M. J. Frechet, Bodipy-backboned polymers as electron donor in bulk heterojunction solar cells, Chem. Commun., 46, 4148–4150, (2010).

[20] J. F. Araneda, W. E. Piers, B. Heyne, M. Parvez, R. McDonald, High Stokes Shift Anilido-Pyridine Boron Difluoride Dyes, Angew. Chem. Int. Ed., 50, 12214 –12217, (2011).

[21] D. Braun, Electronic Injection and Conduction Processes for Polymer Devices, J Polym Sci Part B: Polym Phys 41: 2622–2629, (2003).

[22] P. W. M. Blom, M. J. M. de Jong, J. J. M. Vleggaar, Electron and hole transport in poly(pphenylene vinylene) devices, Appl. Phys. Lett. 68, 3308 (1996).

[23] A. Rose, Space-Charge-Limited Current, Phys. Rev. 97, 1538–1544 (1955).

[24] C. Melzer, E.J. Koop, V.D. Mihailetchi, P.W.M. Blom, Hole Transport in Poly(phenylene vinylene)/Methanofullerene Bulk-Heterojunction Solar Cells, Adv. Mater., 14, 9, (2004).

[25] B. S. Kim, B. Ma, V. R. Donuru, H. Liu, J. M. J. Frechet, Bodipy-backboned polymers as electron donor in bulk Heterojunction solar cells, Chem. Commun., 46, 4148–4150, (2010).

[26] S. Gunes,H. Neugebauer, N. S. Sariciftci, Conjugated Polymer-Based Organic Solar Cells, Chem. Rev. 107, 1324-1338, (2007).

[27] P. W. M. Blom, V. D. Mihailetchi, L. J. A. Koster, D. E. Markov, Device Physics of Polymer:Fullerene Bulk Heterojunction Solar Cells, Adv. Mater. 19, 1551–1566, (2007).

Chapter 5 - Inkjet Printed Optically Active Layer and Ag nanoparticle Current Collecting Grids

This chapter will focus on two major aspects that will advance the field of OPV towards mass production. The first part will focus on using inkjet printing for deposition of the active layer. A systematic study was undertaken to find the optimum parameters for inkjet printing the active layer and which further steps need to be taken to ensure even greater device efficiencies.

The second part will focus on replacing the expensive and brittle ITO in favor of a silver grid architecture that will still ensure sufficient light transmission and carrier selectivity but is significantly less expensive as it does not require energy consuming techniques to deposit. Again, a systematic study was undertaken to find the optimum parameters for a silver ink and PEDOT:PSS combination that yields efficient devices with a doctor bladed active layer.

5.1 Inkjet Printed Optically Active Layer[1]

5.1.1 Introduction

The first highly efficient organic solar cell by inkjet printing was reported by adjusting the chemical properties of a poly(3-hexylthiophene) polymer donor[1] and by using a novel inkjet solvent mixture[2]. Based on this work, control over the nano-morphology of poly(3-hexylthiophene):fullerene blends during the printing process was achieved, which yielded a power conversion efficiency of 3 – 3.5 %. Other recent papers have also reported PCEs for inkjet printed RR-P3HT:PCBM OPVs exceeding 3 % by using additives and combinations of different solvents[3,4]. Despite the recent progress in the field of inkjet printed OPVs, the influence of processing parameters on device PCE has not been investigated in the literature. The only previously published data focusing on processing conditions investigate drop spacing and pulse voltages and report a very low PCE in the range of 8×10^{-4} %[5]. In this chapter we present details on the processing conditions solution viscosity, substrate temperature, drop-spacing and nozzle-to-substrate distance. We show that the choice of parameters are critical to achieving high power conversion efficiency inkjet printed OPVs. Analysis in terms of one-diode equivalent circuit combined with current-voltage characteristics of the devices was performed to reveal the dominant loss mechanisms of the inkjet printed solar cells using these different processing conditions, whereby the device performance analyses help us to identify

[1] This work has been published as M. Neophytou, W. Cambarau, F. Hermerschmidt, C. Waldauf, C. Christodoulou, R. Pacios, S.A. Choulis, Inkjet-printed polymer–fullerene blends for organic electronic applications at Microelectronic Engineering 95, 102–106, (2012)

suitable processing conditions for inkjet printed organic solar cells. By using commercially available materials and a piezoelectric inkjet printer, the optimized printing process can produce OPVs with power conversion efficiency of 3.07 %. This is a PCE similar to that achieved with conventional spin coating and doctor blading processing methods.

5.1.2. Experimental

The application of printing technology as a fabrication tool for organic photovoltaics indicates the potential of these novel materials for future light-activated plastic power sources. One of the key advantages of the inkjet printing technique is the use of Drop-On-Demand (DOD) technology. The controlled deposition of the solution on specific locations on the substrate eliminates the need of patterning for the production of OPV modules. For the trials reported in this chapter ortho-dichlorobenzene (o-DCB) was used as a solvent. The deposition of the RR-P3HT:PCBM layer was performed by using a commercial piezoelectric driven inkjet head with a motorized xyz stage, a fiducial camera for substrate alignment and a drop watcher camera to control the drop shape.

RR-P3HT with average molecular weight of 50 kg mol^{-1} and ~95 % regioregularity was purchased from Rieke materials, [6,6]-phenyl C61 butyric acid methyl ester (PCBM) from Nano-C and the evaporated metal Ca/Ag top electrode materials purchased from Aldrich. Thickness measurements of the deposited layers were performed with a Veeco Dektak 150. A Keithley 2420 source meter was used for the current density vs. voltage characteristics (J/V). The active layer was deposited with

a Dimatix Fujifilm DMP 2831 inkjet printer using 254 μm nozzle spacing and 1 pL droplet volume cartridges.

15 mg RR-P3HT and 12 mg PCBM were diluted separately in pristine o-DCB (solvent amount varied as indicated in Figure 2) and stirred overnight at 85 ˚C. After approximately 12 hours the two separated solutions were mixed and stirred at 85 ˚C until solution homogeneity was achieved. Before inserting the mixture into the cartridge, the ink-formulation was filtered with a 0.2 μm teflon filter and left in a vertical position for 30 minutes to remove air bubbles which could interfere in the printing process. The cartridge temperature was set at 66 ˚C to achieve the appropriate solution viscosity essential to avoid nozzle clogging. The droplet firing voltage was set at 11 V, the tickle control frequency at 5 Hz, meniscus at 5 inches H_2O, slew rate at 0.6 and duration at 3.8 μs. The above parameters provide uniform droplets with large ligaments for the ink-formulations.

RR-P3HT:PCBM blends were printed on top of a 50 nm doctor-bladed PEDOT:PSS (Baytron AL4083) buffer layer. Glass/ITO transparent substrate/electrodes were used for all the devices reported. The total printed area on each substrate was 1 cm^2 and through a shadow mask 10 nm of calcium and 100 nm of silver were thermally evaporated in order to form the cathode for 4 OPV devices of (9 ± 0.05) mm^2 active layer each. For the needs of this study, more than 100 devices were fabricated and analyzed. In order to avoid any oxidation/degradation of the active layer, thermal annealing treatment of 15 minutes at 140 ˚C was performed inside a nitrogen-filled glove box. J/V characteristics under illumination were also measured in these

conditions but due to lack of a solar simulator providing 100 mW/cm^2 inside the glovebox a smaller white light source of 12 mW/cm^2 was preferred.

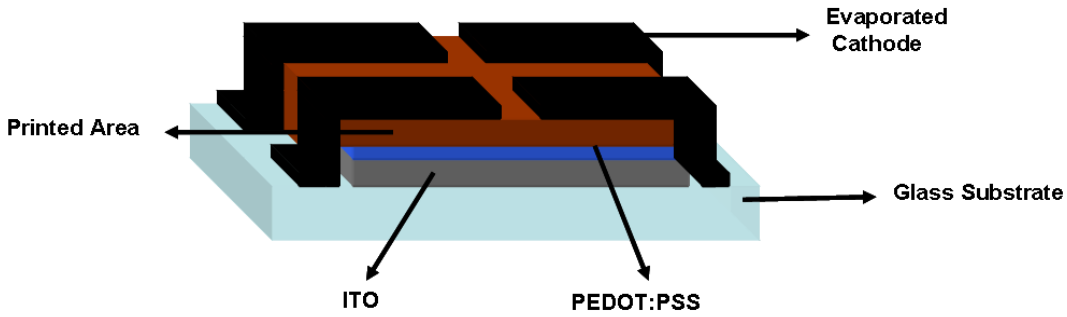

Figure 1: Representation of the device architecture with inkjet printed optically active layer. On top of ITO (grey) a thin layer of PEDOT:PSS (blue) was deposited. Inkjet printed active layer (brown) deposition was followed by thermal evaporation of the Al cathode (black).

5.1.3. Results and Discussion

To investigate the effect of viscosity on the inkjet printed OPVs, RR-P3HT:PCBM in a 1:0.8 (w:w) ratio was diluted in 1 ml and 0.5 ml of pristine o-DCB, providing solutions with two different printable viscosities. While exact viscosity values have not been calculated for this series, the values lie within the jettable range for printing provided by the manufacturer (2 – 30 mPa s) as no nozzle clogging issues were encountered. Figure 2 shows the effect of viscosity on the J/V characteristics under illumination, while Table 1 summarizes the device performance parameters collected for these two ink formulations. As can be seen from Table 1, the higher PCE is obtained from the more viscous solution, which provides thicker active layers with higher photocurrent values. Despite this increase in thickness the fill factor (FF) value of 0.63 was not affected, suggesting that the thicker layer still has

adequate transport properties and no dominant recombination losses for efficient charge collection are present.

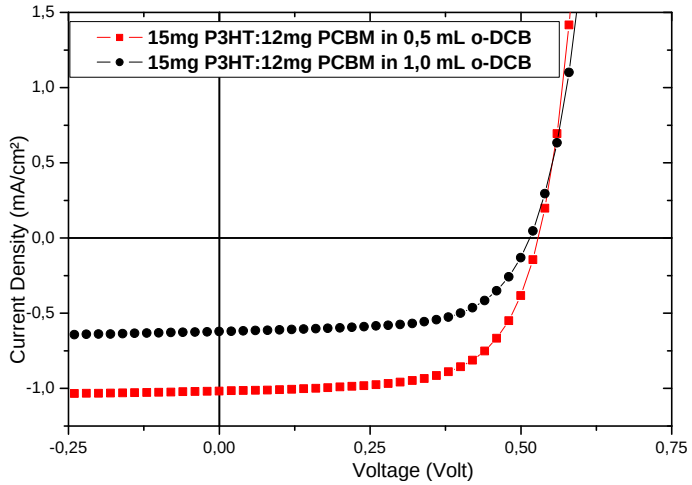

Figure 2: J/V characteristics under illumination represent the effect of solution viscosity on the inkjet printed OPV device performance.

Similarly, the open circuit voltage (Voc) was also not affected (0.52 V) by using a more viscous solution, indicating that the thickness of the active layer was close to the predicted optimum value[6]. The higher viscosity solution (RR-P3HT: PCBM 1:0.8 w:w diluted in 0.5 mL pristine o-DCB) resulted in inkjet printed OPVs with a PCE in the range of 2.6 %. This is due to a higher amount of photons being absorbed by the active layer, as approximately double the thickness (in the range of 250 nm) was achieved as opposed to the less viscous solution.

Table 1: Effect of inkjet-printed ink viscosity on overall device performance

Ink Viscocity	Voc (V)	Jsc (mA/cm²)	FF (%)	PCE (%)
RR-P3HT: PCBM 1:0.8 w:w in **1,0** mL o-DCB	0.517	0.569	63.1	1.55
RR-P3HT: PCBM 1:0.8 w:w in **0,5** mL o-DCB	0.528	1.017	63.7	2.63

We note that investigations of the photovoltaic performance for higher solution viscosities was also performed but in keeping with previously reported observations the small amount of solvent in each droplet mainly affected the printing ability, due to nozzle clogging[7, 8].

Having established the better performing RR-P3HT:PCBM mixture's viscosity, the substrate temperature and its effect on the drying rate of the solvent formulation was investigated. Figure 3 shows this effect of substrate temperature on the J/V characteristics under illumination. Under no temperature addition of the substrate the high boiling point of o-DCB of around 180 ˚C will cause a slow solvent evaporation rate, resulting in non-uniform film formation and high surface roughness active layers[9]. The evaporation rate is affected by the substrate temperature and the experimental results presented below indicate that the chosen substrate temperature is important for high PCE inkjet printed OPVs.

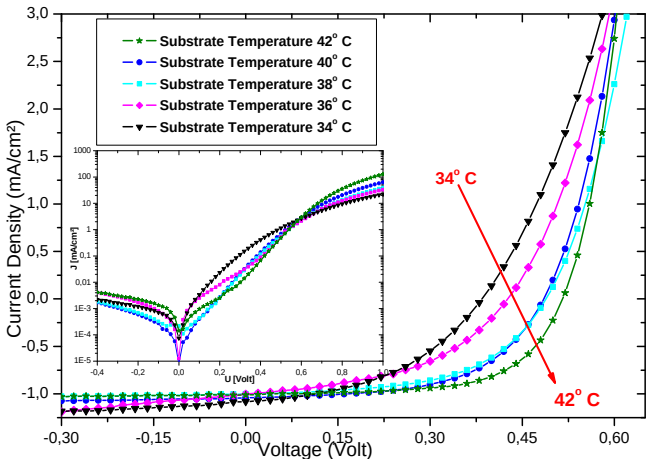

Figure 3: J/V characteristics under illumination represent the effect of substrate temperature on the device performance of RR-P3HT:PCBM based OPVs.

Table 2: Device performance summary when altering substrate temperature

Substrate Temperature	Voc (V)	Jsc (mA/cm²)	FF (%)	PCE (%)
34 ˚C	0.384	1.081	44.7	1.52
36 ˚C	0.426	1.002	46.5	1.63
38 ˚C	0.493	0.935	56.9	2.13
40 ˚C	0.484	1.042	56.2	2.34
42 ˚C	0.515	1.011	62.7	2.68

After printing the desired pattern on every substrate, the inkjet printer's lid was left open so that the vapor pressure of the solvent would not affect the drying process. Previous trials using pristine high boiling solvents such as tetralene showed losses in the short circuit current (Jsc) and Voc, which were identified as losses due to morphological issues and recombination mechanisms within the deposited active layer.

Table 2 summarizes the OPV device parameters obtained as a function of substrate surface temperature. Voc and FF linearly improve from 0.38 V to 0.52 V and 0.45 to 0.63, respectively, as the substrate temperature rises from 34 ˚C to 42 ˚C. This suggesting that modification of the solvent evaporation rate by temperature can be used to control drying speed and increase polymer crystallization, resulting in larger domains of the blend materials and thus improving the morphology during the inkjet printing process. The best PCE of 2.7 % was achieved at 42 ˚C substrate temperature. Above 42 ˚C we observed undesirable topography for the active layer, because at this temperature the solvent evaporates mainly from the droplet's

boundaries. Thus, the direction of liquid flow is from the center towards the edges, resulting in ring-like active layers.

Having now established suitable substrate temperature and solution viscosity, the next inkjet printing processing parameter under investigation was drop spacing. Figures 4 and 5 show representative J/V characteristics in dark and under illumination respectively, as a function of drop spacing conditions. The dark J/V characteristics as a function of drop spacing reveal that despite the fact that in negative polarity and low positive bias the three devices fabricated with different drop spacing conditions behave similarly, differences are observed above 0.45 V.

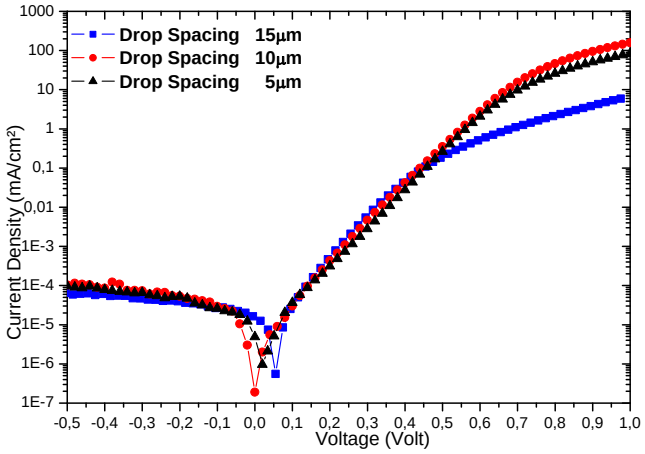

Figure 4: Dark current density vs. voltage characteristics in log/linear representation for different drop spacing values (5 – 15 µm).

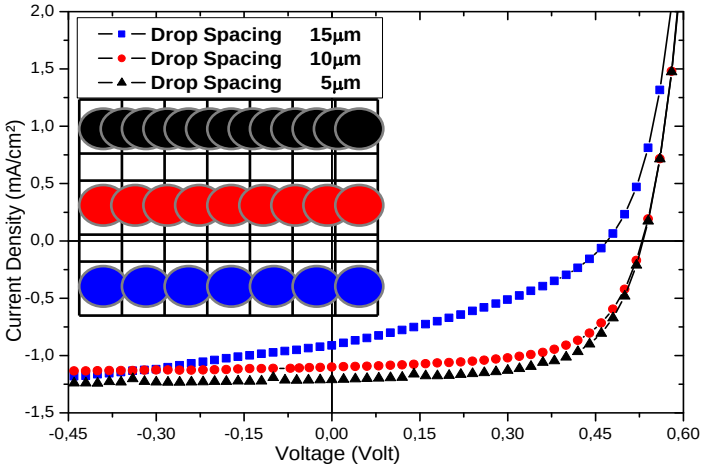

Figure 5: J/V characteristics under illumination when drop spacing varied from 5 – 15 µm. The inset of Figure 5 provides a schematic explanation of the variation of drop spacing and its effect on the resulting active layer film quality.

Table 3: Overall device performance of inkjet printed active layers at various drop spacing distances

Drop Spacing	Voc (V)	Jsc (mA/cm²)	FF (%)	PCE (%)
15 µm	0.469	0.911	35.9	1.16
10 µm	0.529	1.101	62.5	2.76
5 µm	0.530	1.212	63.2	3.07

In a macroscopic device model and at the high voltage linear regime of the dark J/V characteristics, the current flowing through the device is limited by the series resistance (Rs)[10]. The slope of the dark J/V at 1 V for the devices that were fabricated with 15 µm drop spacing indicates transport limitations, mainly limiting the FF value (see Figure 5 bottom plot) and to a lesser extent the Jsc values[11,12] . The poor J/V characteristics under illumination of 15 µm drop spacing (DS15) devices is due to the inhomogeneity of the RR-P3HT:PCBM inkjet-printed active layer since drop merging is only partial.

As the inkjet printer deposits with cartridge angle 3.4˚ and DS15, the diluted mixture was printed in horizontal lines and solidified before it could form a homogenous layer. Therefore, a uniform RR-P3HT:PCBM active layer cannot be achieved for DS15. On the other hand, printing trials with drop spacing of 5 μm (DS5) and 1.1˚ as well as drop spacing of 10 μm (DS10) with 2.3˚ achieved merged inkjet printed active layers. The slightly improved performance with DS5 drop spacing is due to an improved photocurrent value as well as good layer thickness of around 350 nm – a thickness value close to the optimum for inkjet printed RR-P3HT:PCBM blends diluted in pristine o-DCB.

To summarize the inserted scheme of Figure 5, for DS15 the drop distance of 15 μm exceeds the wettability of the solution and the drops never have contact in order to form a homogenous layer. For DS5 and DS10 drop spacing values, the drops mix adequately. Since with DS5 more drops partly or totally cover one pixel and the solution volume per unit area is higher, a significantly thicker active layer is obtained. The achieved thickness for DS5 drop spacing was close to 350 nm resulting in predicted IQE values in the range of 95 %[13,14].

The above results show that the selection of the appropriate drop spacing and cartridge angle at a certain ink viscosity and temperature (to control the evaporation rate of the solvent), can be used to adjust the layer thickness of inkjet printed polymer:fullerene OPVs. The device parameters in Table 3 show a PCE of 3.07 % for 5 μm drop spacing devices. FF values reported for 5 μm and 10 μm drop spacing are also good (63 %), dramatically reducing to 36 % for 15 μm drop spacing. The

observed short circuit current differences for the three devices under investigation are due to differences in the active layer thickness as explained in more detail above. Though no current flows through the series resistance at open circuit conditions and no Voc reduction is observed as expected for 5 and 10 µm drop spacing devices, the devices fabricated with DS15 showed a reduced Voc value of 470 mV, due to a non-uniform active layer. BHJ inkjet printed OPVs with high PCE using pristine solvent formulations have been reported in the literature[15,16]. The highest PCE of 3.07 % presented in this work was achieved with 5 µm drop spacing (DS5).

The final inkjet-printed processing condition under investigation was the nozzle-to-substrate distance. Figure 6 shows representative J/V measurements in the dark (upper plot) and under illumination (inserted plot) for nozzle-to-substrate distances of 1200 µm (circles) and 1400 µm (squares) and with the optimum value of 5 µm drop spacing, substrate temperature of 42 ˚C and chosen solution viscosity (RR-P3HT: PCBM 1:0.8 w:w diluted in 0.5 mL of pristine o-DCB).

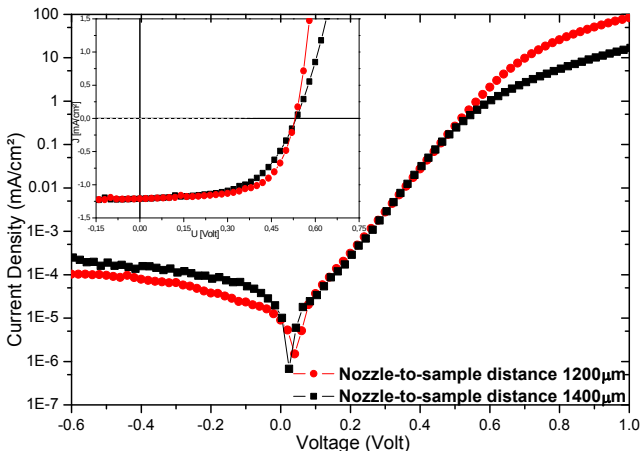

Figure 6: Upper plot (a) J/V characteristics in dark (main) and under illumination (inset) when the nozzle-to-substrate distance was altered from 1200 µm to 1400 µm. Bottom plot

Table 4: Nozzle-to-sample distance effect

Nozzle-to-sample distance	Voc (V)	Jsc (mA/cm²)	FF (%)	PCE (%)
1400 μm	0.542	1.187	56.3	2.74
1200 μm	0.531	1.212	63.2	3.07

The dark J/V characteristics show that the selection of nozzle-to-substrate distance clearly affects the slope of the dark J/V at 1 V, indicating an influence on the active layer transport properties. The major impact of transport limitations is noticeable in the reduced FF of the 1400 μm nozzle-to-substrate distance devices. As the droplets are deposited on the substrate they create a layer with solidified grains stacked one on top of the other. Fast drying of these droplets results in a multi "bi-layer" type structure, which provides slightly higher Voc value but at the same time less efficient transport properties; reflected in the reduced FF obtained. Thus, the illuminated J/V characteristics in Figure 6 (inserted plot), show limited PCE performance for the devices with 1400 μm nozzle-to-substrate distance.

When the solution droplet is released from higher than the optimized distance, it solidifies at a certain degree providing non-favorable morphology for the active layers. The low FF value obtained for the 1400 μm distance of droplet from substrate indicates morphological limitations and low charge carrier collection properties under this condition. The device performance data summarized in Table 4 show that a nozzle-to-substrate distance of 1200 μm is essential for reaching high OPV performance.

To confirm that the above processing conditions described for inkjet printed OPVs are close to optimum values, the J/V characteristics were compared to RR-P3HT:PCBM OPVs prepared with optimized conditions in our labs with spin coating and doctor blading techniques using chloroform/chlorobenzene solvent mixture[17] and pristine chlorobenzene respectively. Figure 7 shows representative J/V in the dark and under illumination and Table 5 summarizes device performance for OPVs fabricated using the above three processing methods. The device performance for all the processing methods is within 3.1 – 3.6 %. The doctor blading cells mainly have higher FF and the spin coated OPVs have higher Jsc compared to the inkjet printed solar cells. We attribute these differences to the small adjustments to thickness and morphological properties of the inkjet printed active layer, necessary because of the more restricted processing conditions applied during the inkjet printing process.

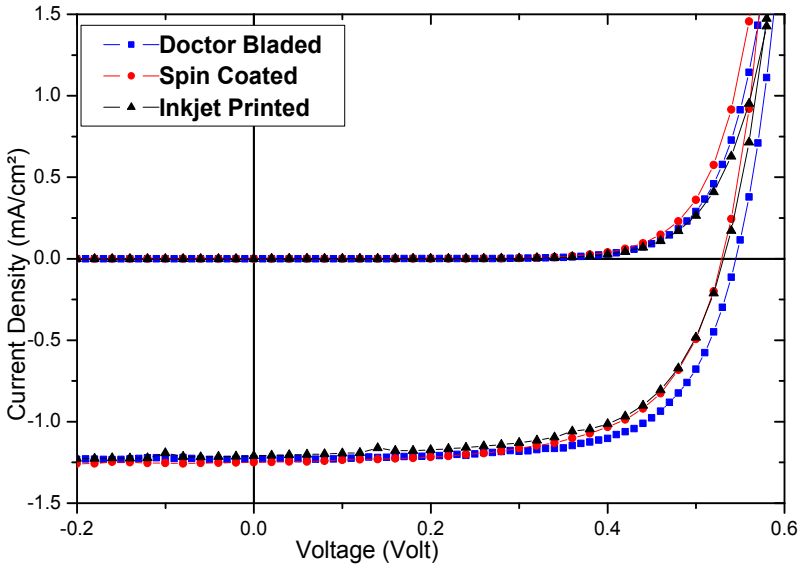

Figure 7: J/V characteristics in dark and under illumination for OPVs processed by inkjet printed in comparison to reference optimized spin coated and doctor bladed OPVs.

Table 5: Overview of PCE device parameters for optimized organic solar cells processed by inkjet printing, in comparison to optimized spin coated and doctor bladed OPVs. For all the devices presented the J/V characteristics under illumination were measured at low light intensity.

Processing method	Voc (V)	Jsc (mA/cm^2)	FF (%)	PCE (%)
Inkjet Printing	0.530	1.212	63.2	3.07
Spin Coating	0.528	1.322	62.7	3.31
Doctor Blading	0.545	1.299	67.0	3.58

5.1.4. Conclusion

The technological attraction in organic electronics applications is their compatibility to printing processes. In this section, we have described in detail the processing conditions of inkjet printed active layers comprising a blend of RR-P3HT:$PC_{61}BM$ using o-DCB solvent. We have shown that solution viscosity, substrate temperature, drop spacing and droplet height are critical parameters for optimized inkjet-printed active layer processing. Considering these parameters, it is shown that efficient inkjet-printed OPVs can be achieved with commercially available materials and pristine solvent formulation. We believe that the above results can be used to provide initial reference processing conditions for inkjet-printed organic electronic applications using polymer-fullerene blend active layers.

5.2. Inkjet Printing Ag nanoparticle Current Collecting Grids[2]

As we have seen in the previous section, a systematic study was undertaken to ensure that inkjet printing the active layers of OPVs produces efficient solar cells. However, in that study, only the active layer was inkjet printed and standard glass/ITO substrates were still used as the main bottom electrode.

This part, then, will focus on replacing ITO with a silver grid/PEDOT:PSS architecture. The Ag grid was achieved by inkjet printing and although PEDOT:PSS was not inkjet printed in this study, it paves the way for the use of printable PEDOT inks towards a fully inkjet printed organic solar cell.

5.2.1. Introduction

Based on the recent progress on power conversion efficiency, lifetime and processing one of the issues needs to urgently be addressed is the materials cost[18]. Cost reduction is considered as the next important milestone for OPVs and replacement of high cost materials on the OPV device structure is critical for the future technological progress of OPVs. Most of the high performance OPV devices reported in the literature use rigid and stiff indium tin oxide (ITO) as the transparent electrode, which is deposited by sputtering at high vacuum and temperatures prohibiting further reduction in fabrication cost. ITO is the most expensive

[2] This work has been published as M. Neophytou, F. Hermerschmidt, A. Savva, E. Georgiou, and S. A. Choulis Highly efficient indium tin oxide free organic photovoltaics using inkjet-printed silver nanoparticle current collecting grid at Applied Physics Letters 101, 193302 (2012).

component of the OPV device structure and the need for inexpensive alternative transparent electrodes is imminent.

Ideally, transparent conductive oxides (TCOs) exhibit high optical transparency while simultaneously being highly conductive so that electric charge carriers extraction can be evenly distributed[19]. Many research groups have reported sputtered or thermally evaporated alternatives to ITO such us fluorine doped tin oxide (FTO)[20], which has high air and chemical stability and is less expensive than ITO. Furthermore, lithographically deposited metal grids[21], single-walled carbon nanotubes[22, 23], ultra thin graphene layers[24] and oxygenated nano-crystalline diamonds[25] are considered as alternative paths to follow for ITO-free organic solar cells. A further promising alternative to these is PEDOT:PSS derivatives[26, 27, 28, 29], a conductive transparent buffer layer which has been extensively studied, but as it exhibits significantly lower conductivity values than those obtained with ITO, the overall device performance is limited. Low conductivity results in high sheet resistance thus decreased capability of the PEDOT:PSS anode to extract charge species efficiently in the cases that is not combined with ITO. In order to diminish resistance losses, inkjet printed Ag-nanoparticle grid lines have been recently integrated with PEDOT:PSS and ITO free OPVs with PCE of 1.47 % have been reported[30]. In this chapter we report an in-depth investigation of an inkjet-printed silver nanoparticle grid combined with different conductivity PEDOT:PSS. We have achieved an ultimate control of the design requirements of current collected grid based on the proposed inkjet-printed process to accurate control the uniformity and dimensions of the silver nanoparticle based grid. The performed measurements

revealed higher transparency of the printed Ag-grid when compared to different thicknesses of ITO. As a result a record power conversion efficiency of 1.96 % is reported for ITO free organic solar cells using the combination of PEDOT:PSS/inkjet printed nanoparticles based current collecting grids.

5.2.2. Experimental

The applied experimental procedure has as follows, on top of a common glass substrate, Ag nanoparticles ink purchased from SunChemical were inkjet-printed with a Fujifilm Dimatix 2832 series printer. A 10 pL cartridge was used and various conditions and deposition parameters were optimized in such a way that desired line height and width were achieved. Inkjet printers deploy drop-of demand (DoD) technology and by altering parameters such as drop spacing the user may control printed grid line thickness. Ink viscosity was manipulated by using different cartridge temperatures, so that improved droplet wettability on the glass substrate was achieved. Printed grid lines were fully covered with doctor bladed PEDOT:PSS layers of different conductivities. Layers were thermally treated at 100 °C for 20 minutes to remove residual solvent. Above these layers a 1:0.8 by weight ratio of P3HT:PCBM was doctor-bladed to achieve a thickness of 280nm. The top electrode, 100 nm Al, was thermally evaporated inside a nitrogen-filled glovebox and the devices were thermally annealed for 15 minutes at 140 °C. Composite materials of the active layer blend were diluted separately overnight in chlorobenzene and mixed one hour prior to deposition. The photovoltaic active area is defined as cathode and anode overlapping, and for this reason an evaporation shadow mask was used. The device area was measured to be 9 mm^2. The device structure is schematically

depicted in Figure 8. For comparison, reference devices of pre-structured ITO substrates were fabricated along with the grid line layers under identical processing conditions.

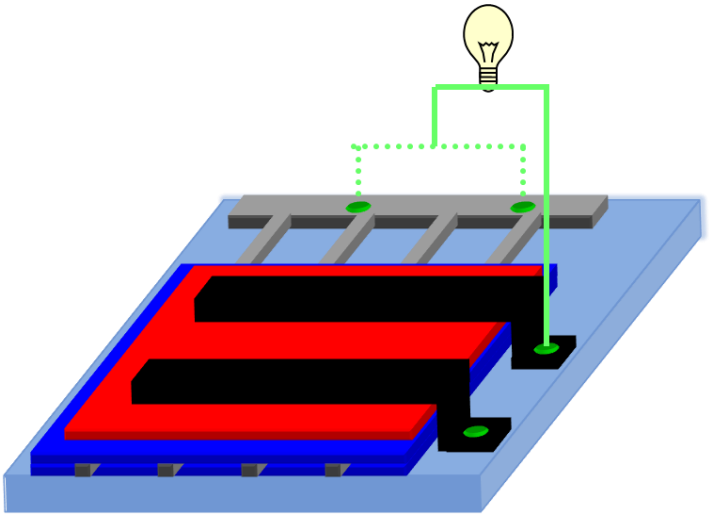

Figure 8: Representation of ITO-free device structure. The silver grid lines (grey) are deposited onto a glass substrate, followed by PEDOT:PSS (blue) and the active layer (red). The Al cathode (black) is thermally evaporated on top

5.2.3. Results and Discussion

As instructed by the manufacturer of the Ag ink, a sintering process is needed so that printed lines achieve optimum conductivity and film properties. A mirror-like appearance (indicating solid silver formation) was visible even after the printed grid lines were sintered for less than a minute at 140 °C on a hot plate. Nonetheless further exposure of up to 20 minutes was needed to ensure that no residual solvent of the Ag nanoparticle ink was causing defects at the evaporated metal cathode. These defects, shown in Figure 9 (top), are visible to naked eye as burst bubbles and are in the range of a few micrometers. Indications that the PEDOT:PSS layer was also damaged were observed and extracted data have shown to decrease device performance.

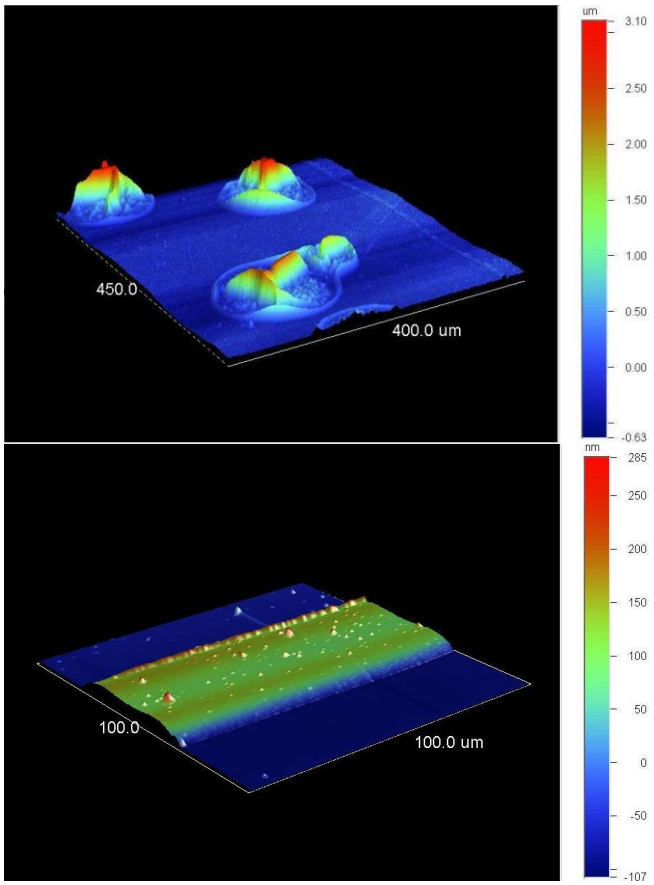

Figure 9: (Top) Surface mapping image contacted with stylus profilometry showing micron-sized bubbles formed on deposited grid lines where the solvent has not evaporated sufficiently. (Bottom) Surface mapping image of an optimized printed line. The overall height of the line is in the region of 190 – 210 nm, with the spike-type shapes showing as more prominent points.

As it will be discussed later in the text, inkjet-printed silver nanoparticle current collecting grid line width and height are co-dependent. By varying the deposition temperature the solvent evaporation rate is altered. At high temperature a so-called coffee-ring effect[31] (solute buildup on one area, leaving a distinct ring shape upon evaporation) was observed and influenced each line formation. Due to the increased evaporation rate, solvent from the edges of the line was rapidly depleted. In order to replenish the loss, solvent from the center of the line created an outward flow.

Shifted nanoparticles were mounted up at the edges of the droplet and resulted in an M-shape line formation[32]. Randomly dispersed spike-type shapes of up to 400 nm, in some rare cases, were reported and consequently penetrated deposited layers, shunting the device. Lack of printed line homogeneity due to coffee-ring line formation could lead to non-uniform conductivity thus increased series resistance in the OPV device performance parameters. Therefore, all efforts have been made to achieve undistorted line shapes. Figure 9b (bottom) shows the spikes observed even in an optimized printed line, however the height of those spikes is only a few tens of nanometers higher than the overall height of the line.

To ensure increased charge carrier selective collection through the Ag grids, they have to be entirely covered with PEDOT:PSS. In order to do so, PEDOT:PSS films should be deposited which are thicker than the printed line height. However, despite the fact that increased thickness results in reduced resistivity values of the PEDOT:PSS films, significant transparency losses occur. In order to avoid additional losses, a balance between these two parameters of resistivity and transparency has to be achieved.

As a general rule an optimized grid structure should allow maximum visible light to pass through and at the same time ensure uniform charge carrier extraction from the entire active area of the photovoltaic cell. Grid lines with small width and height were aimed for in an effort to avoid any undesirable shadow effects. While the width decreases, higher height will be obtained, as the same amount of material from the 10 pL droplet will be collected in a smaller area. Various drop spacing and deposition temperatures were tested. Optimum combination of these two parameters

resulted in a line of 46 µm width and 200 ± 10 nm height. This is significantly thinner than reported elsewhere[30] allowing for more light to reach the active layer P3HT:PCBM blend part of the OPV device structure. Transmission measurements were therefore carried out to ascertain the positive effects of such a thin grid line architecture.

Transmittance measurements were performed on glass with inkjet- printed silver grid and different thickness ITO sputtered on glass substrates, as shown in Figure 10. Pure glass substrates were also used for comparison. The silver nanoparticle inkjet printed grids showed particularly high transmittance (~92 %) in the range of the absorption maxima of the P3HT:PCBM active layer, which are between 490 – 560 nm. The grids with 46 µm width were also compared with ones of 49 µm width. Both types resulted in higher than 90 % transmittance throughout the visible spectrum and one could suggest that they are suitable for broader absorption material systems as well.

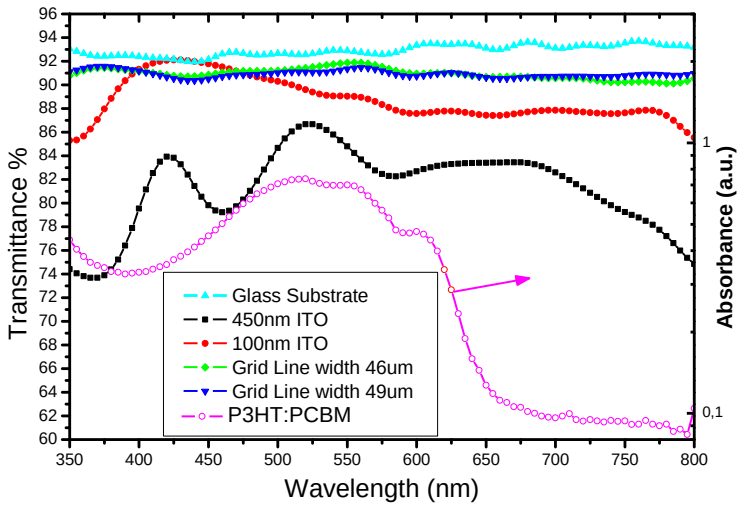

Figure 10: Optical transmittance of glass substrates with various surface covering. The transmittance of the Ag grid lines was compared to 100 nm and 450 nm of ITO coverage as well as a reference. Both grid line widths provide >90 % transmittance. P3HT:PCBM absorbance is included for comparison (open circles).

To investigate the effect of PEDOT:PSS conductivity on overall device performance of ITO-free OPVs using inkjet-printed silver nanoparticle current collecting grids, Clevios P VP AL 4083 and Clevios PH, with conductivity of 0.002 S/cm and 1 S/cm respectively[29], were used as electron blocking and hole transporting buffer layers on the ITO-free OPV device structure. Both dispersions were diluted with isopropanol in a ratio of 1:3,2 in order to reduce the surface tension of pristine PEDOT:PSS. Four lines of silver nanoparticles current collected grids with 46 μm width and ~200 nm height were printed on glass substrates. The pitch size (the horizontal distance of one line from another) was set at 700 μm and no line was printed at the edges of the OPV device structure to avoid leakage current. Total coverage of the cells with inkjet printed Ag nanoparticle grid lines was 6.2 %. We note that ITO-free OPV devices with fewer number of lines were also fabricated but charge carrier collection was significantly reduced[33].

Uneven current collection distribution increased bimolecular recombination. Excitons dissociated away from the Ag grid's position could not be extracted and recombined. This was manifested in reduced shunt resistance (R_{sh}) on current density - voltage characteristics (J/V) that for simplicity are not shown here. Evidently, fewer silver lines did not reduce the PEDOT:PSS resistivity and resulted in high series resistance (R_s) as well. Figures 11, shows J/V characteristics under dark and Figure 12 under illumination of ITO-free OPVs with 46 μm width and ~200 nm height inkjet-printed silver nanoparticle current collecting grids and reference ITO-based OPVs. OPVs device performance characteristics were

measured using a calibrated Newport 92250A solar simulator, under 1 sun (100 mW/cm^2) illumination.

Current density-voltage characteristics were measured for both PEDOT:PSS with embedded Ag nanoparticle grids. For comparison reasons reference devices with ITO electrode were also fabricated and measured. Active layer and evaporated metal cathode were deposited for both architectures at identical conditions (same run). Optimized process for reference cells resulted into higher overall device performance with PCE reaching 3%. Both PEDOT:PSS types, regardless of conductivity, exhibited a good balance of transmittance and resistance at a layer thickness of around 250 nm as shown by relatively high J_{sc} values. A phase separation of conductive PEDOT-rich clusters with insulating PSS-rich edges are reported after film formation. Higher PSS composite in the dispersion only resulted in films with higher resistivity[34]. When replacing the ITO anode with a silver grid and Clevios P VP AL 4083, where the PEDOT:PSS ratio is 1:6 (w/w), series resistance as shown at +1 V (see Figure 11) dominated the overall device performance. According to Ohm's law, in open circuit conditions no reduction in V_{oc} is expected due to R_s and only FF and J_{sc} values are negatively affected, resulting in 28.3 % and 8.9 mA/cm^2 respectively. Generated power in the fourth quadrant is consumed so that the energetic barrier of the increased resistance is overcome.

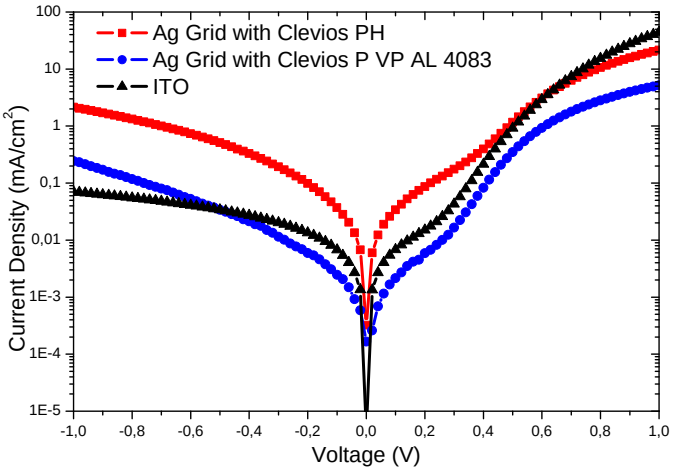

Figure 11: Effect of PEDOT:PSS conductivity on device performance in dark conditions. PEDOT:PSS with 0.002 S/cm conductivity (blue circles) exhibited higher R_s mainly due to the higher PSS concentration, in relation to data obtained with PH (red squares). When compared to the reference structure (black triangles), both devices showed high carrier injection at negative and low positive bias, which is most likely caused by spike-like shapes in the printed line

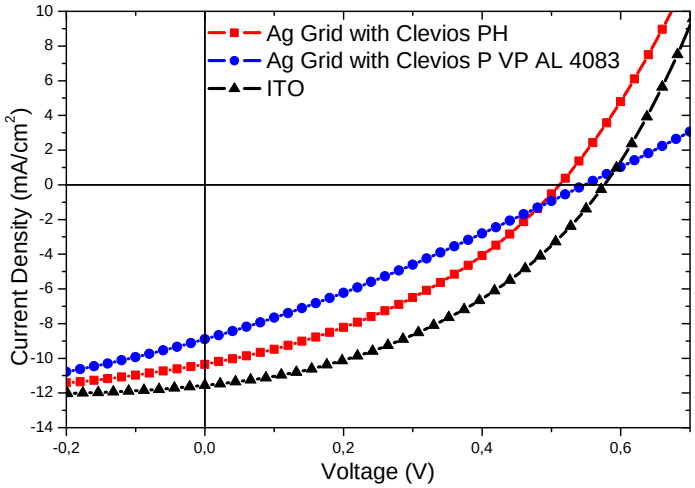

Figure 12: Effect of PEDOT:PSS conductivity on device performance in light conditions. Despite the fact that loss mechanisms dominated device performance for both ITO-free architectures, a PCE of 1.96 % was achieved

Improved FF values of around 37 % are obtained for devices with more conductive hole transporting layers. Charge carrier transportation and collection is enhanced due to better electrical properties of the Clevios PH PEDOT:PSS. At the same time better ohmic contacts between the interfaces are formed. Some losses in V_{oc} in the

range of 510 mV are mainly attributed to increased dark current density values in the negative and low positive bias for these devices. Shunt resistance was reduced as a result of charge carrier bimolecular recombination and this could only suggest that one of the electrodes lacks selective charge extraction. As all other layers for the reference and ITO-free devices were deposited at identical conditions and parameters it was reasonable to assume that losses could be attributed to the Ag grid. Selectivity is to some extent reduced as presumably the Ag spikes have penetrated the PEDOT:PSS film and collect both electron and holes. Fabricated devices with PEDOT:PSS of 10 S/cm conductivity resulted in a power conversion efficiency of 1.96 %. To our knowledge this is among the highest PCE obtained from unmodified PEDOT:PSS/inkjet printed Ag grid ITO-free anodes reported in the literature.

5.2.4 Conclusion

Table 6: Photovoltaic parameters of devices in comparison.

Device	V_{oc} [mV]	J_{sc} [mA/cm^2]	FF [%]	PCE [%]
Clevios P VP AL 4083	548	8.9	28.3	1.38
Clevios PH	510	10.35	36.8	1.96
ITO	570	11.55	45.1	3.04

Table 6 summarizes all device parameters. It is clear that in both PEDOT:PSS/Ag grid anode devices further optimization of line width, height and pitch size is needed in order to maximize carrier transportation and collection. Inkjet printing facilitates mass production organic solar cell fabrication. Brittle and expensive ITO can be efficiently replaced by Ag grid lines embedded into conductive PEDOT:PSS films.

We have demonstrated that inkjet printed Ag grid lines provide high transparency throughout the entire visible spectrum. For low roughness grid lines the coffee-ring effect can be avoided with the optimum combination of drop spacing and deposition temperature. Optimum line width was found to be 46 µm so that shadow effects were minimized. Higher conductivity PEDOT:PSS formulations are needed in order to further reduce line height and transmittance losses. A record PCE in the region of 2 % was achieved, but there is still a long way to go towards fully sustainable inexpensively produced solar cells.

5.3 Bibliography

[1] C.N.Hoth, P.Schilinsky, S.A.Choulis, C.J.Brabec, Printing Highly Efficient Organic Solar Cells, NanoLetters 8, 2806-2813, (2008)

[2] C.N.Hoth, P.Schilinsky, S.A.Choulis, C.J.Brabec, High Photovoltaic Performance of Inkjet Printed Polymer:Fullerene Blends Adv.Mater. 19, 3973-3978, (2007)

[3] S. H.Eom, H. Park, S.H. Mujawar, S. C. Yoon, S.S. Kim, S.I. Na, S.J. Kang, D. Khim, D.Y. Kim, S.H. Lee, High efficiency polymer solar cells via sequential inkjet-printing of PEDOT:PSS and P3HT:PCBM inks with additives, Org. Electron. 11, 1516-1522, (2010)

[4] A. Lange, M. Wegener, C. Boeffel, B. Fischer, A. Wedel, D. Neher, A new approach to the solvent system for inkjet-printed P3HT:PCBM solar cells and its use in devices with printed passive and active layers, Solar Energy Materials & Solar Cells 94, 1816–1821, (2010)

[5] V.Fauzia, A.A. Umar, M.M. Salleh, M.Yahya, Optimization of inkjet Printing Technique Parameters for Fabrication Of Bulk Heterojunction Organic Solar Cells, IEEE International Conference on Semiconductor Electronics, Proceedings, ICSE , 60-63, (2010)

[6] K.M.Coakley, M.D.Mcgehee, Conjugated Polymer Photovoltaic Cells, Chem Mater. 16, 4533-4542, (2004)

[7] J. Perelaer, P. J. Smith, E. van den Bosch, S. S. C. van Grootel, P. H. J. M. Ketelaars, U. S. Schubert, The Spreading of Inkjet-Printed Droplets with Varying Polymer Molar Mass on a Dry Solid Substrate Macromol. Chem. Phys. 210, 495-502, (2009)

[8] J. Perelaer, P. J. Smith, M. M. P. Wijnen, E. van den Bosch, R. Eckardt,P. H. J. M. Ketelaars, U. S. Schubert, Droplet tailoring using evaporative inkjet printing Macromol. Chem. Phys. 210, 387-393, (2009)

[9] C.N.Hoth, P.Schilinsky, S.A.Choulis, C.J.Brabec, Photovoltaic Loss Analysis of Inkjet-Printed Polymer Solar Cells Using Solvent Formulations, Macromol.Symp., 287-292, (2010)

[10] C.Waldauf, M.C.Scharber, P.Schilinsky, J.A.Hauch, C.J.Brabec, Physics of organic bulk heteronjuction devices for photovoltaic applications, Appl. Phys. 99, (2006)

[11] J.D. Servaites, S. Yeganeh, T. J. Marks, M.A.Ratner, Efficiency Enhancement in Organic Photovoltaic Cells:Consequences of Optimizing Series Resistance , Adv. Funct. Mater. 20, 97–104, (2010)

[12] J. Nelson, The Physics of Solar Cells, Imperial College Press, London, England (2003)

[13] G.Dennler, M.C.Scharber , C.J.Brabec , Polymer-Fullerene Bulk-Heterojunction Solar Cells , Adv. Mater. 21, 1323–1338, (2009)

[14] G.Dennler, K.Forberich, M.C.Scharber, C.J.Brabec, Angle dependence of external and internal quantum efficiencies in bulk-heterojuction organic solar cells, J.App. Phys. 102 (2007)

[15] A.Lange, M.Wegener, C.Boeffel, B.Fischer, A.Wedel , D.Neher, A new approach to the solvent system for inkjet-printed P3HT:PCBM solar cells and its use in devices with printed passive and active layers, Solar Energy Materials & Solar Cells 94, 1816–1821, (2010)

[16] S.H.Eom, S.Senthilarasu, P.Uthirakumar, S.C. Yoon, J.Lim, C.Lee, H.S. Lim, J.Lee, S.H. Lee, Polymer solar cells based on inkjet-printed PEDOT:PSS layer, Org. Electron. 10, 536-542, (2009)

[17] Y.S. Kim, Y.Lee, J.. Kim , E.O. Seo , E.W. Lee, W. Lee, S.-H. Han, S.-H. Lee, Effect of solvent on the performance and morphology of polymer photovoltaic devices, Current Applied Physics 10, 985-989, (2010)

[18] C.J.M. Emmot, A. Urbina, J. Nelson, Enviromental and economic assessment of ITO-free electrodes for organic solar cells, Sol. Energy Mater. Sol. Cells, 97, 14-21, (2012)

[19] D.S. Hecht, L. Hu, G. Irvin, Emerging Transparent Electrodes Based on Thin Films of Carbon Nanotubes, Graphene, and Metallic Nanostructures, Adv. Mater, 23, 1482–1513, (2011)

[20] A. Andersson, N. Johansson, P. Broms, N. Yu, D. Lupo, W.R. Salaneck, Fluorine Tin Oxide as an Alternative to Indium Tin Oxide in Polymer LEDs, Adv. Mater, 10, 859, (1998)

[21] M.G. Kang, M.S. Kim, J.S. Kim, L.J. Guo, Organic Solar Cells Using Nanoimprinted Transparent Metal Electrodes, Adv. Mater, 20, 4408,(2008)

[22] A.A. Green, M.C. Hersam, Colored Semitransparent Conductive Coatings Consisting of Monodisperced Metallic Single-Walled Carbon Nanotubes, Nano Lett. 8, 1417, (2008)

[23] J.L. Blackburn, T.M. Barns, M.C. Beared, Y. Kim, R.C. Tenent, T.J. McDonald, B. To, T.J. Coutts, M.J. Heben, Transparent Conductive Single-Walled Carbon Nanotube Networks with Precisely Tunable Ratios of Semiconducting and Metallic Nanotubes, ACS Nano, 2, 1266, (2008)

[24] L.G. De Arco, Y. Zhang, C.W. Schlenker, K. Ryu, M.E. Thompson, C.W. Zhou, Continuous, highly flexible, and transparent graphene films by chemical vapor deposition for organic photovoltaics, ACS Nano, 4, 2865, (2010)

[25] C.H.Y.X. Lim, Y.L. Zhong, S. Janssens, M. Nesladek, K.P. Loh, Oxygen-Terminated Nanocrystalline Diamond Film as an Efficient Anode in Photovoltaics, Adv. Funct. Mater, 20, 1313, (2010)

[26] T. Aernouts, P. Vanlaeke, W. Geens, J. Poortmans, P. Heremans, S. Borghs, R. Mertens, R. Andriessen, L. Leenders,Printable anodes for flexible organic solar cell modules, Thin Solid Films 451, 22, (2004)

[27] S.I. Na, S.S. Kim, J. Jo, D.Y. Kim, Efficient and Flexible ITO-Free Organic Solar Cells Using Highly Conductive Polymer Anodes, Adv. Mater, 20, 4061, (2008)

[28] J. Huang , X. Wang , Y. Kim , A. J. deMello , D. D. C. Bradley and J. C. deMello, High efficiency flexible ITO-free polymer/fullerene photodiodes, Phys. Chem. Chem. Phys., 8, 3904, (2006)

[29] X. Wang , T. Ishwara , W. Gong , M. Campoy-Quiles , J. Nelson, D.D.C. Bradley, High-Performance Metal-Free Solar Cells Using Stamp Transfer Printed Vapor Phase Polymerized Poly(3,4-Ethylenedioxythiophene) Top Anodes, Adv. Funct. Mater, 22, 1454, (2012)

[30] Y. Galagan, B. Zimmermann, E. W.C. Coenen, M. Jørgensen, D.M. Tanenbaum, F. C. Krebs, H. Gorter, S. Sabik, L. H. Slooff, S. C. Veenstra, J. M. Kroon, R. Andriessen, Current Collecting Grids for ITO-Free Solar Cells, Adv. Energy Mater, 2, 103, (2012)

[31] M. Layani, M. Gruchko, O. Milo, I. Balberg, D. Azulay, S. Magdassi, Transparent Conductive Coatings by Printing Coffee Ring Arrays Obtained at Room Temperature, *ACS Nano*, 3 (11), 3537, (2009)

[32] Y. Jang, J. Jo, D.S. Kim, Control of doctor-blade coated poly (3,4-ethylenedioxythiophene) /poly(styrenesulfonate) electrodes shape on prepatterned substrates via microflow control in a drying droplet JOURNAL OF POLYMER SCIENCE PART B: POLYMER PHYSICS, 49, 1590, (2011)

[33] A. Cheknane, Optimal design of electrode grids dimensions for ITO-free organic photovoltaic devicesProg.Photovolt: Res. Appl, 19, 155, (2011)

[34] U. Lang, E. Muller, N. Naujoks, J. Dual, Highly Conductive PEDOT:PSS Electrode with Optimized Solvent and Thermal Post-Treatment for ITO-Free Organic Solar Cells, Adv. Funct. Mater, 19, 1215, (2009)

Chapter 6 – Conclusions and Summary

Establishing a Reference Device System

A major initial target of this thesis was to achieve an optimised and reproducible process for the fabrication of P3HT:PCBM based organic photovoltaics (OPVs). The aim was to create a reference OPV device for our new Molecular Electronics and Photonics (MEP) Research Unit at Cyprus University of Technology – an essential step for all the other studies. Doctor-blading processing parameters such as deposition of the hole transporting layer PEDOT:PSS, active layer composition ratio, selection of appropriate solvents (including investigation of pristine solvents and solvent mixture), layer thickness, thermal annealing processing steps and solvent annealing were optimized and P3HT:PCBM based OPVs with power conversion efficiency (PCE) of more than 3 % can be fabricated. During my internship period within the group of Microsystems at IKERLAN-IK4 Technological Research Centre (Spain), OPVs fabricated with P3HT:PCBM showed a strange kink in the illuminated J/V characteristics of some devices. That s-shape was later identified by collaborators (Jaume University, Spain) as band defects and impurities of the conjugated polymer using capacitance measurements.

Device Performance and Device Loss Analysis Studies for Newly Synthesized Polymer Electron Donors

The optimized parameters obtained for the processing of P3HT:PCBM based OPVs were then used, as described in Chapter 4, to look into newly synthesized polymers developed within the MEP Research Unit and in close collaboration with our chemistry partners at the University of Cyprus. Primarily, a perfluorinated copolymer that follows the structural motif of the well-known APFO-3 copolymer for optoelectronic applications was studied and a direct structure-property relation between the two polymers was attempted. Measurements performed in collaboration with the University of Cyprus showed that the material exhibits complete photoluminescence quenching when blended with PCBM as the electron acceptor. The perfluorinated copolymer (PFTPFBZT) was evaluated for its power conversion efficiency performance on polymer-fullerene bulk heterojunction OPVs relevant to reference APFO-3-PCBM based bulk heterojunction OPVs. The investigations on the device performance showed that PFTPFBZT:PCBM based bulk heterojunction solar cells exhibit low power conversion efficiencies of 0.24 % compared to 1.75 % PCE achieved for reference APFO-3:PCBM. When PFTPFBZT:PCBM was used as the photoactive layer, lower V_{oc} values in comparison to devices with APFO-3:PCBM were obtained. This could be partially explained by the difference in HOMO of the two fluorene-based copolymers. The V_{oc} values achieved are significantly lower than the theoretical maximum potential indicating possible recombination losses. In combination with low FF values obtained, the results indicate morphological limitations for PFTPFBZT:PCBM based OPVs. The low J_{sc}

values for PFTPFBZT:PCBM based OPVs are owed partly due to the moderate E_g of 2.25 eV. Despite the low PCE values the pentafluorophenyl substituted benzimidazole can be an interesting building block for conjugated polymers. Synthetic attempts at maintaining the pentafluorophenyl moiety as a building block, but optimizing the side chains, aiming at improved solubility and shifting of the energy levels to a more favorable direction are suggested for further studies towards higher power conversion efficiency values.

This work was then followed by analysis of a family of five new polymers based on the 4,4-difluoro-4-bora-3*a*,4*a*-diaza-*s*-indacene core (BODIPY) chromophore moiety also synthesized by the synthetic chemistry researchers involved within the MEP research unit. The BODIPY moiety was decorated with a variety of functional groups aiming at enhanced optoelectronic properties and solubility for improving the overall device performance. All copolymers were characterized extensively in collaboration with the University of Cyprus (CY) and Imperial College London (UK). Space charge limited current (SCLC) and atomic force microscopy (AFM) studies were also performed in collaboration with the University of Erlangen (Germany). Solar cell device performance was probed using active layers consisting of the BODIPY conjugated polymer donors and PCBM acceptor. In common with bulk-heterojunction OPVs made from other amorphous conjugated polymers with PCBM, the current density increases with fullerene content reaching a maximum at 75 - 80 wt.%. At 50 wt.% of PCBM a polymeric matrix is formed with embedded isolated PCBM-rich domains. Photogenerated excitons dissociate at the

polymer:PCBM interface but due to the lack of interpenetrating percolated networks, they bimolecularly recombine. On the other hand for 75 and 80 wt.% the formed electron acceptor-rich clusters grow significantly, providing more efficient pathways for charged species to reach the respective electrodes. The BODIPY polymer derivative leading to the best device performance (PBTT) when blended with PCBM showed a short circuit current density (J_{sc}) of 4 mA/cm^2, V_{oc} of around 1 V, fill factor of 34 % and PCE of 1.2 %. SCLC measurements revealed that the PBTT:PCBM blends have better transport properties compared to the other studied BODIPY derivatives when blended with PCBM. As carriers were more efficiently transported towards the electrodes a J_{sc} value of 4 mA/cm^2 was obtained for PBTT:PCBM based OPVs. AFM measurements indicated phase separation for the BODIPY:PCBM blends under study, in good agreement with the low FF values observed (up to 34 %). Despite the very high open circuit voltage values obtained for the BODIPY:PCBM material system (around 1V), J_{sc} and FF values ranging from 0.3 - 4 mA/cm^2 and 24-34% respectively, are much lower compared to reference P3HT:PCBM based OPVs (V_{oc} of 0.57 V, FF of 45.1 % and J_{sc} of 11.55 mA/cm^2). Morphology limitations and low carrier mobility values for the BODIPY:PCBM materials system affect J_{sc} and FF, which in turn affect the achievability of higher PCE values. BODIPY:PCBM based devices exhibited hole mobility values reaching a maximum of 6.9×10^{-5} cm^{2}V^{-1}s^{-1}, when at the same time P3HT:PCBM solar cells show mobilities around two orders of magnitude higher. AFM measurements have revealed that main bottleneck for further device performance improvement is linked with obtained morphology. In order to address

this, BODIPY polymers with higher molecular weight and probably branched alkyl chains are needed.

Inkjet Printed Optically Active Layer

The final part of this thesis focused on more advanced processing techniques for the fabrication of OPVs and alternative pathways to eliminate high cost device components. Cost reduction is considered as the next important milestone for OPVs. The application of printing technology as a fabrication tool for organic photovoltaics and replacement of high cost materials in the OPV device structure is critical for the future technological progress of OPVs – enhancing the potential of the use of novel materials for future light-activated plastic power sources. Understanding and gaining control over the printing process is an essential step towards cost reduction and commercialization of OPVs. In the first part of chapter 5, details of the inkjet printing processing conditions of the P3HT:PCBM active layers such as solution viscosity, substrate temperature, drop-spacing and droplet height were presented. The choice of the above parameters is critical to achieving high power conversion efficiency inkjet printed OPVs. By using materials and a piezoelectric inkjet printer which are commercially available the optimized printing process can produce OPVs with power conversion efficiency in the range of 3 % – a PCE achieved under similar experimental conditions for optimized reference OPVs fabricated with conventional spin coating and doctor blading processing methods.

Record Efficiency Achieved for ITO Free Organic Solar Cells

In the second part of chapter 5, concepts to develop ITO-free OPVs are described. Most of the high performance OPV devices reported in the literature use rigid and stiff indium tin oxide (ITO) as the transparent electrode. ITO is deposited by sputtering at high vacuum and temperatures, prohibiting further reduction in fabrication cost. The need for inexpensive alternative transparent electrodes is imminent as ITO is one of the most expensive components of the OPV devices. The thesis concludes with a detailed optimisation process of an inkjet printed silver nanoparticle grid combined with different conductivity PEDOT:PSS as alternative to ITO to produce a low cost OPV bottom electrode. Ultimate control of the design requirements of the current collecting grid was achieved by using the proposed inkjet printing process to accurately control the uniformity and dimensions of the silver nanoparticle based grid. The performed measurements revealed higher light transmittance in almost all the visible range of the printed Ag grid when compared to different thicknesses of sputtered ITO. Processing challenges are described in detail and the proposed optimised inkjet printing process resulted in a record power conversion efficiency of 2 % for ITO-free P3HT:PCBM based OPVs using the combination of PEDOT:PSS/inkjet printed nanoparticles based current collecting grids [6]. Despite the recent progress and achievements in the field of OPVs there is still a long way to go towards fully printed and sustainable inexpensively produced OPVs and my future research plans will be focused on contributing to that direction.

Appendix:

List of publications:

JOURNAL PUBLICATIONS AS FIRST AUTHOR (ISI Web of Science)

- **M. Neophytou**, W. Cambarau, F. Hermerschmidt, C. Waldauf, C. Christodoulou, R. Pacios, S. A. Choulis, Inkjet-printed polymer–fullerene blends for organic electronic applications, Microelectronic Engineering 95, pp. 102–106, (2012).

(experimental work including ink formulation selection, device processing, characterization and data evaluation, discussion with supervisors, manuscript written, submission and review process)

Journal of Microelectronic Engineering, ELSEVIER, **Impact Factor: 1.557**

- **M. Neophytou,** H. A. Ioannidou, T. A. Ioannou, C. L. Chochos, S. P. Economopoulos, P. A. Koutentis, G. Itskos, S. A. Choulis, 2-(2,3,4,5,6-Pentafluorophenyl)-1H-benzo[d]imidazole, A Fluorine-Rich Building Block for the Preparation of Conjugated Polymer Donors for Organic Solar Cells Applications, Polymer Chemistry 3, pp. 2236-2243 (2012).

(experimental work including processing optimisation, device preparation, characterization and data evaluation, discussion with supervisors,manuscript written, submission and review process)

Journal of Polymer Chemistry, Royal Society of Chemistry, **Impact Factor: 5.32**

- **M. Neophytou**, F. Hermerschmidt, A. Savva, E. Georgiou, S. A. Choulis, Highly efficient indium tin oxide-free organic photovoltaics using inkjet-printed silver nanoparticle current collecting grid, Applied Physics Letters 101, 193302 (2012).

(experimental work including ink formulation selection, device preparation, optimization, characterization and data evaluation, discussion with supervisors, manuscript written, submission and review process)

Applied Physics Letters, American Institute of Physics, **Impact Factor: 3.844**

- **M. Neophytou**, D. Baran, C. J. Brabec and S. A. Choulis, *Photovoltaic loss analysis of BODIPY:PCBM based organic solar cells*, Organic Electronics, **Manuscript in preparation (2012).**

JOURNAL PUBLICATIONS AS CO-AUTHOR (ISI Web of Science)

- P. P. Boix, G. G. Belmonte, U. Muñecas, **M. Neophytou**, C. Waldauf, R. Pacios, Determination of gap defect states in organic bulk heterojunction solar cells from capacitance measurements, Applied Physics Letters 95, p. 233302, (2009).

(experimental work including solution preparation and device performance optimization of P3HT:PCBM at different ratio concentrations)

- A. Othonos, G. Itskos, **M. Neophytou**, S. A. Choulis, Excitation dynamics of a low bandgap silicon-bridged dithiophene copolymer and its composites with fullerenes, Applied Physics Letters 100, p. 153303, (2012)

(experimental work including processing optimisation and sample preparation)

- S. P. Economopoulos, C. L. Chochos, H. A. Ioannidou, **M. Neophytou**, J. Frost, S. Tuladhar, M. Shahid, J. Nelson, M. Heeney, D. D. C. Bradley, G. Itskos, P. A. Koutentis, S. A. Choulis, Novel BODIPY-based conjugated polymers. Synthesis, characterization and computational study, Journal of Materials Chemistry, Submitted, (2012).

(experimental work including ink formulation and processing optimisation, sample preparation)

PROCEEDINGS PAPERS (Scopus)

- J. C. Nolasco, R. Cabré, R. Pacios, C. Waldauf, **M. Neophytou**, E. Palomares, L. F. Marsal, J. Pallares, Conduction mechanisms of P3HT:PCBM solar cell, Proceedings of the 2009 Spanish Conference on Electron Devices, CDE'09 , art. no. 4800517, pp. 398-401.

CONFERENCES

- **M. Neophytou**, C. Waldauf ,S. A. Choulis, R. Pacios, Optimization of organic bulk heterojunction solar cells – the benefits of mixing Poster at E-MRS 2009 Spring Meeting June 8 – 12 Strasbourg, France, Symposium A.

- **M. Neophytou**, C. Waldauf, R. Pacios, S. A. Choulis, Comparison of different processing techniques for organic photoactive layers, with respect to efficiency and lifetime. Poster at Hybrid and Photovoltaics Conference, Benidorm Spain 2009.

- J. C. Nolasco, R. Cabré, L. Marsal **M. Neophytou**, M. Campoy-Quiles, C. Waldauf , R. Pacios, Conduction mechanisms of P3HT:PCBM solar cell. Poster at the 2009 Spanish Conference on Electron Devices, CDE'09.

- **M. Neophytou**, Inkjet Printing Organic Solar Cells, OREA Summer School, Chania, Crete, Greece, 2010 (Oral Presentation).

- **M. Neophytou**, C. Waldauf, R. Pacios, S. A Choulis "Organic solar cells: A potential source for low cost renewable energy", Oral Speech at the 2nd International Conference on Renewable Energy Sources and Energy Efficiency, Cyprus 2010 (Oral Presentation).

- S. A. Choulis, C. L. Chochos. **M. Neophytou**, C. Christodoulou, G. Florides, P. Eleftheriou "Molecular Electronics and Photonics" 4th North America - Greece - Cyprus Workshop on Paramagnetic Materials, Invited, June 14-18 2011, Patras, Greece.

- **M.Neophytou**, “Investigation of the Processing Parameters for Efficient Organic Solar Cells”, 2nd Workshop on Nanostructured Materials & Devices, October 17 2012, Nicosia, Cyprus (Oral presentation)